

DIGITAL ACCESS TO SCHOLARSHIP AT HARVARD
DASH.HARVARD.EDU

HARVARD LIBRARY


Examining the role of succinate signaling in tissue remodeling

Citation

Reddy, Anita. 2023. Examining the role of succinate signaling in tissue remodeling. Doctoral dissertation, Harvard University Graduate School of Arts and Sciences.

Link

https://nrs.harvard.edu/URN-3:HUL.INSTREPOS:37377882

Terms of use

This article was downloaded from Harvard University's DASH repository, and is made available under the terms and conditions applicable to Other Posted Material (LAA), as set forth at

https://harvardwiki.atlassian.net/wiki/external/NGY5NDE4ZjgzNTc5NDQzMGIzZWZhMGFlOWI2M2EwYTg

Accessibility

https://accessibility.huit.harvard.edu/digital-accessibility-policy

Share Your Story

The Harvard community has made this article openly available.
Please share how this access benefits you. Submit a story

HARVARD
Kenneth C. Griffin

GRADUATE SCHOOL
OF ARTS AND SCIENCES

DISSERTATION ACCEPTANCE CERTIFICATE

The undersigned, appointed by the

Division of Medical Sciences

in the subject of Biological and Biomedical Sciences

have examined a dissertation entitled

Examining the role of succinate signaling in tissue remodeling

presented by Anita Reddy

candidate for the degree of Doctor of Philosophy and hereby certify that it is worthy of acceptance.

Signature: Andrew Kruse
Andrew Kruse (Oct 19, 2023 15:26 EDT)

Typed Name: Dr. Andrew Kruse

Signature: Naama Kanarek
Naama Kanarek (Oct 18, 2023 16:48 EDT)

Typed Name: Dr. Naama Kanarek

Signature: Brendan Manning
Brendan Manning (Oct 18, 2023 18:51 EDT)

Typed Name: Dr. Brendan Manning

Signature: Kathryn Wellen
Kathryn Wellen (Oct 18, 2023 15:12 EDT)

Typed Name: Dr. Kathryn Wellen

Date: October 18, 2023

Examining the role of succinate signaling in tissue remodeling

A DISSERTATION PRESENTED
BY
ANITA REDDY
TO
THE DIVISION OF MEDICAL SCIENCES

IN PARTIAL FULFILLMENT OF THE REQUIREMENTS
FOR THE DEGREE OF
DOCTOR OF PHILOSOPHY IN THE SUBJECT OF
BIOLOGICAL AND BIOMEDICAL SCIENCES

HARVARD UNIVERSITY
CAMBRIDGE, MA
OCTOBER 2023

© 2023- ANITA REDDY

ALL RIGHTS RESERVED

Dissertation advisor: Professor Edward T. Chouchani Anita Reddy

Examining the role of succinate signaling in tissue remodeling

Abstract

While the benefits of exercise on systemic health are undeniable, vigorous muscle contraction, like the ones associated with exercise, puts considerable mechanical and energetic strain on muscle fibers. To meet these newfound demands, skeletal muscle must undergo extensive remodeling. This is a highly coordinated process that involves the participation of numerous non-myofibril cell populations such as satellite cells, stromal cells, immune cells, and endothelial cells. How exercising muscle communicates with these cells to initiate the remodeling process remains poorly understood. We performed comparative metabolomics analysis on exercised skeletal muscle to identify potential signaling molecules that preferentially increase in the local extracellular environment of muscle, following exercise. Using this approach, we identified succinate, a tricarboxylic acid (TCA) cycle intermediate, as a potential exercise signaling molecule in both mice and humans. Succinate is a ligand for a g-protein coupled receptor, succinate receptor 1 (SUCNR1). Using a hybrid resistance-endurance training model, we implicate succinate-SUCNR1 signaling in a host of remodeling processes such as fast-twitch myosin protein expression, innervation, and extracellular matrix remodeling. These changes manifest as a SUCNR1-dependent increase in strength. Additionally, we show that SUCNR1 is exclusively localized to non-myofibrillar cells within skeletal muscle. Moreover, we identify a novel pH-gated transport mechanism for succinate where monocarboxylate transporter 1 (MCT1) is repurposed to allow for succinate secretion from skeletal muscle, during exercise. We also show this transport mechanism to be relevant in brown adipose tissue (BAT) where succinate sequestration by BAT has been linked to many favorable outcomes including reduced systemic

tissue inflammation and increased energy expenditure. Overall, we identify a novel role for succinate as an exercise-responsive metabolite, implicate succinate-SUCNR1 signaling in many muscle remodeling processes, and characterize a new transport mechanism for succinate.

Table of Contents

Preamble

	Title Page	i
	Copyright	ii
	Abstract	iii
	Table of Contents	v
	List of Figures	vi
	Acknowledgments	viii

Main Chapters

Chapter One	Introduction	1
Chapter Two	Succinate signaling contributes to muscle adaptation following exercise	33
Chapter Three	Monocarboxylate transporters facilitate succinate uptake into brown adipocytes	88
Chapter Four	Discussion and Future Perspectives	118

List of Figures

Figure 1.1 Oxidation of succinate to fumarate by succinate dehydrogenase 3

Figure 1.2 Structure of ubiquinone and ubiquinol 4

Figure 1.3 Schematic depicting enzymatic reactions that donate electrons to ubiquinone (Q**)** 5

Figure 1.4 SUCNR1 is coupled to $G\alpha_i$, $G\alpha_q$, and $G\alpha_s$ subunits 7

Figure 1.5 Schematic depicting the properties of white, beige, and brown adipocytes 10

Figure 1.6 β-adrenergic signaling promotes thermogenesis by activating UCP1 12

Figure 1.7 Organization of muscle fiber 17

Figure 1.8 Skeletal muscle contraction 19

Figure 2.1 Schematic depicting succinate release from skeletal muscle 35

Figure 2.2 Succinate is selectively secreted by exercising skeletal muscle in both mice and humans 39

Figure S2.1 Metabolite Profiling of Mouse and Human Exercise Samples and Characterization of pH-Dependent Succinate Release 42

Figure 2.3 Cytosolic acidification drives succinate secretion 46

Figure 2.4 pH-dependent secretion of succinate 49

Figure S2.2 Depletion of MCT isoforms in C2C12 myoblasts and characterization of MCT1-dependent succinate transport 51

Figure 2.5 Succinate-SUCNR1 signaling controls cell non-autonomous transcriptional responses to acute exercise 53

Figure S2.3 Direct effect of succinate on muscle cells and comparison of WT and SUCNR1 TA proteomes 57

Figure 2.6 Succinate signaling mediates muscle adaptation to exercise 61

Figure S2.4 Quantification of blood vessel and fiber volume in WT and SUCNR1 KO TA muscle and correlation analysis of human physiological parameters and peak venous succinate concentration following exercise 65

Figure 3.1 Brown adipocytes import extracellular succinate in a pH dependent manner 94

Figure 3.2 Monocarboxylate transporters (MCTs) facilitate succinate uptake in brown adipocytes 96

Figure 3.3 Inhibition of MCT1 attenuates succinate uptake into mouse BAT *in vivo* 101

Figure 4.1 Schematic depicting pH-gated succinate release from skeletal muscle 118

Figure 4.2 Schematic depicting paracrine succinate-SUCNR1 signaling 119

Figure 4.3 Proposed model of NE-driven succinate transport 121

Figure 4.4 Exercise promotes the transcription of pro- and anti-inflammatory cytokines 125

Figure 4.5 Gene-expression data from WT and SUCNR1 KO mice following exhaustive treadmill running 127

Acknowledgements

There are so many people I must thank that have helped get me to this spot. First and foremost, I would like to thank Ed Chouchani, my PhD mentor. Without his support and guidance, I would not be here. I have learned so much from Ed. Working in his lab has made me a stronger and better scientist. When I was rotating in Ed's lab, I remember having trouble trying to make a buffer. I messaged him about it and not five minutes later he was there at the bench, helping me. While this might seem small, this moment really stuck with me and showed me his commitment to the lab. Throughout the years Ed has helped me troubleshoot countless experiments and has showed me the answer is usually in the details. One of the skills I am most grateful to have learned from Ed is the ability to communicate my science clearly and effectively. Through working on manuscripts and giving countless practice talks, Ed has taught me how to craft the narrative of a project and present it in a way that allows people to better understand the core message. His approach to science has deeply influenced my own scientific inquiry and I am so thankful that he accepted me as a graduate student in his lab. I would also like to thank my dissertation advisory committee (DAC) members: Bruce Spiegelman, Diane Mathis, and Andrew Kruse. Their advice and suggestions, over the years, have improved my science and strengthened my project. I am so grateful that they agreed to serve on my committee.

Working in Ed's lab, I have been so fortunate to have worked with so many amazing scientists whose scientific ability is only rivaled by their kindness. The person who has perhaps most greatly shaped my PhD is Evanna Mills. While a postdoc in Ed's lab, Evanna and I first grew close, bonding over our love of Love Island and good food. Over the years Evanna has provided me immense support, for which I'm eternally grateful. When science got tough, which it almost always inevitably does, Evanna was there to lend a shoulder to lean on and offer advice. Her belief in me gave me the strength to preserve through the toughest parts of my PhD. I feel so

grateful to have had the opportunity to work beside Evanna. She has taught me to be more confident in my science. I greatly admire Evanna, both as a scientist and a person. Her scientific rigor is only paralleled by her deep care for those around her. Next, I would like to thank Martha Ordonez. I first met Martha during my second year of graduate school when she rotated in the Chouchani Lab. While we didn't talk much during the rotation, Martha has since grown to be one of my closest friends. I know I can always turn to Martha when I'm having a tough day or when I have exciting result to share. Martha has provided so much joy throughout my PhD. I always look forward to seeing her in lab and awaiting whatever ridiculous conversations we may have. Time in lab always flies by with Martha. Whether she's humoring my crazy hypotheticals or recounting her weekend, I always enjoy talking to Martha. I admire her strength, resilience, and perseverance. She helps me to see the bright side of every situation and encourages me to be more confident, reminding me that I've "got this." If I'm ever having a bad day, I know I can turn to Martha for support and comfort. If I'm feeling overwhelmed, Martha is usually the first one to offer help. I'm so grateful that she decided to join Ed's lab. I would also like to thank Haopeng Xiao, a postdoc in Ed's lab. Haopeng and I have sat next to each other for over five year and through that time he has become a close friend and confidant. Haopeng is always there with encouraging words and helpful advice. I always feel comfortable sharing both scientific and personal problems with him knowing he'll offer me words of support and encouragement. He has made my time in lab both fun and enriching. I am so thankful that we have been bay-mates for so long and to have gotten so close. There are so many other people in the Chouchani lab that have made my time here so enjoyable. Thank you to my co-author Luiz Bozi, without his tremendous effort the muscle paper would not have been possible. Also, his positivity is infectious and always puts me in a better mood. Thank you to Narek Darabedian, a former member of the lab. He always made the lab such a fun place to work and were so helpful. I would also like to thank all the

remaining members of the Chouchani Lab, both past and present. You all have made my experience in the lab infinitely better and have helped shape me as a scientist.

Before I joined Ed's lab as a graduate student, I worked as a research technician in Marcia Haigis's lab. In her lab, I first fell in love with metabolism. Working in the Haigis lab exposed me to academic research and greatly inspired me to apply to graduate school. Marcia's support and mentorship were instrumental in me getting into graduate school and joining the BBS program. For that I will be eternally grateful. Working in Marcia's lab I have met some of the most amazing scientists and people. I would like to start by thanking one of the first postdocs I've worked for who has since become a close friend, Sejal Vyas. When I first joined Marcia's lab, Sejal was responsible for training me. She taught me many lab techniques and was always so patient whenever I made a mistake. Sejal's calming demeanor always instantly puts me at ease and gives me perspective. She helps me not sweat the little stuff and to not dwell. Some of my fondest memories are dinner parties at Sejal's home. Not only is Sejal a fantastic chef, but she's also the most welcoming hostess. Dinners at Sejal's are always filled with laughter, games, and amazing food. I am so grateful to have gotten to know Sejal and to call her a friend. Next, I would like to thank Jessica Spinelli. I first got to know Jessica when she was a graduate student in Marcia's lab. The thing that initially struck me when I first met Jessica was her enthusiasm and warmth, which has only grown throughout the years. Jessica's energy is infectious and invigorating. I'm so inspired by her both as a scientist and a person. Spending time with Jessica it's evident that she deeply cares about the people in her life and strives to make everyone feel included. I would also like to thank Giulia Notarangelo. I always have so much fun when I'm around Giulia. Whether we're talking about Taylor Swift or driving everyone crazy during code names, I'm always having a good time when Giulia is around. Next, I would like to thank Stacy Mulei. Stacy has been such a source of warmth. She always encourages me to see things from a different perspective and I always enjoy spending time with her. I would also like to thank Elma Zaganjor and Haejin Yoon

and all other members of the Haigis lab I have worked with. I greatly appreciate all the support I have received from you all over the years.

In addition to all the people I have met in the Haigis and Chouchani labs, there are people I've met along my scientific journey outside of these labs that have greatly improved my time as a PhD student. I would like to start by thanking Irene Wong. I first met Irene through the BBS program when we were both first year students. We quickly became friends as we commiserated over p-sets and finals. Irene has been there for me through all the good times and bad times, throughout my PhD. All my fondest grad school memories involve Irene. From BBS retreat to blueberry picking to seeing live shows at Sonia, I've had so much fun with Irene. I would also like to thank Adrija Navarro. I also met Adrija Navarro during my first year of graduate school. One of my first memories of Adrija was when she took us sailing on the Charles. Since then, I've had countless memorable nights with Adrija. Whether it's house parties, nights at Sonia, or dinner at her apartment spending time Adrija is always a great time. I'm so grateful for both Irene and Adrija. Spending time with them has kept me sane throughout grad school and provided much needed time away from lab when things got tough, or experiments were not going well, and for that I am forever thankful.

In addition to all the people I met through science, my friends outside of science are perhaps some of the oldest and closest to me. I would like to thank my college friends, Molly MacDonald, Kim Burk, Lily Rasouli, Megan Mabee, Hiba Bilal, Laura Pendergast Johnson, and Sarah Quintiliani, affectionately known as "the biddies." Their support throughout the years has been immeasurable. I know I can always count on them when things get tough. Hanging out with "the biddies" gives me perspective and makes the problems I face in lab feel small. I cherish all the memories we have made from theme parties to late night study sessions. I am so grateful to have met them and to have them all in my life. I would also like to thank Molly and her husband Mike. Our beach days at Crane beach and nights out bar hopping have been some of the most

fun I've had. I'm so glad they both decided to move to Boston. I would also like to thank Kim, one of my closest friends. I always have so much fun visiting Kim. I know I can tell her anything and not feel judged. Kim has provided me with immense support throughout my PhD journey, for which I will be eternally grateful.

Next, I would like to thank Leah Doherty. I met Leah a mere three years ago, but she has left such a mark on my life. In this short amount of time, Leah has become almost like a sister to me. The closeness I feel to Leah is only rivaled by the closeness I feel to my actual sister, Niki. Living with Leah during my fourth and fifth years of my PhD has been some of my favorite times in Boston. Leah's warmth, kindness, and silliness brought so much joy to my life. Leah has been by my side through all the bad and good times. I could always count on Leah to make me feel better after a rough day and to provide laughter and joy. I loved all our little adventures from trying to find the best soft-serve ice cream in Boston to taking an ill-fated, impromptu trip to Kimballs Farm that ended in us getting Covid. I am forever grateful for this friendship and know my life has only been made better by having Leah in it.

Finally, but most importantly, I would like to thank my family. My family has been the greatest source of strength and support throughout my PhD journey. They have helped me in so many ways. I would not be here without them. I am forever indebted to my parents and all the sacrifices they made for my sister and me. I am thankful for the work ethic my parents instilled in us, showing and telling us that anything is possible with just a little hard work. I would like to thank my mom for always believing in me and reassuring me that things will be okay. Her confidence in me made me believe that I can handle any situation I face. I would also like to thank my dad who has always made me believe I can achieve anything I put my mind to. Lastly, but certainly not least, I would like to thank my sister Niki, by best friend and greatest confidant. I am serious when I say I would not have been able to complete my PhD without her. She has been a constant source of strength, support, and joy throughout this process. She is the first person I turn to when

things are tough, knowing that she will have the right thing to say to make me feel better. While she is my younger sister, I look up to Niki in many ways. I admire her intelligence, work ethic, and wit, but perhaps above all her warmth, compassion, and kindness are my favorite qualities of hers. Niki has been my emotional rock throughout my PhD, offering words of encouragement when things got tough and celebrating all the triumphs with me. She has helped me maintain perspective and has reassured me when I believed the worst. Niki has brought so much joy into my life and has made my PhD so much more enjoyable. She is my biggest cheerleader, and I am so grateful to have her in my life. Overall, I am so thankful to have so many amazing people in my life, cheering me on. Without their support, getting to this point in my PhD would have been infinitely harder and far less fun. Thank you everyone, your presence has been invaluable to me.

Introduction

Life hinges on the ability of living organisms to extract nutrients from food and convert it into energy, a process known as metabolism. The intermediary molecules involved in this process are known as metabolites and play a major role in health and disease. The metabolic profile of an individual, that is the concentration and identity of metabolites present either in the circulation or a given tissue, is illuminating and can reflect the health of that individual. Metabolite concentrations change rapidly in response to environmental stimuli such as cold exposure or exercise and renormalize quickly once the perturbation has ended. These changes can also be more persistent in response to a chronic stimulus like nutrient imbalance which is seen with type 2 diabetes and obesity. Since metabolite concentrations can serve as a proxy for health status and are dynamically regulated, metabolites are poised to act as signaling molecules and can promptly convey changes in bioenergetic status to the surrounding environment. Indeed, there is growing interest in understanding the signaling properties of metabolites and the role they play in tissue remodeling, the maintenance of systemic health, and the onset of disease.

One metabolite that has garnered considerable interest for its signaling abilities is the tricarboxylic acid (TCA) cycle intermediate succinate. Since the de-orphaning of g-protein coupled receptor 91 (GPCR91), better known as succinate receptor 1 (SUCNR1), succinate has emerged as a powerful signaling molecule that is involved in processes that contribute to both the maintenance and breakdown of systemic health. Much of succinate's signaling prowess lies in its

ability to serve as a ligand for SUCNR1. Succinate-SUCNR1 signaling has both beneficial and detrimental effects on systemic health that are largely dependent on the frequency of signaling. For instance, acute, pulsatile bouts of succinate signaling typically confer positive health benefits while chronic, incessant signaling contributes to many disease states[1-5]. The frequency of succinate signaling is dependent on the persistence of extracellular succinate, that is whether circulating succinate levels renormalize to baseline or remain chronically elevated. In fact, elevated circulating succinate is a signature for many diseases such as hypertension and type II diabetes [3,5,6]. Thus, understanding how to reduce circulating succinate and subsequently limit succinate signaling is of interest. Additionally, localization of SUCNR1 is poorly defined and the pathways downstream of SUCNR1 agonism are not well characterized. Identifying which cell types express the receptor and which pathways are activated upon succinate-SUCNR1 engagement will offer us a better understanding of the role of this signaling modality in health and disease.

In this dissertation, I elucidate a plasma membrane transport mechanism that regulates succinate exchange between cells and the circulation. I focus my attention on two tissues that I show are key modulators of systemic succinate in mice and humans: skeletal muscle and brown adipose tissue (BAT). Specifically, I uncover a newfound role for monocarboxylate transporter 1 (MCT1) as a succinate transporter. Additionally, I illuminate the contributions of succinate signaling in strength adaptation following exercise. Combined, these chapters highlight the benefits of succinate signaling, its contribution to muscle remodeling and adaptation to exercise, and the environmental conditions that foster succinate transport. Overall, I hope this body of work will provide readers with a newfound appreciation for the signaling abilities of metabolites and offer a better understanding of how this signaling is regulated.

Succinate: a bioenergetic signal

Central to mitochondrial metabolism is succinate. This metabolite links the TCA cycle to the electron transport chain (ETC), two major metabolic pathways whose main objective is to generate energy in the form of adenosine triphosphate (ATP). Succinate is produced from

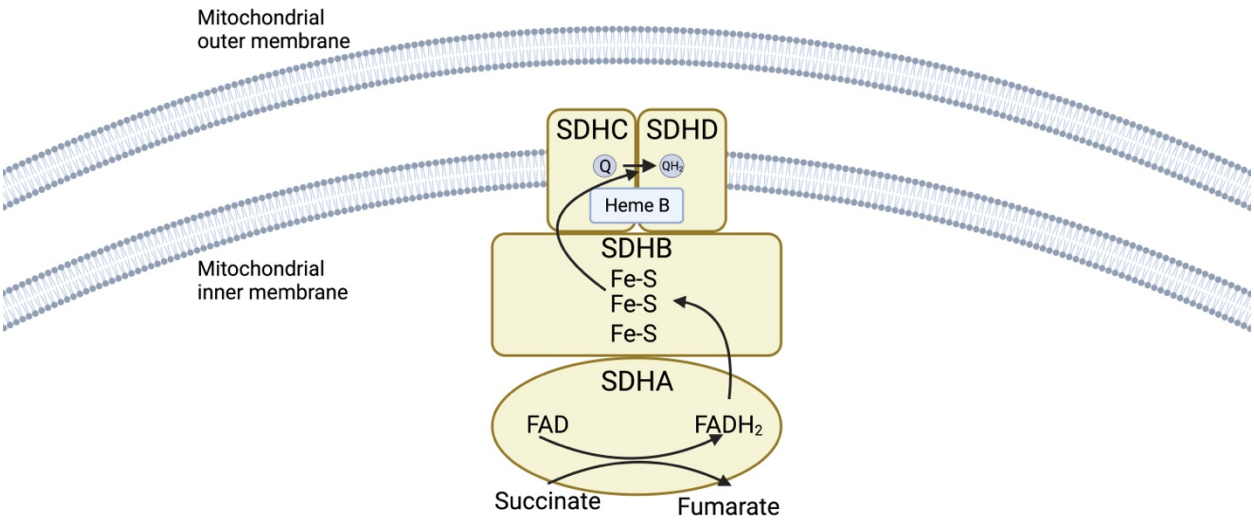


Figure 1.1 | Oxidation of succinate to fumarate by succinate dehydrogenase. Succinate oxidation to fumarate is coupled to the reduction of flavin adenine dinucleotide (FAD) to $FADH_2$. $FADH_2$ passes the accepted electrons to iron-sulfur clusters in SDHB. These electrons are ultimately transferred to ubiquinone (Q) which then results in the formation of ubiquinol (QH_2).

succinyl-CoA by the enzyme succinyl-CoA synthetase. This reaction generates free coenzyme A (CoA) and one molecule of ATP or guanine triphosphate (GTP), depending on the isoform of the enzyme[7]. Following this reaction, succinate is then oxidized by succinate dehydrogenase (SDH), also known as complex II, to produce fumarate. SDH sits in the inner membrane of the mitochondria and is a part of the ETC and the TCA cycle. This protein consists of four subunits: SDHA, SDHB, SDHC, and SDHD, all of which are encoded by nuclear DNA[8]. The SDHA and SDHB subunits reside in the mitochondrial matrix, while the C and D subunits comprise the transmembrane domain of the protein[9]. SDHA contains a dicarboxylate binding site and a bound

flavin adenine dinucleotide (FAD) cofactor[10]. When succinate binds to SDHA, the protein facilitates the transfer of electrons from succinate to FAD forming $FADH_2$ and fumarate (figure 1.1). These electrons are shuttled from $FADH_2$ to iron-sulfur (Fe-S) clusters in SDHB which then transfers them to the redox-sensitive molecule ubiquinone resulting in the formation of ubiquinol[9].

Ubiquinone is comprised of a redox-responsive benzoquinone head and a lipophilic isoprenoid tail, and is largely confined to the mitochondrial inner membrane[11]. The oxidation of succinate cannot occur without reduction of ubiquinone. However, succinate is not the only metabolite that relies on ubiquinone reduction for its conversion. Ubiquinone is involved in many metabolic reactions and accepts electrons from numerous pathways ranging from *de novo* pyrimidine biosynthesis to fatty acid oxidation, making this molecule a metabolic hub[11] (figure 1.3). Because of its involvement in diverse branches of metabolism, ubiquinone can serve as a barometer for the energetic status of the cell with changes in ubiquinone redox state reflecting changes in nutrient abundance. Ubiquinone can be replenished by complex III which oxidizes

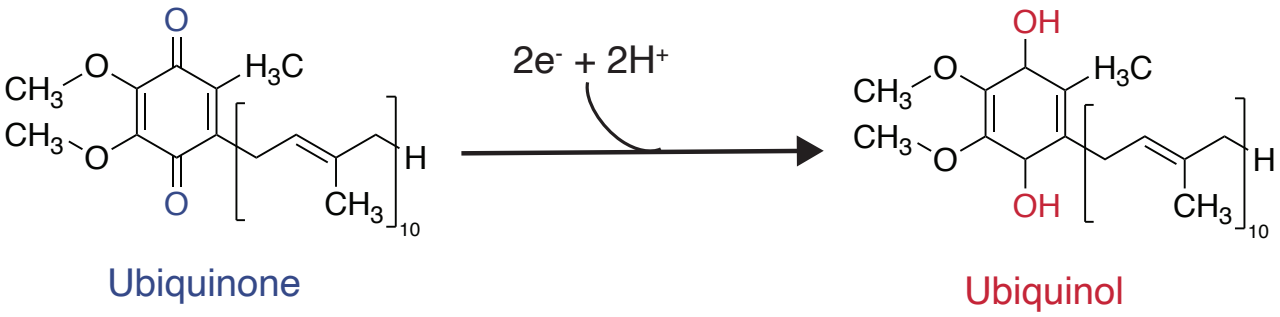


Figure 1.2 | Structure of ubiquinone and ubiquinol. Reaction depicting the reduction of ubiquinone to ubiquinol.

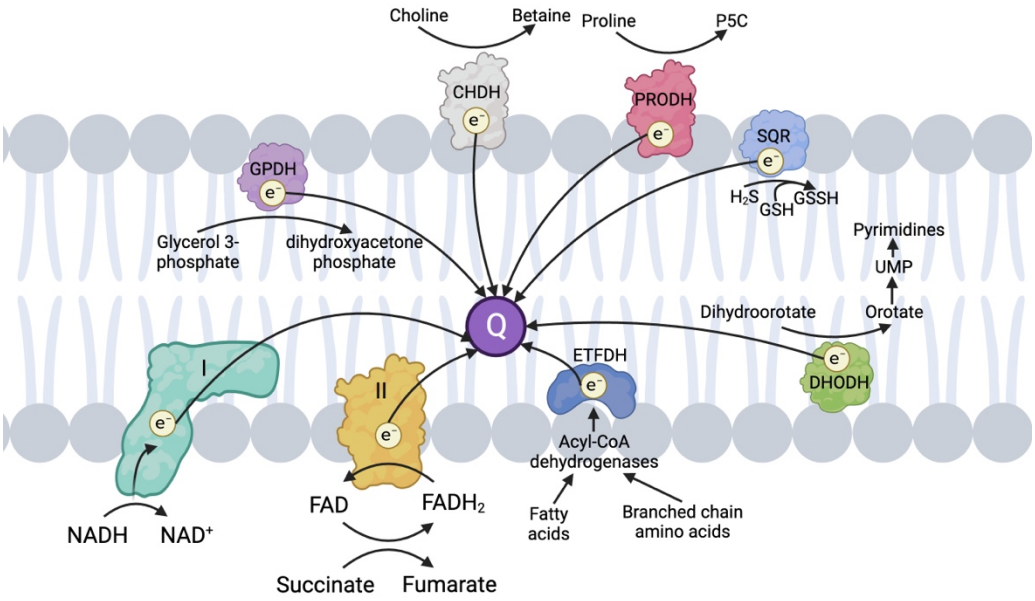


Figure 1.3 | Schematic depicting enzymatic reactions that donate electrons to ubiquinone (Q). Abbreviations: glycerol-3-phosphate dehydrogenase (GPDH), choline dehydrogenase (CHDH), proline dehydrogenase (PRODH), sulfide quinone oxidoreductase (SQR), glutathione (GSH), glutathione persulfide (GSSH), dihydroorotate dehydrogenase (DHODH), electron transfer flavoprotein dehydrogenase (ETFDH)

ubiquinol to produce ubiquinone[12,13]. Complex III passes these electrons to cytochrome C while transferring protons across the mitochondrial inner membrane[14]. The coupling of electron transfer to proton translocation allows ubiquinone to serve as a central electron shuttle and establish the proton gradient, which is required for ATP synthase activiety[15]. Thus, the oxidation of ubiquinol is dependent on the proton motive force and subsequently ATP demand, while the reduction of ubiquinone is determined by metabolic flux[15]. A high ratio of ubiquinol to ubiquinone indicates an energetic imbalance, signaling a discrepancy in electron supply and demand. Additionally, the regeneration of ubiquinone is contingent on oxygen being able to serve as the final electron

accceptor[16]. Thus, the redox status of ubiquinone reflects the bioenergetic status of the cell by integrating nutrient abundance, ATP demand, and oxygen availability. Because succinate oxidation is coupled to the reduction of ubiquinone, changes in intracellular succinate concentrations reflect the redox status of the ubiquinone pool and thus the bioenergetic status of the cell. Imbalances in energy supply and demand result in the accumulation and secretion of succinate[17-20].

Succinate accumulation in health and disease

Succinate is a dynamic metabolite, whose abundance changes rapidly in response to a wide array of interventions. Accumulation of intra- and extracellular succinate can signify metabolic distress, or a discrepancy in nutrient supply and demand. Succinate concentrations can be used as a biomarker for numerous physiological and pathophysiological states. For example, elevated serum succinate is associated with metabolic disorders like obesity, type II diabetes, and hypertension[3,5,6,21]. The increase in extracellular succinate associated with obesity is thought to originate from succinate-producing strains of microbiota residing in the gut that are enriched in obese individuals[6]. Moreover, serum succinate levels are a good predictor of poor metabolic health. Extracellular succinate concentrations positively correlate with serum triglyceride levels, visceral fat abundance, and blood pressure[5]. In patients who have undergone bariatric surgery, serum succinate levels negatively correlate with type II diabetes remission[22]. Succinate accumulation is also a signature of tissue ischemia, with concentrations increasing 3 – 19-fold compared to non-ischemic controls[17]. In fact, plasma succinate concentrations following myocardial infarction correlate with the extent of ischemia experienced[23]. The rapid oxidation of succinate upon reperfusion contributes to ischemia-reperfusion induced injury through the production of reactive oxygen species (ROS) by reverse electron transport at complex I[17]. Succinate accretion also has immunomodulatory effects. Previous findings report succinate

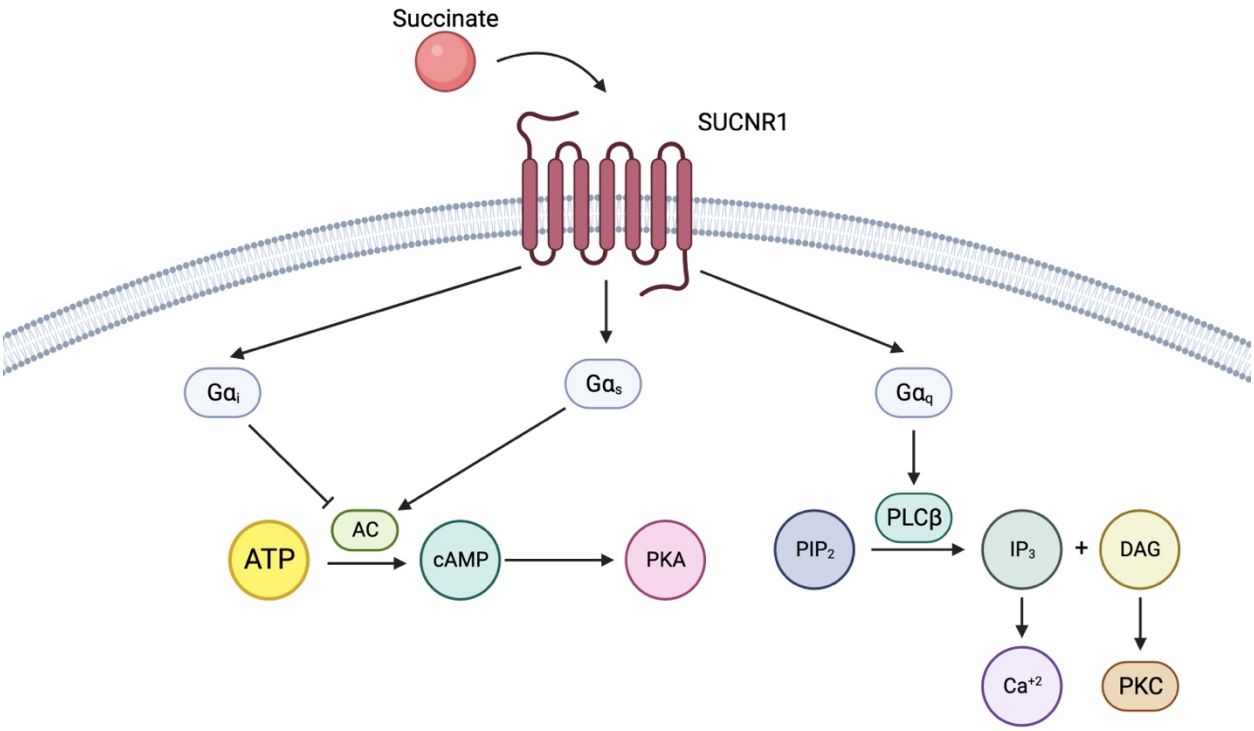


Figure 1.4 | SUCNR1 is coupled to $G\alpha_i$, $G\alpha_q$, and $G\alpha_s$ subunits. SUCNR1 signaling, when coupled to $G\alpha_i$, results in the inhibition of adenylyl cyclase (AC) which causes a decrease in cyclic-adenosine monophosphate (cAMP) and inhibition of protein kinase A (PKA). Contrarily, Gas signaling activates AC and stimulates PKA signaling. Signaling through Gaq activates phospholipase C beta (PLCβ) which cleaves phosphatidylinositol 4,5-bisphosphate (PIP_2) to form inositol triphosphate (IP_3) and diacylglycerol (DAG), which results in the activation of protein kinase C (PKC).

accumulation promotes the production of pro-inflammatory cytokine interleukin-1β (IL-1β), in lipopolysaccharide (LPS)-stimulated macrophages [18,24].

Elevated succinate is not always associated with pathophysiological states. For instance, succinate naturally accumulates in the retina, a chronically hypoxic niche within the eye. Accumulated succinate is transported to the neighboring retinal pigment epithelium where it is used as fuel[25]. Additionally, succinate released by shivering muscles in the neck during cold

exposure results in succinate accumulation in BAT and promotes thermogenesis, highlighting another benefit of increased succinate[26]. Perhaps most notably, increased succinate is a hallmark of exhaustive exercise[4,27-29]. Researchers observed increased plasma succinate immediately following high-intensity treadmill running, in humans, with concentrations peaking at 125 μM[4]. Moreover, plasma succinate concentrations following exercise can be a good predictor of athletic performance. Plasma metabolomics performed on marathon runners immediately following running observed a positive correlation between plasma succinate and running speed, suggesting a benefit of succinate release[27].

While extracellular succinate has been well-documented, the mechanism of succinate transport is unknown. In fact, many believe extracellular succinate to be purely a result of non-specific cell damage. However, we have evidence to believe the contrary; succinate transport is selective. We hypothesize that succinate release and uptake are induced by transient changes in pH driven by physiological events (e.g. exercise, cold exposure). This hypothesis is further explored in chapters two and three of this dissertation.

Contribution of SUCNR1-succinate signaling to metabolic disorders

The accumulation of succinate is not purely incidental. Succinate itself can influence systemic health largely by activating SUCNR1 (figure 1.4). SUCNR1 is highly expressed on metabolically active tissues like kidney, liver, and adipose tissue[30]. This receptor is highly specific for succinate and is not activated by other TCA cycle intermediates[31]. Structurally similar metabolites maleate and methylmalonate can engage the receptor but are 5 – 10 fold less potent than succinate[32]. Moreover, succinate only serves as a ligand for SUCNR1 and does not bind to or activate additional receptors[31]. The half-maximal effective concentration (EC_{50}) of succinate for human SUCNR1 is between 28 – 56 μM[31]. In healthy adults, plasma succinate concentrations range from 1 – 10 μM, which is well below the required concentration for receptor activation[3,33]. However, succinate can rapidly increase in response to metabolic perturbations, making

succinate signaling a possibility in these contexts. In fact, succinate-SUCNR1 signaling occurs during many altered metabolic states and is a direct response to an elevation of extracellular succinate. This is most prominent during metabolic disorders like obesity or type II diabetes where circulating succinate rapidly accumulates and remains elevated at concentrations allowing for receptor activation[3,5,6,21]. SUCNR1 is highly expressed on white adipocytes and macrophages, two cell types that play a major role in obesity and type II diabetes[21,30,34]. Succinate-SUCNR1 signaling can exacerbate symptoms associated with these disorders leading to a worsened prognosis. For example, succinate signaling inhibits lipolysis in white adipose tissue (WAT) and leads to an increase in subcutaneous and epididymal tissue weight compared to SUCNR1 KO mice[30,35]. Additionally, wild-type (WT) mice had increased levels of plasma cholesterol following high-fat feeding, compared to SUCNR1 KO mice[21].

Succinate signaling also contributes to the progression of inflammation during metabolic disorders. For example, SUCNR1 KO mice experienced less inflammation following high fat feeding which was marked by reduced inflammatory gene expression and a decrease in macrophages present in adipose tissue[21]. Similar findings have been reported in non-alcoholic fatty liver disease (NAFLD) where SUCNR1 KO mice experienced reduced liver inflammation following western diet[1]. Additionally, succinate can serve as a chemokine, attracting innate immune cells to sites of high succinate, in a SUCNR1-dependent manner[1,21,34]. Succinate is also involved in the production of pro-inflammatory cytokine interleukin-1β (IL-1β), which occurs in a SUCNR1-dependent and independent manner[18,24,34,36]. In these ways, succinate fosters a pro-

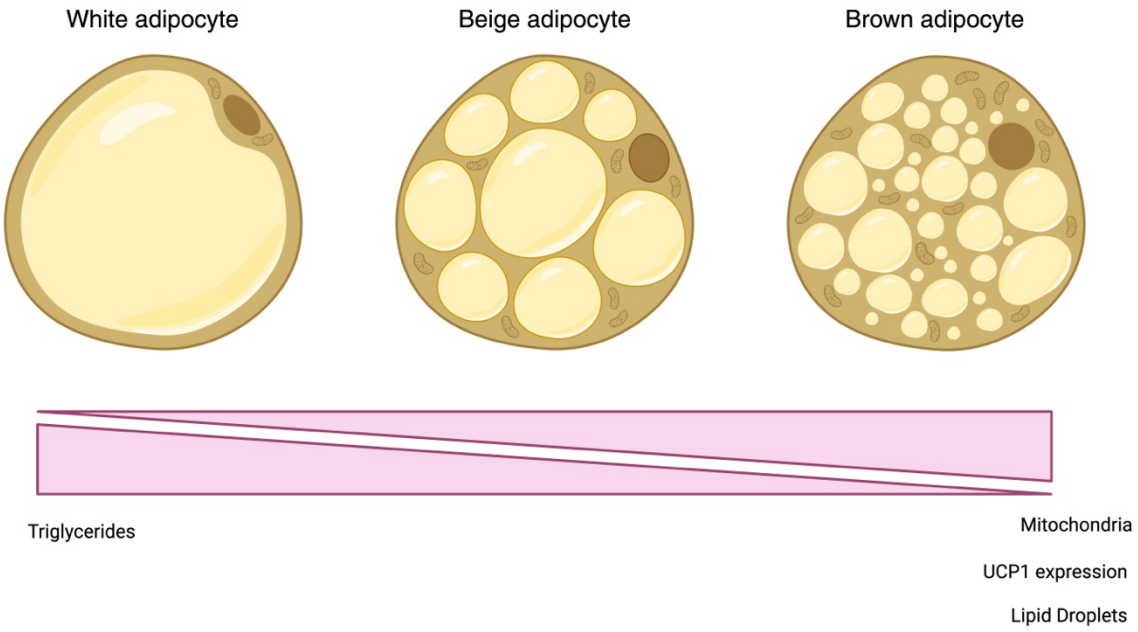


Figure 1.5 | Schematic depicting the properties of white, beige, and brown adipocytes. White adipocytes contain the least number of mitochondria, have the greatest lipid content, and do not express UCP1. Brown adipocytes have the greatest number of mitochondria, smaller lipid droplets, and express UCP1. Beige adipocytes have an intermediary number of mitochondria and lipid droplets and can be induced to express UCP1.

inflammatory environment by recruiting immune cells to sites of high succinate concentration and by promoting inflammatory cytokine production. It should be noted that there have been conflicting reports about the role of succinate signaling in the inflammatory response. Mice with a myeloid-specific deletion of SUCNR1 experience an increase in pro-inflammatory cytokine transcripts in liver, subcutaneous adipose tissue (SAT), and visceral adipose tissue, suggesting SUCNR1 has an anti-inflammatory role in this setting[37]. These contrary results likely arise from cell-type differences in Gα subunit expression. SUCNR1 is thought to be coupled to $G\alpha_i$ and $G\alpha_q$ subunits but new findings suggest the receptor can also couple to $G\alpha_s$ subunits (figure 1.4)[38]. Succinate signaling through $G\alpha_i$ and $G\alpha_q$ is thought to promote inflammation while signaling through $G\alpha_s$ is

believed to have anti-inflammatory effects[38]. However, more work needs to be done to fully understand the effects of Gα subunit expression and the downstream pathways involved in SUCNR1-mediated inflammation.

BAT: a succinate sink

Chronic elevation of extracellular succinate contributes to the pathophysiology of several metabolic disorders largely by increased SUCNR1 activation. Therefore, reducing aberrant succinate signaling by lowering the concentration of circulating succinate is important. However, the mechanism underlying succinate transport and how it is regulated is poorly understood. We have previously observed beige and brown adipose tissue (BAT) to have a high capacity for succinate sequestration[1,26]. Brown adipocytes are specialized fat cells with thermogenic abilities that are activated upon cold exposure. Brown adipocytes differ from white adipocytes in mitochondrial content and lipid droplet morphology (figure 1.5)[39]. Their thermogenic ability lies in the activity of uncoupling protein 1 (UCP1). UCP1 is a mitochondrial protein that sits in the inner membrane. During cold exposure, UCP1 is activated by fatty acids that are released from triglycerides in response to norepinephrine stimulation of adrenoreceptors (figure 1.6). Once activated, UCP1 dissipates the proton gradient established by complexes 1 and 3 of the electron transport chain by allowing protons an alternative path into the mitochondrial matrix. Because protons are no longer confined to pass through ATP synthase, BAT can futilely burn fuel independently of ATP demand and generate heat.

While UCP1 activity is largely induced by adrenoreceptor agonism, succinate can also increase the activity of this protein. During cold conditions, BAT readily imports circulating succinate released by shivering muscles in the neck[26]. Once inside, succinate is rapidly metabolized, producing reactive oxygen species (ROS) as a byproduct. This ROS reacts with UCP1, leading to the sulfenylation of cysteine 253 on UCP1[26,40]. This modification heightens the

activity of UCP1 resulting in increased thermogenic activity[26,40]. Brown adipocytes, however, are not the only cell type to express this protein. Beige adipocytes also express UCP1 and have thermogenic abilities. These fat cells reside within white adipose tissue (WAT) depots (figure

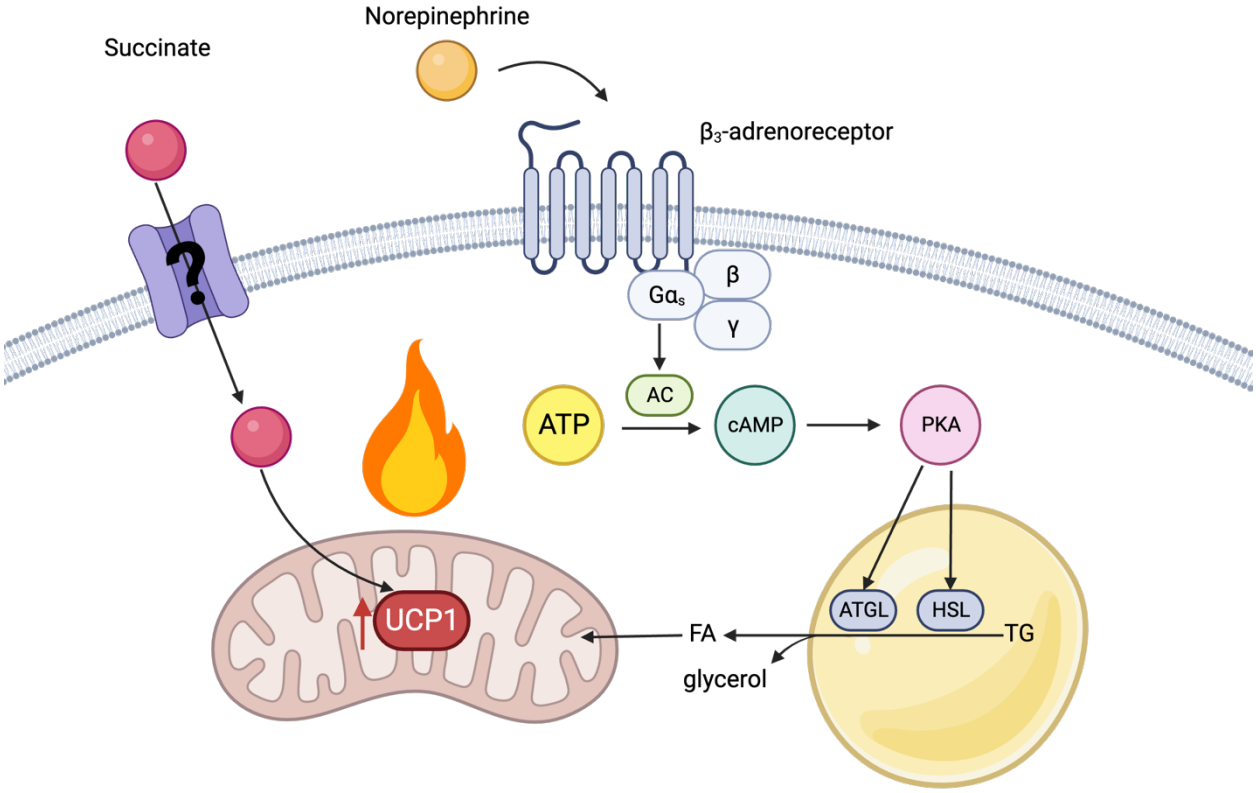


Figure 1.6 | β-adrenergic signaling promotes thermogenesis by activating UCP1. During cold exposure, sympathetic nerves innervating brown adipose tissue release norepinephrine which stimulates β_3-adrenoceptors present on adipocytes. This leads to the activation of adenylyl cyclase (AC) and promotes to conversion of ATP to cyclic AMP (cAMP). cAMP activates protein kinase A (PKA) which phosphorylates lipolytic proteins adipose triglyceride lipase (ATGL) and hormone-sensitive lipase (HSL). Phosphorylation of these proteins fosters the conversion of triglycerides (TG) to fatty acids (FA). FA are released from lipid droplets and enter mitochondria where the activate uncoupling protein 1 (UCP1). Increased UCP1 activity generates heat. Additionally, succinate uptake during cold exposure heightens UCP1 activity, largely through the production of reactive oxygen species (ROS).

1.5)[41] and can upregulate UCP1 expression upon cold exposure, although basally their expression is similar to that of WAT[41].

Additionally, the sequestration of succinate by brown and beige adipocytes protects against chronic inflammation associated with various metabolic disorders. For example, UCP1 knockout mice experienced increased liver inflammation following western diet and concomitantly had an increase in succinate in the local, extracellular environment of the liver, compared to wild-type mice[1]. The increased inflammation experienced by UCP1 knockout mice can be attributed to an increase in succinate signaling resulting from the elevation of liver extracellular succinate, where mice lacking both UCP1 and SUCNR1 experienced less liver inflammation than their UCP1 counterparts[1]. While it is established that brown and beige adipocytes can readily uptake circulating succinate and protect from succinate-induced inflammation, the mechanism of succinate transport into these cells and the transporter(s) responsible remain unknown. How BAT transports succinate, the proteins involved in this process, and the environmental conditions that foster uptake will be explored in chapter three of this dissertation.

Succinate accumulation in exercising skeletal muscle

While BAT serves as a sink for circulating succinate, the source of extracellular succinate remains largely unknown. However, many findings suggest that muscle is a major secreter of succinate. In fact, during cold exposure, shivering muscles in the neck release a large amount of succinate and significantly contribute to the extracellular pool[26]. Additionally, elevated plasma succinate is a signature of exercise[4,27-29]. This increase is most likely due to increased skeletal muscle activity, the most energetically active organ during exercise. Metabolically, exercising muscle is primed to accumulate succinate, mainly because of its low oxygen tension. During exercise, ATP consumption dramatically increases in skeletal muscle to support increased contraction. ATP turnover in working skeletal muscle during exhaustive exercise can increase more than 100-fold compared to resting muscle[42]. To meet this newfound demand, fuel utilization

increases. The type of fuel consumed by working muscle is largely dependent on the intensity of exercise. During lower intensity exercise, circulating free fatty acids liberated from adipose tissue and glucose produced by the liver or obtained orally are predominantly used[43]. As exercise intensity increases, muscles rely mainly on glycogen stores to meet their metabolic demands[43]. This increase in skeletal muscle metabolism is highlighted by an increase in glycolysis, mitochondrial respiration, and an accumulation of certain TCA cycle intermediates, one of them being succinate[28].

In addition to increased fuel utilization, more oxygen is consumed by exercising muscle due to increased mitochondrial respiration. Even during submaximal exercise, oxygen consumption increases rapidly with myoglobin, a specialized oxygen-binding molecule found in skeletal muscle, desaturation rising to about 50%[44]. To support this increased oxygen consumption, during exercise arteries vasodilate to deliver more blood to skeletal muscle while blood flow to peripheral organs decreases. This allows for greater oxygen deliver to skeletal muscle and supports increased ETC activity. However, there is a maximum amount of oxygen that skeletal muscle can use during exercise. This is known as VO_2 max. VO_2 max is largely dependent on genetics, age, and altitude. It can be improved with training and is positively correlated with cardiovascular fitness and longevity[45,46]. VO_2 max is largely limited by the amount of blood the heart can pump to the rest of the body, otherwise known as cardiac output[47]. In a study performed on healthy subjects who were subjected to three weeks of bed rest followed by eight weeks of exhaustive endurance training, researchers found a ~25% decrease in cardiac output following bed rest and a subsequent return to baseline levels following the training period. Very little change in maximum oxygen uptake, arteriovenous oxygen difference, and heart rate was observed[48]. Since blood flow cannot meet the oxygen demands of exercising muscle, oxygen tension drops almost 7-fold from 34 mmHg to 3 – 5 mmHg, rendering the tissue mildly hypoxic[49-51]. In fact, this drop in oxygen is enough to stabilize hypoxia inducible factor-1 alpha (HIF-1α), a

transcriptional regulator activated during hypoxia that is responsible for the transcription of genes involved in angiogenesis and erythropoiesis[52,53]. This hypoxic environment fosters succinate accumulation. Work done in aquatic, diving mammals reports an increase in succinate in working muscles under low oxygen conditions[54]. The concentration of succinate is likely attributed to the redox state of the ubiquinone pool. Succinate oxidation to fumarate is coupled to the reduction of ubiquinone to ubiquinol. Under low oxygen conditions, ubiquinone cannot be replenished resulting in an accumulation of succinate[17]. While much evidence indicates that skeletal muscle accumulates succinate, it is still unknown if skeletal muscle secretes succinate and if so, what the transport mechanism may be. Moreover, the role of succinate signaling in muscle adaptation to exercise is unexplored and localization of the receptor, SUCNR1, uncharacterized. The mechanism of succinate secretion from exercising muscle and the role of succinate signaling in muscle remodeling following exercise will be covered in chapter two of this dissertation.

Skeletal muscle adaptations to exercise

The benefits of exercise are far-reaching. Exercise lessens the likelihood of numerous diseases including hypertension[55], type II diabetes[56], obesity[57], coronary heart disease[58], depression[59], and breast cancer[60]. Some of the most notable effects of exercise can be seen in skeletal muscle. Exercise improves muscle health and function which ultimately improves overall health. Muscle mass and strength are good predictors of longevity and health[61-63]. While exercise is ultimately beneficial for skeletal muscle, it is a strenuous process that incurs damage. Skeletal muscle must undergo extensive remodeling to meet the energetic and mechanical demands of exercise. These adaptations ultimately improve skeletal muscle health and function. Some of these changes include but are not limited to angiogenesis, increased motor neuron innervation, muscle hypertrophy, increased insulin sensitivity, and fiber type switching. These adaptations allow muscle to meet the newfound demands of exercise and become more resistant to fatigue.

The type of remodeling muscles undergo are largely dependent on the type of training and frequency.

Vascular Remodeling

With the onset of exercise comes an increase in muscle contraction and subsequently increased ATP consumption. To support this newfound ATP demand, skeletal muscles consume more fuels and become more energetically active. As a result of this increased metabolic flux, skeletal muscles utilize more oxygen to meet the increased energy demands. However, there is a limit to how much oxygen skeletal muscles can consume, otherwise known as VO_2 max. To overcome this limitation, skeletal muscles undergo angiogenesis and arteriogenesis, the formation of new capillaries and arteries. Prolonged endurance and resistance training results in structural changes to arteries, specifically increases in arterial diameter and decreases in arterial wall thickness, mainly in the femoral and brachial arteries[64-67]. These changes are triggered by shear stress and radial pressure that blood vessels experience due to increased blood flow during exercise[68-70]. Shear stress stimulates the production of nitric oxide by endothelial cells which initiates extracellular matrix (ECM) remodeling, leading to an enlargement of vessels[70]. This increase in arterial diameter allows for an increase in blood flow and thus oxygen delivery, allowing individuals to adapt to exercise.

At the other end of the vessel, exercise also stimulates an increase in capillaries. This is stimulated by both endurance and resistance exercise[71-74]. Angiogenesis can occur one of two ways, through intussusception or sprouting. Intussusception involves the splitting of a single capillary into two and is more commonly seen during development, while sprouting angiogenesis is commonly seen following exercise and involves the budding of existing capillaries to form new vessels[75]. At the center of exercise-induced angiogenesis is the pro-angiogenic factor vascular endothelial growth factor (VEGF). Induction of VEGF protein and mRNA occurs following both endurance and resistance exercise[76-78]. This increase in VEGF is thought to be partly mediated

by the master transcriptional co-activator PPARɣ coactivator-1α (PGC-1α) which binds to the nuclear receptor ERRα to promote the transcription of Vegf[79]. VEGF binding to its receptor, VEGFR-2, promotes the growth of new capillaries. The increase in capillaries allows for increased diffusion of oxygen into skeletal muscles, allowing the organ to better meet the demands of exercise. Moreover, capillarity has also been positively associated with critical power, or the maximum power output that can be sustained with time[80].

Fiber type switching

Muscle fibers are comprised of many contractile proteins that work in concert to generate muscle contractions. Two proteins that play a large role in this process are actin and myosin (figure 1.7). Together these proteins generate muscle contraction when they slide past one another resulting in a shortening of the sarcomere[81]. The force generated by muscle fibers and how resistant they

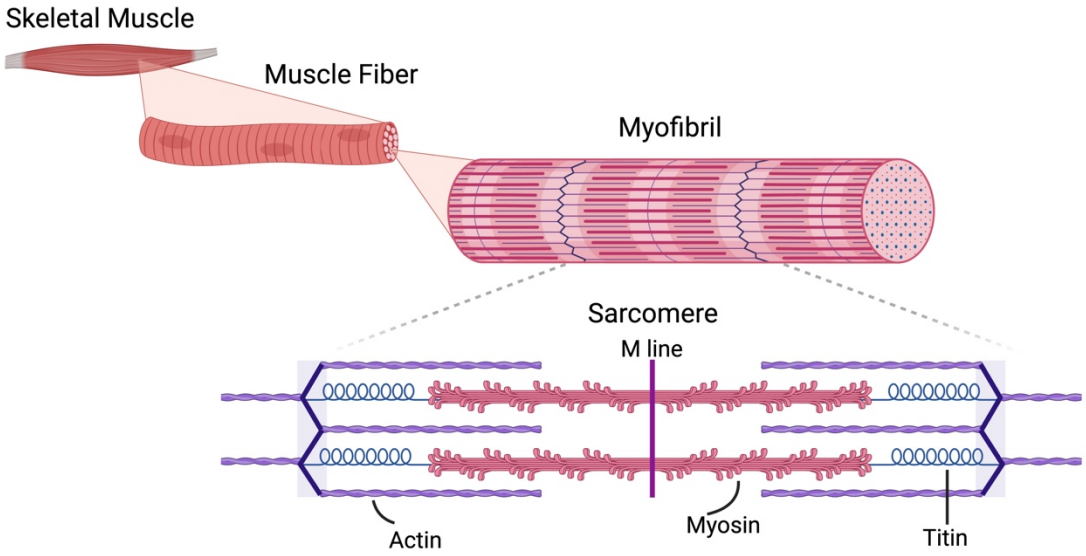


Figure 1.7 | Organization of muscle fiber. Skeletal muscle is comprised of multiple muscle fibers that consist of bundles of myofibrils. Each myofibril contains numerous sarcomeres which are the smallest contractile unit of skeletal muscle. This image was created with BioRender.

are to fatigue are variable and are dependent on the isoforms of actin, myosin, and other contractile proteins, such as tropomyosin, and troponin, expressed in the muscle[82]. Muscle fibers can be broadly divided into two categories: type I and type II. Type I fibers, also known as slow twitch fibers, are highly oxidative, slower contracting, and less powerful[83]. The slower contractions of these fibers allow them to be more resistant to fatigue. Slow twitch fibers are primarily involved in endurance and other exercises where the mechanical load is low, but the duration of exercise is long[84-86]. These fibers are rich in mitochondria and myoglobin, allowing them to be more oxidative. Conversely, type II fibers, also known as fast twitch fibers, are quick contracting and more powerful. There are two classes of fast twitch fibers in humans: IIa and IId/x. Type IIa fibers are highly oxidative while type IId/x fibers are glycolytic[83]. In mice there exists an additional fiber type, type IIb, which are even faster contracting and more glycolytic than type IId/x fibers[87]. Fast twitch muscle fibers mainly participate in explosive, powerful muscle contractions, like those associated with resistance exercise, and are more prone to fatigue compared to slow twitch fibers. Muscle fibers are often classified by the myosin heavy chain (MyHC) isoforms that they express. Skeletal muscles commonly exist in a mixed state with both type I and type II fibers present. However, certain muscles, like the soleus, while mixed, predominantly express a singular fiber type[88]. While debated, many studies support the notion that fibers can switch between types, with exercise being the preeminent initiator of this process. Endurance exercise promotes the expression of slow-twitch fiber genes and the conversion of glycolytic fibers to oxidative[89-93]. These adaptations prime the muscle for future bouts of prolonged, low-mechanical load exercise. This is best highlighted by the higher proportion of type I fibers present in endurance athletes compared to the average individual[84-86].

Motor Neuron Adaptations

Increased strength is one of the most noticeable adaptations to exercise. It allows the muscle to become more resistant to fatigue and produce more power. This adaptation is driven by resistance exercise[94-98]. In fact, elderly individuals that performed just one resistance exercise workout per week for 24 weeks gained approximately a 40% in-

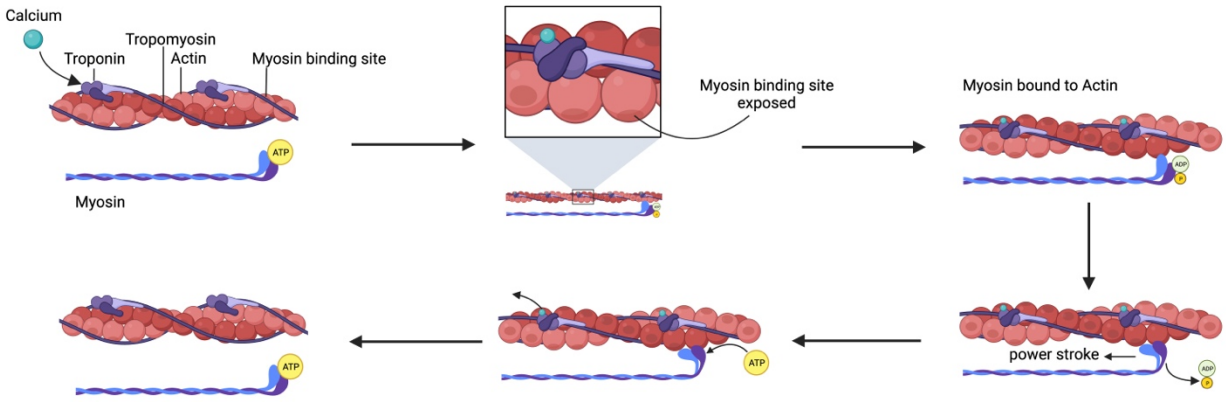


Figure 1.8 | Skeletal muscle contraction. Binding of calcium to troponin causes shifting of tropomyosin, resulting in the exposure of myosin binding sites on actin. The head of myosin hydrolyzes bound ATP to ADP and inorganic phosphate (P_i). The hydrolysis allows myosin to bind actin with ADP and P_i still attached. ADP and P_i detach from myosin causing the myosin head to move to a cocked position and the bound actin to move along with it. This is known as the power stroke. Contraction ends with ATP binds myosin, causing the protein to detach from actin and move to a relaxed state.

ease in strength[98]. While there are numerous factors that contribute to increased strength, neurological adaptations are perhaps the most notable. Motor neurons play an integral role in muscle contraction. Contraction is initiated when motor neurons release the neurotransmitter acetylcholine (ACh) into the neuromuscular junction[81]. The binding of ACh to nicotinic receptors present on the surface of skeletal muscle ultimately causes myosin and actin filaments to slide past each other resulting in the shortening of the sarcomere, the contractile unit of skeletal muscle (figure 1.8)[99]. Contraction ends when acetylcholinesterases degrade ACh and sarcoplasmic

reticulum Ca^{+2}-ATPase (SERCA) transports calcium ions from the cytosol to sarcoplasmic reticulum[99,100]. Typically, one motor neuron innervates many muscle fibers and together they are referred to as a motor unit. A key factor that determines the strength of muscle contraction is how many motor units are recruited to participate in the contraction[101]. That is, how many motor neurons fire and signal to muscle fibers. In fact, during the early months of training there is an increase in neuronal activity as measured by electromyography (EMG), suggesting an increase in the number of fibers recruited for contraction[102-106]. This increase in central nervous system activity plays a major role in strength. In fact, imagined muscle contractions resulted in approximately a 20% increase in plantar flexor torque and elbow flexor strength following a 7 – 8-week training period[107,108]. Additionally, exercise is a potent regulator of neuronal growth and promotes re-innervation of skeletal muscles that have undergone peripheral nerve lesions[109,110]. While the effects of exercise on the central nervous system are well established, the mechanism underlying these changes and the signaling molecules involved in mediating these adaptations remain poorly understood. This will be explored in chapter two of this dissertation.

Muscle Hypertrophy

In addition to neuronal adaptations, skeletal muscle hypertrophy, the increase in muscle mass, significantly contributes to increased strength following resistance training. However, hypertrophy is typically only observed after several months of training while neuronal adaptations are seen during the initial period of training[105]. Hypertrophy is distinct from hyperplasia, the formation of new muscle fibers, and is marked by an increase in fiber cross-sectional area (CSA), resulting from an increase in myofibrils or an enlargement of the sarcoplasm[111]. Immediately following a single bout of exercise, mRNA transcript levels of numerous genes rise and return to baseline several hours following cessation of exercise[43]. As exercise training continues, these short-lived increases in mRNA transcript levels result in a more stable elevation and ultimately leads to an increase in protein synthesis[43]. Numerous growth factors and cytokines can initiate

the hypertrophic process. Some of the most notable of these external signals include insulin growth factor-1 (IGF-1) and the pro-inflammatory cytokine interleukin-6 (IL-6). IGF-1 serum levels rise following acute and prolonging endurance and resistance exercise[112-114]. The increase in IGF-1 following exercise is partly mediated by an alternative isoform of PCG-1α, PGC-1α4. PGC-1α4 plays a significant role in the hypertrophic process and regulates the transcription of Igf-1[115]. Mice that overexpressed PGC-1a4 showed ~60% increase in fiber CSA[115]. Binding of IGF-1 to its receptor, IGF-1 receptor, ultimately results in the activation of the master anabolic regulator, mammalian target of rapamycin (mTOR), which is required for skeletal muscle hypertrophy. When this protein is inhibited, hypertrophy is blocked.[116]

In addition to myogenic signaling pathways, satellite cells, a muscle specific stem cell, are thought to play a key role in muscle hypertrophy. Satellite cells are governed by external signaling molecules, namely cytokines, and possess the ability to differentiate and form new myotubes. The exercise-responsive cytokine, IL-6 is a prominent regulator of satellite cell proliferation while the anti-inflammatory cytokine IL-10 promotes their differentiation, which may be mediated by macrophages[117-119]. In fact, genetic depletion of IL-6 in mice resulted in a reduction in fiber CSA and a decrease in satellite cell proliferation[119]. The new myotubes formed by activated satellite cells can fuse to existing myofibers, contributing to an increase in myofiber volume and myonuclei number, a process known as myonuclear accretion[120]. Myonuclear accretion is stimulated by exercise and often contributes to hypertrophy[121-123]. The exact mechanism underlying this process is poorly understood but is thought to be attributed to an increase in the amount of mRNA transcribed[124]. An increase in myonuclei is commonly seen following both prolonged resistance and endurance training, however, endurance training fails to elicit a hypertrophic response despite the increase in myonuclear number[123]. While myonuclear accretion is not typically seen following a single acute bout of exercise, this process can occur as quickly as two weeks following training. In fact, two weeks of high intensity interval training (HIIT) resulted in an increase in myonuclei

present on muscle fibers[122]. Overall, muscle hypertrophy allows individuals to meet subsequent bouts of resistance exercise and handle increased mechanical load.

Adaptations in glucose metabolism following exercise

Exercise is a bioenergetic process that relies on the generation of ATP through the oxidation of fatty acids and carbohydrates. Hydrolysis of ATP fuels muscle contraction and is required for proper muscle function. During intense exercise, the rate of ATP demand can rise more than 100-fold[42]. Muscle fatigue occurs when skeletal muscles cannot re-synthesize ATP quick enough to meet the demand[125]. ATP depletion during exercise is most pronounced in glycolytic, fast-twitch type IId/x fibers that express fast-twitch myosin isoforms with the greatest ATPase activity[87,126,127]. However, continued exercise training induces adaptations that allow skeletal muscles to circumvent this limitation. One notable adaptation seen with prolonged exercise is increased glucose uptake[128-131]. Exercise induced glucose uptake is largely executed by increased glucose transporter type 4 (GLUT4) translocation to the plasma membrane[132,133]. In addition to GLUT4 translocation, exercise increases the sensitivity of skeletal muscles to insulin[134-138]. The effects of exercise on glucose uptake and insulin sensitivity are quite profound. A single bout of running can improve glucose uptake up to 48 hours following exercise[139]. Moreover, this adaptation ameliorates metabolic disorders like type II diabetes. In fact, diet combined with exercise is the best known intervention for type II diabetes[140]. However, there is a subpopulation that does not show improved glucose uptake following exercise. The mechanism for this lack of response is poorly understood[141,142].

Role of accessory cells in muscle remodeling

While muscle fibers contribute to most of the biomass of skeletal muscle, numerous non-myofibrillar cells reside within the muscle. Some of these cell types include macrophages, regulatory T-cells (Tregs), stromal cells, endothelial cells, and satellite cells. These cells play a major role in muscle repair following damage caused by acute trauma as well as exercise-induced

muscle injury, which is often seen following intense or unaccustomed exercise[143-146]. Immune cells play a particularly important role in the regenerative process following muscle damage. At the onset of injury, tissue-resident macrophages recruit circulating neutrophils to the site of damage through the secretion of cytokine-induced neutrophil chemoattractant (CXCL1) and monocyte chemoattractant protein 1 (MCP-1)[147,148]. Neutrophil infiltration is necessary for proper muscle regeneration to occur. When neutrophils are depleted from the circulation, muscle repair is hindered[149]. Once in the muscle, neutrophils further the inflammatory environment by recruiting pro-inflammatory macrophages and monocytes[150]. The inflammatory environment of damaged skeletal muscles conditions recruited macrophages and monocytes to a pro-inflammatory signature. These pro-inflammatory macrophages and monocytes release more pro-inflammatory cytokines like tumor necrosis factor-alpha (TNF-α), IL-1β, and interferon-gamma (IFN-γ). These release of IL-1β stimulates the production of anti-inflammatory cytokines IL-10 and transforming growth factor-beta (TGF-β). This new anti-inflammatory environment causes macrophages adopt an anti-inflammatory phenotype and secrete more IL-10 and TGF-β, thus resolving the initial inflammatory response [151]. The initial inflammation seen following injury is not purely incidental, it is in fact required for proper muscle growth. When inflammation is blocked by non-steroidal anti-inflammatory drugs (NSAIDS), subjects experienced reduced muscle hypertrophy and strength following 8-weeks of resistance training[152]. The influence of inflammation on muscle regeneration is thought to be mediated by satellite cells. Pro-inflammatory cytokines foster the proliferation of these stem cells while anti-inflammatory cytokines promote their differentiation into new myofibrils. For example, the pro-inflammatory cytokine IL-6 promotes satellite cell proliferation while the anti-inflammatory cytokine interleukin-4 (IL-4) supports satellite cell fusion[119,153]. Tight control of the inflammatory response is required for proper muscle regeneration to occur. When IL-10 is prematurely expressed in fibers, muscle regeneration is impaired highlighted by a reduction in fiber CSA[154]. In addition to macrophages, Tregs are also instrumental in the

regenerative process. These immune cells are key regulators of both the inflammatory response and the satellite cell niche[155].

Another cell type central to muscle regeneration is the stromal cell. These cells are bipotential stem cells that possess the ability to differentiate into either fibroblasts or adipocytes[156-158]. Stromal cells participate in the regenerative process by clearing debris following injury which is a prerequisite for muscle growth[159]. These stem cells also foster the differentiation of satellite cells by promoting an anti-inflammatory phenotype in macrophages[160]. Additionally, stromal cells play a prominent role in extracellular matrix (ECM) remodeling. These cells can regulate the expression of specialized ECM degrading enzymes, metalloproteinases, thus preventing fibrosis and promoting satellite cell migration and differentiation[161]. While it is evident that non-parenchymal cells are crucial for muscle repair, their role in non-damaging exercise and adaptation to exercise is poorly defined. Moreover, how exercising muscle signals to these cell populations is not understood. These questions will be addressed in chapter two of this dissertation.

Conclusion

The coupling of succinate oxidation to the reduction of ubiquinone allows succinate to serve as a gauge for the redox status of the limitedly mobile ubiquinone pool, making succinate a prime bioenergetic signal that relays the nutrient and oxygen status of the cell. Understanding the role of succinate and succinate signaling during physiological events such as exercise can offer greater insight into how cells and tissues communicate with their environment to adapt to environmental stressors. In this dissertation, I uncover the role of succinate and succinate signaling in muscle adaptation to exercise and elucidate the mechanism of succinate transport in skeletal muscle and brown and beige fat. Overall, the findings from this work highlight the importance of metabolites as signaling molecules and offer a better understanding of how skeletal muscle adapts to bioenergetic stress.

References

1. Mills, E.L.*, et al.* UCP1 governs liver extracellular succinate and inflammatory pathogenesis. *Nat Metab* **3**, 604-617 (2021).
2. Reddy, A.*, et al.* pH-Gated Succinate Secretion Regulates Muscle Remodeling in Response to Exercise. *Cell* **183**, 62-75 e17 (2020).
3. Sadagopan, N.*, et al.* Circulating succinate is elevated in rodent models of hypertension and metabolic disease. *Am J Hypertens* **20**, 1209-1215 (2007).
4. Hochachka, P.W. & Dressendorfer, R.H. Succinate accumulation in man during exercise. *Eur J Appl Physiol Occup Physiol* **35**, 235-242 (1976).
5. Osuna-Prieto, F.J.*, et al.* Elevated plasma succinate levels are linked to higher cardiovascular disease risk factors in young adults. *Cardiovasc Diabetol* **20**, 151 (2021).
6. Serena, C.*, et al.* Elevated circulating levels of succinate in human obesity are linked to specific gut microbiota. *ISME J* **12**, 1642-1657 (2018).
7. Van Hove, J.L.*, et al.* Succinyl-CoA ligase deficiency: a mitochondrial hepatoencephalomyopathy. *Pediatr Res* **68**, 159-164 (2010).
8. Bezawork-Geleta, A., Rohlena, J., Dong, L., Pacak, K. & Neuzil, J. Mitochondrial Complex II: At the Crossroads. *Trends Biochem Sci* **42**, 312-325 (2017).
9. Rutter, J., Winge, D.R. & Schiffman, J.D. Succinate dehydrogenase - Assembly, regulation and role in human disease. *Mitochondrion* **10**, 393-401 (2010).
10. Cecchini, G. Function and structure of complex II of the respiratory chain. *Annu Rev Biochem* **72**, 77-109 (2003).
11. Wang, Y. & Hekimi, S. Understanding Ubiquinone. *Trends Cell Biol* **26**, 367-378 (2016).
12. Crofts, A.R. Proton-coupled electron transfer at the Qo-site of the bc1 complex controls the rate of ubihydroquinone oxidation. *Biochim Biophys Acta* **1655**, 77-92 (2004).
13. Brandt, U. Bifurcated ubihydroquinone oxidation in the cytochrome bc1 complex by proton-gated charge transfer. *FEBS Lett* **387**, 1-6 (1996).
14. Brandt, U. & Trumpower, B. The protonmotive Q cycle in mitochondria and bacteria. *Crit Rev Biochem Mol Biol* **29**, 165-197 (1994).
15. Murphy, M.P. & Chouchani, E.T. Why succinate? Physiological regulation by a mitochondrial coenzyme Q sentinel. *Nat Chem Biol* **18**, 461-469 (2022).
16. Arias-Mayenco, I.*, et al.* Acute O(2) Sensing: Role of Coenzyme QH(2)/Q Ratio and Mitochondrial ROS Compartmentalization. *Cell Metab* **28**, 145-158 e144 (2018).
17. Chouchani, E.T.*, et al.* Ischaemic accumulation of succinate controls reperfusion injury through mitochondrial ROS. *Nature* **515**, 431-435 (2014).
18. Tannahill, G.M.*, et al.* Succinate is an inflammatory signal that induces IL-1beta through HIF-1alpha. *Nature* **496**, 238-242 (2013).
19. Guo, Y., Cho, S.W., Saxena, D. & Li, X. Multifaceted Actions of Succinate as a Signaling Transmitter Vary with Its Cellular Locations. *Endocrinol Metab (Seoul)* **35**, 36-43 (2020).
20. Prag, H.A.*, et al.* Mechanism of succinate efflux upon reperfusion of the ischaemic heart. *Cardiovasc Res* **117**, 1188-1201 (2021).
21. van Diepen, J.A.*, et al.* SUCNR1-mediated chemotaxis of macrophages aggravates obesity-induced inflammation and diabetes. *Diabetologia* **60**, 1304-1313 (2017).
22. Ceperuelo-Mallafre, V.*, et al.* Preoperative Circulating Succinate Levels as a Biomarker for Diabetes Remission After Bariatric Surgery. *Diabetes Care* **42**, 1956-1965 (2019).
23. Kohlhauer, M.*, et al.* Metabolomic Profiling in Acute ST-Segment-Elevation Myocardial Infarction Identifies Succinate as an Early Marker of Human Ischemia-Reperfusion Injury. *J Am Heart Assoc* **7**(2018).
24. Mills, E.L.*, et al.* Succinate Dehydrogenase Supports Metabolic Repurposing of Mitochondria to Drive Inflammatory Macrophages. *Cell* **167**, 457-470 e413 (2016).

25. Bisbach, C.M.*, et al.* Succinate Can Shuttle Reducing Power from the Hypoxic Retina to the O(2)-Rich Pigment Epithelium. *Cell Rep* **31**, 107606 (2020).
26. Mills, E.L.*, et al.* Accumulation of succinate controls activation of adipose tissue thermogenesis. *Nature* **560**, 102-106 (2018).
27. Lewis, G.D.*, et al.* Metabolic signatures of exercise in human plasma. *Sci Transl Med* **2**, 33ra37 (2010).
28. Gibala, M.J., MacLean, D.A., Graham, T.E. & Saltin, B. Tricarboxylic acid cycle intermediate pool size and estimated cycle flux in human muscle during exercise. *Am J Physiol* **275**, E235-242 (1998).
29. Gibala, M.J., MacLean, D.A., Graham, T.E. & Saltin, B. Anaplerotic processes in human skeletal muscle during brief dynamic exercise. *J Physiol* **502 (Pt 3)**, 703-713 (1997).
30. Regard, J.B., Sato, I.T. & Coughlin, S.R. Anatomical profiling of G protein-coupled receptor expression. *Cell* **135**, 561-571 (2008).
31. He, W.*, et al.* Citric acid cycle intermediates as ligands for orphan G-protein-coupled receptors. *Nature* **429**, 188-193 (2004).
32. Ariza, A.C., Deen, P.M. & Robben, J.H. The succinate receptor as a novel therapeutic target for oxidative and metabolic stress-related conditions. *Front Endocrinol (Lausanne)* **3**, 22 (2012).
33. Kushnir, M.M., Komaromy-Hiller, G., Shushan, B., Urry, F.M. & Roberts, W.L. Analysis of dicarboxylic acids by tandem mass spectrometry. High-throughput quantitative measurement of methylmalonic acid in serum, plasma, and urine. *Clin Chem* **47**, 1993-2002 (2001).
34. Rubic, T.*, et al.* Triggering the succinate receptor GPR91 on dendritic cells enhances immunity. *Nat Immunol* **9**, 1261-1269 (2008).
35. McCreath, K.J.*, et al.* Targeted disruption of the SUCNR1 metabolic receptor leads to dichotomous effects on obesity. *Diabetes* **64**, 1154-1167 (2015).
36. Littlewood-Evans, A.*, et al.* GPR91 senses extracellular succinate released from inflammatory macrophages and exacerbates rheumatoid arthritis. *J Exp Med* **213**, 1655-1662 (2016).
37. Keiran, N.*, et al.* SUCNR1 controls an anti-inflammatory program in macrophages to regulate the metabolic response to obesity. *Nat Immunol* **20**, 581-592 (2019).
38. Krzak, G., Willis, C.M., Smith, J.A., Pluchino, S. & Peruzzotti-Jametti, L. Succinate Receptor 1: An Emerging Regulator of Myeloid Cell Function in Inflammation. *Trends Immunol* **42**, 45-58 (2021).
39. Townsend, K. & Tseng, Y.H. Brown adipose tissue: Recent insights into development, metabolic function and therapeutic potential. *Adipocyte* **1**, 13-24 (2012).
40. Chouchani, E.T.*, et al.* Mitochondrial ROS regulate thermogenic energy expenditure and sulfenylation of UCP1. *Nature* **532**, 112-116 (2016).
41. Wu, J.*, et al.* Beige adipocytes are a distinct type of thermogenic fat cell in mouse and human. *Cell* **150**, 366-376 (2012).
42. Gaitanos, G.C., Williams, C., Boobis, L.H. & Brooks, S. Human muscle metabolism during intermittent maximal exercise. *J Appl Physiol (1985)* **75**, 712-719 (1993).
43. Egan, B. & Zierath, J.R. Exercise metabolism and the molecular regulation of skeletal muscle adaptation. *Cell Metab* **17**, 162-184 (2013).
44. Richardson, R.S., Noyszewski, E.A., Kendrick, K.F., Leigh, J.S. & Wagner, P.D. Myoglobin O2 desaturation during exercise. Evidence of limited O2 transport. *J Clin Invest* **96**, 1916-1926 (1995).

45. Mandsager, K.*, et al.* Association of Cardiorespiratory Fitness With Long-term Mortality Among Adults Undergoing Exercise Treadmill Testing. *JAMA Netw Open* **1**, e183605 (2018).
46. Helgerud, J.*, et al.* Aerobic high-intensity intervals improve VO2max more than moderate training. *Med Sci Sports Exerc* **39**, 665-671 (2007).
47. Bassett, D.R., Jr. & Howley, E.T. Limiting factors for maximum oxygen uptake and determinants of endurance performance. *Med Sci Sports Exerc* **32**, 70-84 (2000).
48. Saltin, B.*, et al.* Response to exercise after bed rest and after training. *Circulation* **38**, VII1-78 (1968).
49. Mole, P.A.*, et al.* Myoglobin desaturation with exercise intensity in human gastrocnemius muscle. *Am J Physiol* **277**, R173-180 (1999).
50. Richardson, R.S.*, et al.* Human skeletal muscle intracellular oxygenation: the impact of ambient oxygen availability. *J Physiol* **571**, 415-424 (2006).
51. Richardson, R.S., Newcomer, S.C. & Noyszewski, E.A. Skeletal muscle intracellular PO(2) assessed by myoglobin desaturation: response to graded exercise. *J Appl Physiol (1985)* **91**, 2679-2685 (2001).
52. Ameln, H.*, et al.* Physiological activation of hypoxia inducible factor-1 in human skeletal muscle. *FASEB J* **19**, 1009-1011 (2005).
53. Lee, J.W., Bae, S.H., Jeong, J.W., Kim, S.H. & Kim, K.W. Hypoxia-inducible factor (HIF-1)alpha: its protein stability and biological functions. *Exp Mol Med* **36**, 1-12 (2004).
54. Hochachka, P.W., Owen, T.G., Allen, J.F. & Whittow, G.C. Multiple end products of anaerobiosis in diving vertebrates. *Comp Biochem Physiol B* **50**, 17-22 (1975).
55. Pescatello, L.S., MacDonald, H.V., Lamberti, L. & Johnson, B.T. Exercise for Hypertension: A Prescription Update Integrating Existing Recommendations with Emerging Research. *Curr Hypertens Rep* **17**, 87 (2015).
56. Colberg, S.R.*, et al.* Exercise and type 2 diabetes: the American College of Sports Medicine and the American Diabetes Association: joint position statement. *Diabetes Care* **33**, e147-167 (2010).
57. Heath, G.W.*, et al.* Evidence-based intervention in physical activity: lessons from around the world. *Lancet* **380**, 272-281 (2012).
58. Fernandez-Rubio, H.*, et al.* Exercise Training and Interventions for Coronary Artery Disease. *J Cardiovasc Dev Dis* **9**(2022).
59. De Moor, M.H., Beem, A.L., Stubbe, J.H., Boomsma, D.I. & De Geus, E.J. Regular exercise, anxiety, depression and personality: a population-based study. *Prev Med* **42**, 273-279 (2006).
60. Chen, X.*, et al.* Exercise after diagnosis of breast cancer in association with survival. *Cancer Prev Res (Phila)* **4**, 1409-1418 (2011).
61. Abramowitz, M.K.*, et al.* Muscle mass, BMI, and mortality among adults in the United States: A population-based cohort study. *PLoS One* **13**, e0194697 (2018).
62. Srikanthan, P. & Karlamangla, A.S. Muscle mass index as a predictor of longevity in older adults. *Am J Med* **127**, 547-553 (2014).
63. Metter, E.J., Talbot, L.A., Schrager, M. & Conwit, R. Skeletal muscle strength as a predictor of all-cause mortality in healthy men. *J Gerontol A Biol Sci Med Sci* **57**, B359-365 (2002).
64. Dinenno, F.A.*, et al.* Regular endurance exercise induces expansive arterial remodelling in the trained limbs of healthy men. *J Physiol* **534**, 287-295 (2001).
65. Stebbings, G.K., Morse, C.I., McMahon, G.E. & Onambele, G.L. Resting arterial diameter and blood flow changes with resistance training and detraining in healthy young individuals. *J Athl Train* **48**, 209-219 (2013).

66. Hafner, N.M., Womack, C.J., Luden, N.D. & Todd, M.K. Arterial adaptations to training among first time marathoners. *Cardiovasc Ultrasound* **14**, 19 (2016).
67. Naylor, L.H., O'Driscoll, G., Fitzsimons, M., Arnolda, L.F. & Green, D.J. Effects of training resumption on conduit arterial diameter in elite rowers. *Med Sci Sports Exerc* **38**, 86-92 (2006).
68. Galie, P.A.*, et al.* Fluid shear stress threshold regulates angiogenic sprouting. *Proc Natl Acad Sci U S A* **111**, 7968-7973 (2014).
69. Hoefer, I.E., den Adel, B. & Daemen, M.J. Biomechanical factors as triggers of vascular growth. *Cardiovasc Res* **99**, 276-283 (2013).
70. Kolluru, G.K.*, et al.* Shear stress promotes nitric oxide production in endothelial cells by sub-cellular delocalization of eNOS: A basis for shear stress mediated angiogenesis. *Nitric Oxide* **22**, 304-315 (2010).
71. Brodal, P., Ingjer, F. & Hermansen, L. Capillary supply of skeletal muscle fibers in untrained and endurance-trained men. *Am J Physiol* **232**, H705-712 (1977).
72. Carrow, R.E., Brown, R.E. & Van Huss, W.D. Fiber sizes and capillary to fiber ratios in skeletal muscle of exercised rats. *Anat Rec* **159**, 33-39 (1967).
73. Ingjer, F. Effects of endurance training on muscle fibre ATP-ase activity, capillary supply and mitochondrial content in man. *J Physiol* **294**, 419-432 (1979).
74. Tesch, P.A., Thorsson, A. & Kaiser, P. Muscle capillary supply and fiber type characteristics in weight and power lifters. *J Appl Physiol Respir Environ Exerc Physiol* **56**, 35-38 (1984).
75. Prior, B.M., Yang, H.T. & Terjung, R.L. What makes vessels grow with exercise training? *J Appl Physiol (1985)* **97**, 1119-1128 (2004).
76. Gavin, T.P., Drew, J.L., Kubik, C.J., Pofahl, W.E. & Hickner, R.C. Acute resistance exercise increases skeletal muscle angiogenic growth factor expression. *Acta Physiol (Oxf)* **191**, 139-146 (2007).
77. Kivela, R.*, et al.* Exercise-induced expression of angiogenic growth factors in skeletal muscle and in capillaries of healthy and diabetic mice. *Cardiovasc Diabetol* **7**, 13 (2008).
78. Kraus, R.M., Stallings, H.W., 3rd, Yeager, R.C. & Gavin, T.P. Circulating plasma VEGF response to exercise in sedentary and endurance-trained men. *J Appl Physiol (1985)* **96**, 1445-1450 (2004).
79. Chinsomboon, J.*, et al.* The transcriptional coactivator PGC-1alpha mediates exercise-induced angiogenesis in skeletal muscle. *Proc Natl Acad Sci U S A* **106**, 21401-21406 (2009).
80. Mitchell, E.A., Martin, N.R.W., Bailey, S.J. & Ferguson, R.A. Critical power is positively related to skeletal muscle capillarity and type I muscle fibers in endurance-trained individuals. *J Appl Physiol (1985)* **125**, 737-745 (2018).
81. Kuo, I.Y. & Ehrlich, B.E. Signaling in muscle contraction. *Cold Spring Harb Perspect Biol* **7**, a006023 (2015).
82. Widrick, J.J., Trappe, S.W., Costill, D.L. & Fitts, R.H. Force-velocity and force-power properties of single muscle fibers from elite master runners and sedentary men. *Am J Physiol* **271**, C676-683 (1996).
83. Schiaffino, S. & Reggiani, C. Fiber types in mammalian skeletal muscles. *Physiol Rev* **91**, 1447-1531 (2011).
84. Costill, D.L.*, et al.* Skeletal muscle enzymes and fiber composition in male and female track athletes. *J Appl Physiol* **40**, 149-154 (1976).
85. Costill, D.L., Fink, W.J. & Pollock, M.L. Muscle fiber composition and enzyme activities of elite distance runners. *Med Sci Sports* **8**, 96-100 (1976).

86. Fink, W.J., Costill, D.L. & Pollock, M.L. Submaximal and maximal working capacity of elite distance runners. Part II. Muscle fiber composition and enzyme activities. *Ann N Y Acad Sci* **301**, 323-327 (1977).
87. Scott, W., Stevens, J. & Binder-Macleod, S.A. Human skeletal muscle fiber type classifications. *Phys Ther* **81**, 1810-1816 (2001).
88. Gollnick, P.D., Sjodin, B., Karlsson, J., Jansson, E. & Saltin, B. Human soleus muscle: a comparison of fiber composition and enzyme activities with other leg muscles. *Pflugers Arch* **348**, 247-255 (1974).
89. Akimoto, T., Ribar, T.J., Williams, R.S. & Yan, Z. Skeletal muscle adaptation in response to voluntary running in Ca2+/calmodulin-dependent protein kinase IV-deficient mice. *Am J Physiol Cell Physiol* **287**, C1311-1319 (2004).
90. Allen, D.L.*, et al.* Cardiac and skeletal muscle adaptations to voluntary wheel running in the mouse. *J Appl Physiol (1985)* **90**, 1900-1908 (2001).
91. Ehlers, M.L., Celona, B. & Black, B.L. NFATc1 controls skeletal muscle fiber type and is a negative regulator of MyoD activity. *Cell Rep* **8**, 1639-1648 (2014).
92. Gehlert, S.*, et al.* Cycling exercise-induced myofiber transitions in skeletal muscle depend on basal fiber type distribution. *Eur J Appl Physiol* **112**, 2393-2402 (2012).
93. Jarvis, J.C., Mokrusch, T., Kwende, M.M., Sutherland, H. & Salmons, S. Fast-to-slow transformation in stimulated rat muscle. *Muscle Nerve* **19**, 1469-1475 (1996).
94. Larsson, A.*, et al.* Resistance exercise improves muscle strength, health status and pain intensity in fibromyalgia--a randomized controlled trial. *Arthritis Res Ther* **17**, 161 (2015).
95. McBride, J.M., Blaak, J.B. & Triplett-McBride, T. Effect of resistance exercise volume and complexity on EMG, strength, and regional body composition. *Eur J Appl Physiol* **90**, 626-632 (2003).
96. Radaelli, R.*, et al.* Dose-response of 1, 3, and 5 sets of resistance exercise on strength, local muscular endurance, and hypertrophy. *J Strength Cond Res* **29**, 1349-1358 (2015).
97. Schoenfeld, B.J.*, et al.* Resistance Training Volume Enhances Muscle Hypertrophy but Not Strength in Trained Men. *Med Sci Sports Exerc* **51**, 94-103 (2019).
98. Taaffe, D.R., Duret, C., Wheeler, S. & Marcus, R. Once-weekly resistance exercise improves muscle strength and neuromuscular performance in older adults. *J Am Geriatr Soc* **47**, 1208-1214 (1999).
99. Pham, S. & Puckett, Y. Physiology, Skeletal Muscle Contraction. in *StatPearls* (Treasure Island (FL), 2023).
100. Trang, A. & Khandhar, P.B. Physiology, Acetylcholinesterase. in *StatPearls* (Treasure Island (FL), 2023).
101. Del Vecchio, A.*, et al.* The increase in muscle force after 4 weeks of strength training is mediated by adaptations in motor unit recruitment and rate coding. *J Physiol* **597**, 1873-1887 (2019).
102. Hakkinen, K.*, et al.* Neuromuscular adaptations during bilateral versus unilateral strength training in middle-aged and elderly men and women. *Acta Physiol Scand* **158**, 77-88 (1996).
103. Hakkinen, K. & Komi, P.V. Electromyographic changes during strength training and detraining. *Med Sci Sports Exerc* **15**, 455-460 (1983).
104. Hakkinen, K., Kraemer, W.J., Newton, R.U. & Alen, M. Changes in electromyographic activity, muscle fibre and force production characteristics during heavy resistance/power strength training in middle-aged and older men and women. *Acta Physiol Scand* **171**, 51-62 (2001).
105. Moritani, T. & deVries, H.A. Neural factors versus hypertrophy in the time course of muscle strength gain. *Am J Phys Med* **58**, 115-130 (1979).

106. Narici, M.V., Roi, G.S., Landoni, L., Minetti, A.E. & Cerretelli, P. Changes in force, cross-sectional area and neural activation during strength training and detraining of the human quadriceps. *Eur J Appl Physiol Occup Physiol* **59**, 310-319 (1989).
107. Herbert, R.D., Dean, C. & Gandevia, S.C. Effects of real and imagined training on voluntary muscle activation during maximal isometric contractions. *Acta Physiol Scand* **163**, 361-368 (1998).
108. Zijdewind, I., Toering, S.T., Bessem, B., Van Der Laan, O. & Diercks, R.L. Effects of imagery motor training on torque production of ankle plantar flexor muscles. *Muscle Nerve* **28**, 168-173 (2003).
109. Di Palma, M.*, et al.* The impact of different exercise protocols on rat soleus muscle reinnervation and recovery following peripheral nerve lesion and regeneration. *Front Physiol* **13**, 948985 (2022).
110. Udina, E., Puigdemasa, A. & Navarro, X. Passive and active exercise improve regeneration and muscle reinnervation after peripheral nerve injury in the rat. *Muscle Nerve* **43**, 500-509 (2011).
111. Roberts, M.D., Haun, C.T., Vann, C.G., Osburn, S.C. & Young, K.C. Sarcoplasmic Hypertrophy in Skeletal Muscle: A Scientific "Unicorn" or Resistance Training Adaptation? *Front Physiol* **11**, 816 (2020).
112. Arazi, H., Babaei, P., Moghimi, M. & Asadi, A. Acute effects of strength and endurance exercise on serum BDNF and IGF-1 levels in older men. *BMC Geriatr* **21**, 50 (2021).
113. Chicharro, J.L.*, et al.* Effects of an endurance cycling competition on resting serum insulin-like growth factor I (IGF-I) and its binding proteins IGFBP-1 and IGFBP-3. *Br J Sports Med* **35**, 303-307 (2001).
114. Tsai, C.L., Wang, C.H., Pan, C.Y. & Chen, F.C. The effects of long-term resistance exercise on the relationship between neurocognitive performance and GH, IGF-1, and homocysteine levels in the elderly. *Front Behav Neurosci* **9**, 23 (2015).
115. Ruas, J.L.*, et al.* A PGC-1alpha isoform induced by resistance training regulates skeletal muscle hypertrophy. *Cell* **151**, 1319-1331 (2012).
116. Bodine, S.C.*, et al.* Akt/mTOR pathway is a crucial regulator of skeletal muscle hypertrophy and can prevent muscle atrophy in vivo. *Nat Cell Biol* **3**, 1014-1019 (2001).
117. Deng, B., Wehling-Henricks, M., Villalta, S.A., Wang, Y. & Tidball, J.G. IL-10 triggers changes in macrophage phenotype that promote muscle growth and regeneration. *J Immunol* **189**, 3669-3680 (2012).
118. Steensberg, A.*, et al.* Production of interleukin-6 in contracting human skeletal muscles can account for the exercise-induced increase in plasma interleukin-6. *J Physiol* **529 Pt 1**, 237-242 (2000).
119. Serrano, A.L., Baeza-Raja, B., Perdiguero, E., Jardi, M. & Munoz-Canoves, P. Interleukin-6 is an essential regulator of satellite cell-mediated skeletal muscle hypertrophy. *Cell Metab* **7**, 33-44 (2008).
120. Pallafacchina, G., Blaauw, B. & Schiaffino, S. Role of satellite cells in muscle growth and maintenance of muscle mass. *Nutr Metab Cardiovasc Dis* **23 Suppl 1**, S12-18 (2013).
121. Abou Sawan, S.*, et al.* Satellite cell and myonuclear accretion is related to training-induced skeletal muscle fiber hypertrophy in young males and females. *J Appl Physiol (1985)* **131**, 871-880 (2021).
122. Goh, Q.*, et al.* Myonuclear accretion is a determinant of exercise-induced remodeling in skeletal muscle. *Elife* **8**(2019).
123. Masschelein, E.*, et al.* Exercise promotes satellite cell contribution to myofibers in a load-dependent manner. *Skelet Muscle* **10**, 21 (2020).

124. Bamman, M.M., Roberts, B.M. & Adams, G.R. Molecular Regulation of Exercise-Induced Muscle Fiber Hypertrophy. *Cold Spring Harb Perspect Med* **8**(2018).
125. Allen, D.G., Lamb, G.D. & Westerblad, H. Skeletal muscle fatigue: cellular mechanisms. *Physiol Rev* **88**, 287-332 (2008).
126. Karatzaferi, C., de Haan, A., Ferguson, R.A., van Mechelen, W. & Sargeant, A.J. Phosphocreatine and ATP content in human single muscle fibres before and after maximum dynamic exercise. *Pflugers Arch* **442**, 467-474 (2001).
127. Gorza, L. Identification of a novel type 2 fiber population in mammalian skeletal muscle by combined use of histochemical myosin ATPase and anti-myosin monoclonal antibodies. *J Histochem Cytochem* **38**, 257-265 (1990).
128. Berger, M., Hagg, S. & Ruderman, N.B. Glucose metabolism in perfused skeletal muscle. Interaction of insulin and exercise on glucose uptake. *Biochem J* **146**, 231-238 (1975).
129. Hargreaves, M., McConell, G. & Proietto, J. Influence of muscle glycogen on glycogenolysis and glucose uptake during exercise in humans. *J Appl Physiol (1985)* **78**, 288-292 (1995).
130. Richter, E.A., Ploug, T. & Galbo, H. Increased muscle glucose uptake after exercise. No need for insulin during exercise. *Diabetes* **34**, 1041-1048 (1985).
131. Wahren, J., Felig, P., Ahlborg, G. & Jorfeldt, L. Glucose metabolism during leg exercise in man. *J Clin Invest* **50**, 2715-2725 (1971).
132. Kennedy, J.W.*, et al.* Acute exercise induces GLUT4 translocation in skeletal muscle of normal human subjects and subjects with type 2 diabetes. *Diabetes* **48**, 1192-1197 (1999).
133. Sylow, L.*, et al.* Rac1 governs exercise-stimulated glucose uptake in skeletal muscle through regulation of GLUT4 translocation in mice. *J Physiol* **594**, 4997-5008 (2016).
134. Houmard, J.A.*, et al.* Effect of the volume and intensity of exercise training on insulin sensitivity. *J Appl Physiol (1985)* **96**, 101-106 (2004).
135. King, D.S.*, et al.* Effects of exercise and lack of exercise on insulin sensitivity and responsiveness. *J Appl Physiol (1985)* **64**, 1942-1946 (1988).
136. Koopman, R.*, et al.* A single session of resistance exercise enhances insulin sensitivity for at least 24 h in healthy men. *Eur J Appl Physiol* **94**, 180-187 (2005).
137. Mondon, C.E., Dolkas, C.B. & Reaven, G.M. Site of enhanced insulin sensitivity in exercise-trained rats at rest. *Am J Physiol* **239**, E169-177 (1980).
138. Newsom, S.A., Everett, A.C., Hinko, A. & Horowitz, J.F. A single session of low-intensity exercise is sufficient to enhance insulin sensitivity into the next day in obese adults. *Diabetes Care* **36**, 2516-2522 (2013).
139. Ortega, J.F., Fernandez-Elias, V.E., Hamouti, N., Pallares, J.G. & Mora-Rodriguez, R. Higher insulin-sensitizing response after sprint interval compared to continuous exercise. *Int J Sports Med* **36**, 209-214 (2015).
140. Knowler, W.C.*, et al.* Reduction in the incidence of type 2 diabetes with lifestyle intervention or metformin. *N Engl J Med* **346**, 393-403 (2002).
141. Stephens, N.A.*, et al.* A transcriptional signature of "exercise resistance" in skeletal muscle of individuals with type 2 diabetes mellitus. *Metabolism* **64**, 999-1004 (2015).
142. Stephens, N.A. & Sparks, L.M. Resistance to the beneficial effects of exercise in type 2 diabetes: are some individuals programmed to fail? *J Clin Endocrinol Metab* **100**, 43-52 (2015).
143. Nosaka, K. & Clarkson, P.M. Muscle damage following repeated bouts of high force eccentric exercise. *Med Sci Sports Exerc* **27**, 1263-1269 (1995).
144. Lavender, A.P. & Nosaka, K. Comparison between old and young men for changes in makers of muscle damage following voluntary eccentric exercise of the elbow flexors. *Appl Physiol Nutr Metab* **31**, 218-225 (2006).

145. Howatson, G. & Milak, A. Exercise-induced muscle damage following a bout of sport specific repeated sprints. *J Strength Cond Res* **23**, 2419-2424 (2009).
146. Bailey, D.M.*, et al.* Influence of cold-water immersion on indices of muscle damage following prolonged intermittent shuttle running. *J Sports Sci* **25**, 1163-1170 (2007).
147. Brigitte, M.*, et al.* Muscle resident macrophages control the immune cell reaction in a mouse model of notexin-induced myoinjury. *Arthritis Rheum* **62**, 268-279 (2010).
148. Nunes-Silva, A.*, et al.* Treadmill exercise induces neutrophil recruitment into muscle tissue in a reactive oxygen species-dependent manner. An intravital microscopy study. *PLoS One* **9**, e96464 (2014).
149. Graca, F.A.*, et al.* Platelet-derived chemokines promote skeletal muscle regeneration by guiding neutrophil recruitment to injured muscles. *Nat Commun* **14**, 2900 (2023).
150. Tidball, J.G. Regulation of muscle growth and regeneration by the immune system. *Nat Rev Immunol* **17**, 165-178 (2017).
151. Arnold, L.*, et al.* Inflammatory monocytes recruited after skeletal muscle injury switch into antiinflammatory macrophages to support myogenesis. *J Exp Med* **204**, 1057-1069 (2007).
152. Lilja, M.*, et al.* High doses of anti-inflammatory drugs compromise muscle strength and hypertrophic adaptations to resistance training in young adults. *Acta Physiol (Oxf)* **222**(2018).
153. Horsley, V., Jansen, K.M., Mills, S.T. & Pavlath, G.K. IL-4 acts as a myoblast recruitment factor during mammalian muscle growth. *Cell* **113**, 483-494 (2003).
154. Perdiguero, E.*, et al.* p38/MKP-1-regulated AKT coordinates macrophage transitions and resolution of inflammation during tissue repair. *J Cell Biol* **195**, 307-322 (2011).
155. Burzyn, D.*, et al.* A special population of regulatory T cells potentiates muscle repair. *Cell* **155**, 1282-1295 (2013).
156. Joe, A.W.*, et al.* Muscle injury activates resident fibro/adipogenic progenitors that facilitate myogenesis. *Nat Cell Biol* **12**, 153-163 (2010).
157. Uezumi, A., Fukada, S., Yamamoto, N., Takeda, S. & Tsuchida, K. Mesenchymal progenitors distinct from satellite cells contribute to ectopic fat cell formation in skeletal muscle. *Nat Cell Biol* **12**, 143-152 (2010).
158. Uezumi, A.*, et al.* Fibrosis and adipogenesis originate from a common mesenchymal progenitor in skeletal muscle. *J Cell Sci* **124**, 3654-3664 (2011).
159. Heredia, J.E.*, et al.* Type 2 innate signals stimulate fibro/adipogenic progenitors to facilitate muscle regeneration. *Cell* **153**, 376-388 (2013).
160. Qiu, X.*, et al.* Mesenchymal stem cells and extracellular matrix scaffold promote muscle regeneration by synergistically regulating macrophage polarization toward the M2 phenotype. *Stem Cell Res Ther* **9**, 88 (2018).
161. Sassoli, C.*, et al.* Defining the role of mesenchymal stromal cells on the regulation of matrix metalloproteinases in skeletal muscle cells. *Exp Cell Res* **323**, 297-313 (2014).

Chapter Two

Succinate signaling contributes to muscle adaptation following exercise

Citation. This chapter has been assembled with modification from the following manuscript:

pH-Gated Succinate Secretion Regulates Muscle Remodeling in Response to Exercise

Cell **183,** 62-75 e17 (2020).

Anita Reddy[1,2,9], Luiz H.M. Bozi[1,2,3,9], Omar K. Yaghi[4], Evanna L. Mills[1,2], Haopeng Xiao[1,2], Hilary E. Nicholson[5], Margherita Paschini[6], Joao A. Paulo[2], Ryan Garrity[1], Dina Laznik-Gogoslavaski[1], Julio C.B. Ferreira[3], Christian S. Carl[7], Kim A. Sjøberg[7], Jørgen F.P. Wojtaszewski[7], Jacob F. Jeppesen[8], Bente Kiens[7], Steven P. Gygi[2], Erik A. Richter[7], Diane Mathis[4], Edward T. Chouchani[1,2,10]

[1] Department of Cancer Biology, Dana-Farber Cancer Institute, Boston, MA, USA

[2] Department of Cell Biology, Harvard Medical School, Boston, MA, USA

[3] Institute of Biomedical Sciences, University of Sao Paulo, Sao Paulo, Brazil

[4] Department of Immunology, Harvard Medical School, Boston, MA 02115, USA

[5] Department of Medical Oncology, Dana-Farber Cancer Institute, Harvard Medical School, Boston, MA, USA

[6] Stem Cell Program, Division of Hematology/Oncology, Boston Children's Hospital, Boston, MA 02115, USA

[7] Section of Molecular Physiology, Department of Nutrition, Exercise and Sports, Faculty of Science, University of Copenhagen, Copenhagen, Denmark

[8] Global Drug Discovery, Novo Nordisk A/S, Copenhagen, Denmark

[9] These authors contributed equally

[10] Corresponding author

Contributions: A.R., L.H.M.B., E.L.M., H.X., H.E.N., J.A.P., R.G., D.L.-B., C.S.C., K.A.S., J.F.P.W., B.K., and E.A.R. performed the experiments. O.K.Y., M.P., J.C.B.F., J.F.J., J.W., B.K., S.P.G., E.A.R., D.M., and E.T.C. oversaw the experiments and data analyses. E.T.C. wrote the manuscript with assistance from all other authors.

Acknowledgements: We thank Mike Murphy, Fred Goldberg, and Bruce Spiegelman for helpful discussions; Bill Kaelin for assistance with cellular hypoxia experiments; the Nikon Imaging Facility at Harvard Medical School for assistance with light and fluorescence microscopy; and the Harvard Center for Biological Imaging for assistance with *in situ* hybridization microscopy. We thank the Neurobiology Department and the Neurobiology Imaging Facility for consultations and instrument availability, which supported this work. This facility is supported in part by the Neural Imaging Center as part of NINDS P30 Core Center grant NS072030. This work was supported by the American Heart Asso'iation and NIH DK123095 (to E.T.C.), the JPB Foundation and NIH AR070334 (to D.M.), NIH NIGMS T32GM007753 (to O.K.Y.), Sao Paulo Research Foundation 2019/07221-9 (to L.H.M.B.), and the National Cancer Center (to H.X.). The human studies were supported by Novo Nordisk A/S.

Abstract

Skeletal muscle remodeling, following exercise, requires the participation of numerous non-myofibrillar cells that reside within the muscle milieu. This process is coordinated by paracrine factors released by working skeletal muscle that communicate with these populations to initiate remodeling. We identify the tricarboxylic (TCA) cycle intermediate, succinate, as an exercise-responsive metabolite that is selectively secreted by skeletal muscle during exercise. Selective secretion of succinate is mediated by the transient protonation of the metabolite that occurs due to acute cytosolic acidification during exercise (**figure 2.1**). Protonation of succinate transforms the metabolite from a dicarboxylate to a monocarboxylate, making it amenable for secretion via monocarboxylate transporter 1 (MCT1). Once secreted, succinate engages its cognate receptor,

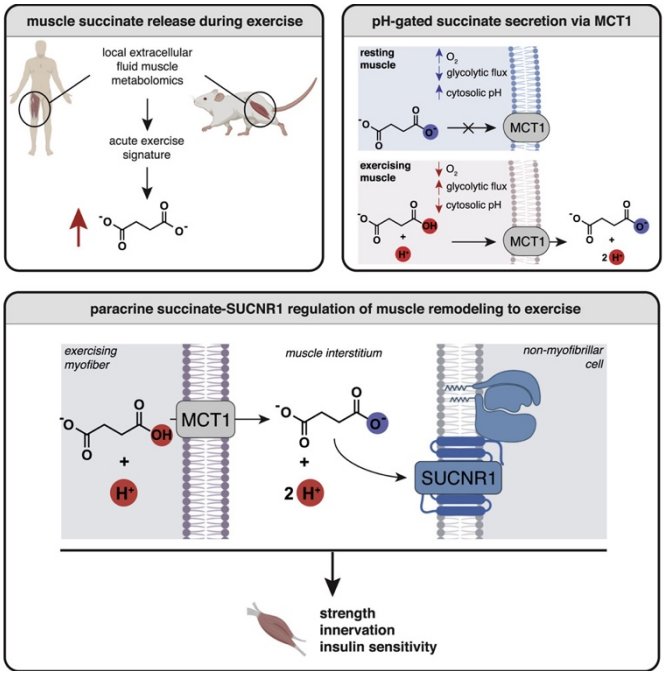


Figure 2.1 | Schematic depicting succinate release from skeletal muscle.

succinate receptor 1 (SUCNR1), which is localized exclusively to non-myofibrillar cells, and initiates transcription of muscle-remodeling pathways. Succinate signaling is required for exercise-induced innervation, extracellular matrix remodeling, and increased strength following training. Overall, we identify succinate as an exercise-responsive metabolite that relays the bioenergetic status of contracting muscles to the surrounding environment and facilitates exercise-induced muscle adaptation.

Introduction

Skeletal muscle remodeling following exercise has many beneficial effects on systemic health. This process is mediated by paracrine factors secreted by contracting muscle fibers and involves the participation of non-parenchymal cells that reside within the muscle tissue. These cell populations facilitate angiogenic, neurotrophic, and myogenic signaling pathways that underly muscle adaptation to exercise. How these processes are initiated following exercise remains poorly understood. Metabolite concentrations change rapidly and metabolite signaling can occur quickly, making this signaling modality amenable to muscle remodeling, which occurs shortly following exercise[3-7]. We hypothesize that exercising muscle selectively secretes key metabolites during exercise that signal to the surrounding environment to initiate the remodeling process.

We performed metabolomics on exercised tibialis anterior (TA) skeletal muscle, TA extracellular fluid, and plasma to identify exercise-responsive metabolites that are secreted by muscle. Through this analysis we show that skeletal muscle selectively releases the mitochondrial metabolite succinate during exercise. Acute decreases in cytosolic pH, due to altered muscle metabolism, drive exercise-induced succinate release. Cytosolic acidification promotes the protonation of succinate, transforming the metabolite from a dicarboxylate to a monocarboxylate. Protonated succinate is now amenable for transport via monocarboxylate transporter 1 (MCT1).

Once secreted, succinate engages its cognate receptor, succinate receptor 1 (SUCNR1). We show this receptor to be exclusively localized to non-myofibrillar cells in skeletal muscle. Succinate signaling initiates the transcription of several remodeling pathways, and is critical for innervation, extracellular matrix remodeling, and increased strength seen following training. Additionally, we observe a significant correlation between peak femoral vein succinate abundance and post-exercise insulin sensitivity, in humans.

Results

Mouse and Human Muscle Secrete Succinate during Exercise

Using a comparative metabolomics approach, we determined which metabolites are selectively secreted by skeletal muscle, *in vivo* (figure 2.2a). We subjected wild-type (WT) mice to a single bout of acute treadmill running which is known to initiate muscle remodeling and promote systemic health benefits[4-7]. Mice either walked on a treadmill or ran till exhaustion. Immediately following running, the tibialis anterior (TA) muscle, which is engaged during this exercise, was harvested[8]. Additionally, the extracellular fluid (figures S2.1a and S2.1b) and plasma were also collected. We then filtered metabolites based on the following criteria: (1) metabolite increases extracellularly following exercise (figure 2.2b; see figures S2.1a and S2.1b and methods for a description of interstitial fluid isolation and quality control [QC]); (2) metabolite is enriched in the extracellular fluid compared to bulk muscle (figure 2.2c); (3) metabolite preferentially accumulates in the local extracellular environment compared to bulk plasma (figure 2.2d). Metabolites that fulfilled all three criteria were deemed to be a signature of exercise-responsive metabolite release. Only one metabolite fulfilled these criteria: the mitochondrial metabolite, succinate. We also performed this analysis in gastrocnemius (GA) muscle, another

major muscle engaged with exercise. We see a similar pattern of succinate accumulation in this muscle (figure 2.2e – 2.2g).

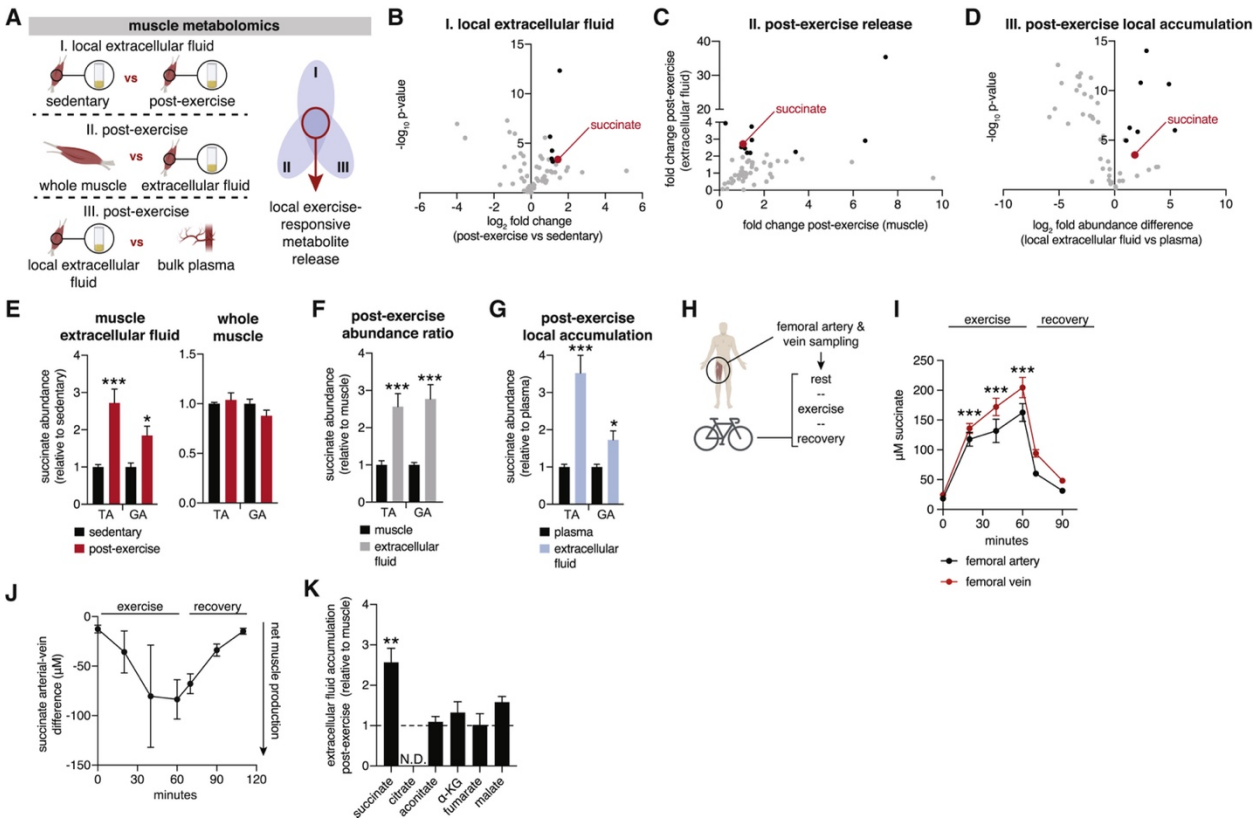


Figure 2.2 | Succinate is selectively secreted by exercising skeletal muscle in both mice and humans. (a) Comparative metabolomics approach to identify locally released metabolites. (b – d) Summary of results from comparative approach. Metabolites that fulfilled a criterion are highlighted in black, while metabolites that fulfill all three criteria are indicated in red. (b) Relative enrichment of metabolites in the extracellular fluid following exercise. Metabolites that were $\log_2$ fold change ≥ 1 and $-\log_{10}$ p-value > 3 were considered to be preferentially accumulated (n = 8). (c) Post-exercise fold change of each metabolite in extracellular fluid vs. muscle tissue (n = 8). (d) Relative enrichment of metabolites in extracellular fluid vs bulk plasma (n = 8). Selectively enriched metabolites in the extracellular fluid were defined as $\log_2$ fold change ≥ 1 and $-\log_{10}$ p-value > 3. (e) Selective enrichment of succinate in the extracellular fluid of tibialis anterior (TA) and gastrocnemius (GA) muscle post-exercise, not observed in whole muscle (n = 8).

Figure 2.2 l Succinate is selectively secreted by exercising skeletal muscle in both mice and humans (cont.). (f) Enrichment of succinate in extracellular fluid compared to whole muscle, post-exercise (n = 8). (g) Succinate preferentially accumulates in the extracellular fluid of TA and GA muscle compared to bulk plasma (n = 8). (h) Experimental setup to determine succinate concentration in humans during exercise. (i) Succinate concentration in femoral vein and femoral artery in humans during and following exercise (n = 10). (j) Femoral artery-vein difference of succinate in humans during and following exercise (n = 10). (k) Relative abundance of mitochondrial metabolites in extracellular fluid, post-exercise, compared to abundance of metabolite in muscle, post-exercise (n = 8).

Data are represented as mean ± SEM. *p < 0.05, **p < 0.01, ***p < 0.005 (two-tailed Student's t test for pairwise comparisons, one-way ANOVA for multiple comparisons involving one independent variable).

We next examined if succinate secretion occurs in humans during exercise. We recruited 10 healthy, non-obese, non-smoker male subjects 25 – 30 years old. Participants were catharized in their femoral artery and vein to allow for sampling of blood during and following exercise as described Kleinert et al., 2018[9]. Subjects exercised on a bike ergometer at 67% VO_2 max for 60 min followed by a 30 min recovery period (figure 2.2h). Succinate concentrations rapidly rose upon exercise to ~200 μM in the femoral vein, and quickly renormalized during recovery (figure 2.2i). Increases in succinate in the femoral vein and artery mirrored an increase in lactate that was also observed (figure S2.1c). The arterial-venous (A-V) difference of metabolite abundance is a benchmark to determine if a tissue is a consumer or producer of a given metabolite[10]. During exercise, the A-V difference of succinate quickly decreases and then renormalizes upon recovery, indicating that exercising muscle is a source of succinate (figure 2.1j and figure S2.1d). Together, these data demonstrate that, in mice and humans, exercising muscle releases succinate.

Cytosolic acidification drives succinate secretion from muscle cells via MCT1

Selective secretion of succinate from skeletal muscle was unexpected since mitochondrial dicarboxylates, like succinate, are traditionally thought to be impenetrable to most plasma membranes[11-14]. However, extracellular succinate concentrations are dynamic and rapidly increase in response to many physiological events such as hypoxia, exercise, and cold exposure[14-16]. Because succinate is thought to be exclusively intracellular, its accumulation extracellularly is thought to be a result of cell rupture[17].

However, this view is inconsistent with what we observe. We do not detect a general increase in all mitochondrial metabolites (figure 2.1k) nor do we see an accumulation of other known intracellular metabolites (figure S2.1e), which disputes the notion of general cellular leakage. Succinate secretion was specific to this mitochondrial metabolite, with structurally similar metabolites not accumulating (figure 2.1k). To understand the difference between succinate and other TCA cycle intermediates that allows for its secretion, we compared the chemical properties of succinate to other mitochondrial dicarboxylates. We noted that succinate had a high monorcarboxylic acid dissociation constant (pKa) compared to other intermediates (figure 2.2a and 2.2b). This property of succinate would allow for a significant portion of the succinate pool to exist in the monocarboxylate form during exercise. The cytosolic pH of exercising muscle has been reported to drop to 6.4 – 6.8 depending on the intensity of the exercise, and quickly alkalinizes upon recovery[18-20]. Therefore, we hypothesized that the monocarboxylate form of succinate may be the form being secreted during exercise (figure 2.2c).

To test this hypothesis, we first determined if perturbations that drive cytosolic acidification can promote succinate secretion from skeletal muscle cells. Cytosolic acidification during exercise

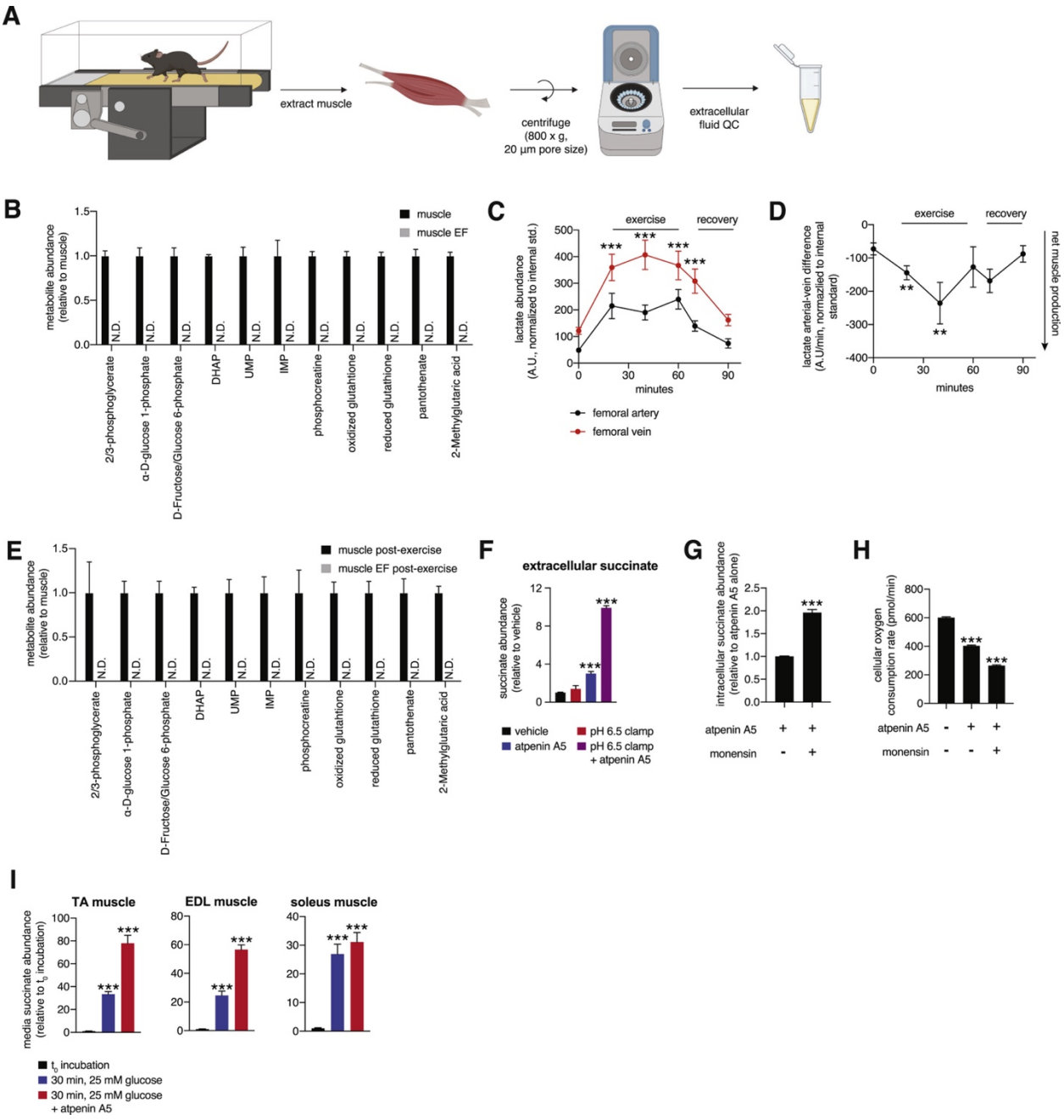


Figure S2.1 | Metabolite Profiling of Mouse and Human Exercise Samples and Characterization of pH-Dependent Succinate Release. (a) Schematic depicting protocol for extracting extracellular fluid from skeletal muscle. Method was based on established protocols[1,2]. (b) Quality control (QC) analysis of known intracellular metabolites in muscle and extracellular fluid. Metabolites are not detected in extracellular fluid, indicating no

Figure S2.1 | Metabolite Profiling of Mouse and Human Exercise Samples and Characterization of pH-Dependent Succinate Release (cont). (b) contamination from intracellular metabolites (n = 8). (c) Lactate concentration in femoral artery and vein in humans during and following exercise (n = 10). (d) Femoral arterial-venous difference of lactate in humans during and following exercise (n = 10). (e) Relative abundance of intracellular metabolites in extracellular fluid compared to whole muscle following exercise. Intracellular metabolites are not detected in extracellular fluid following exercise, indicating an absence of non-specific release of metabolites (n = 8). (f) Equilibration of cytosolic pH to acidic extracellular environment potentiates succinate release by atpenin A5 (n = 6). (g) Cytosolic alkalization driven by monensin increases intracellular succinate (n = 6). (h) Cytosolic alkalization driven by monensin inhibits mitochondrial respiration (n = 20). (i) Incubation of TA, EDL, and soleus muscle, *ex vivo,* in high-glucose buffer promotes succinate release by atpenin A5 (n = 6).

Data are represented as mean ± s.e.m. $**p < 0.01$; $***p < 0.005$ (two-tailed Student's t test for pairwise comparisons, one-way ANOVA for multiple comparisons involving one independent variable).

is a result of increased glycolysis and lactate production occurring partly due to local hypoxia[18-20]. In fact, subjecting muscle cells to hypoxia drives cytosolic acidification[18,21]. Hypoxia was sufficient to drive selective succinate release from skeletal muscle cells (figure 2.2d). Additionally, treating cells with mitochondrial inhibitors to increase glycolytic flux resulted in a decrease in cytosolic pH (figure 2.2e) and fostered succinate secretion from skeletal muscle cells (figure 2.2f and 2.2g). We also used the small molecule 5-(N-ethyl-N-isopropyl) amiloride (EIPA) to equilibrate the intracellular pH of cells to acidic medium (pH = 6.4). This resulted in a modest release of succinate (figure S2.1f). However, when we administered atpenin A5 to inhibit oxidative phosphorylation in

combination with EIPA, we observe a significant release of succinate (figure S2.1f). These findings indicate a succinate gradient across the plasma membrane in addition to cytosolic pH is required for succinate transport in skeletal muscle cells.

Next, to determine the necessity of cytosolic acidification for succinate release, we treated cells with the small molecule monensin, a sodium/proton antiporter that can alkalinize cytosolic pH (figure 2.3h)[22]. Monensin administration in combination with atpenin A5 inhibited cytosolic acidification and attenuated succinate release (figure 2.3i). Inhibition of succinate release by monensin resulted in an accumulation of intracellular succinate (figure S2.1g) and a decrease in mitochondrial respiration (figure S2.1h). Similarly, treating cells that have been subjected to hypoxia with monensin resulted in a decrease in succinate release (figure 2.3k). Next, we wanted to determine if pH-dependent succinate release occurs in intact muscle. We incubated isolated TA, extensor digitorum longus (EDL), and soleus muscle in high glucose media, *ex vivo*, to increase glycolytic flux and drive lactate production. High glucose media was sufficient to drive succinate release in TA, EDL, and soleus muscle (figure S2.1i). This response was potentiated by the addition of atpenin A5 in TA and EDL tissue (figure S2.1i). We then examined the pH dependency of succinate release in EDL by administering monensin in combination with atpenin A5. Monensin, when administered with atpenin A5, significantly attenuated succinate release (figure 2.3l).

To further elucidate the mechanism underpinning succinate secretion in skeletal muscle cells and tissue, we sought to identify the transporter that mediates this process. Using proteomic mass spectrometry (MS) we determined which plasma membrane proteins are highly expressed on TA and GA tissue, skeletal muscles that are capable of transporting succinate (figure 2.2e). The canonical plasma membrane dicarboxylate transporter, solute carrier family 13 member 3

Figure 2.3 | Cytosolic acidification drives succinate secretion. (a) Schematic depicting the pKa of mitochondrial dicarboxylates and abundance of protonated metabolite at various physiological pH conditions. (b) Relationship between pKa and metabolite abundance in (b) extracellular fluid (n = 8). (c) Schematic depicting the proposed mechanism of succinate secretion. (d) Mitochondrial carboxylate abundance in media following C2C12 myoblast hypoxia (n = 6). (e) Inhibition of mitochondrial respiration by antimycin A or atpenin A5 causes cytosolic acidification in C2C12 myoblasts (n = 4). (f) Promotion of glycolysis through acute inhibition of oxidative phosphorylation with antimycin A drives succinate release from C2C12 myoblasts (n = 6). (g) Promotion of glycolysis through acute inhibition of oxidative phosphorylation with atpenin A5 drives succinate release from C2C12 myoblasts (n = 6). (h) Schematic depicting the mechanism of monensin. (i) Monensin prevents cytosolic acidification caused by inhibition of oxidative phosphorylation with atpenin A5 in C2C12 myoblasts (n = 4). (j) Monensin attenuates succinate secretion driven by inhibition of mitochondrial respiration with atpenin A5 in C2C12 myoblasts (n = 6). (k) Monensin attenuates hypoxia-induced succinate secretion in C2C12 myoblasts. pH values denote extracellular pH clamp (n = 6). (l) Monensin inhibits succinate release driven by inhibition of mitochondrial respiration with atpenin A5, *ex vivo*, in EDL muscle (n = 5).

Data are represented as mean ± SEM. $*p$ or $\#p < 0.05$, $**p < 0.01$, $***p$ or $\#\#\#p < 0.005$ (two-tailed Student's t test for pairwise comparisons, one-way ANOVA for multiple comparisons involving one independent variable). # label significance assessed by ANOVA when comparing to a condition other than control.

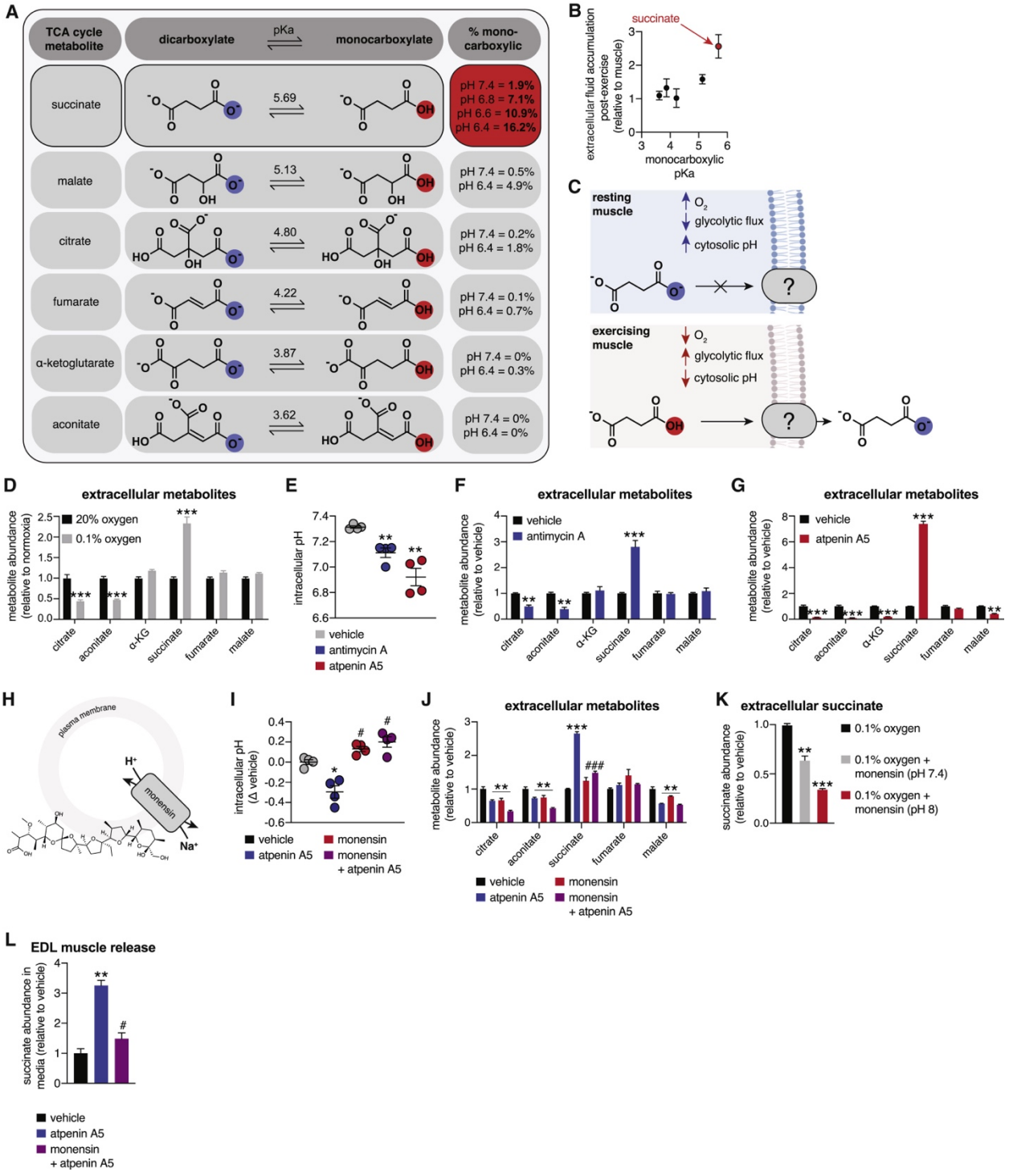


Figure 2.3 l (caption on preceding page)

was not detected on TA or GA tissue[23]. Of the ~3800 proteins quantified, only two were known transporters of carboxylates: monocarboxylate transporter 1 (MCT1) and monocarboxylate transporter 4 (MCT4) (figure 2.4a). MCT1 and MCT4 are not thought to transport succinate and instead facilitate the transport of small monocarboxylates like lactate and pyruvate[24]. Given the pH dependency of succinate transport, we hypothesized that skeletal muscle could selectively transport the monocarboxylate form of succinate (figure 2.4b). This selectivity could explain the pH dependency for succinate secretion. Genetic depletion of MCT1 with small interfering RNA (siRNA) resulted in a decrease in succinate release following induction of cytosolic acidification with atpenin A5 (figure 2.4c, S2.2a, and S2.2d). This response was absent in cells not subjected to cytosolic acidification (figure 2.4c). siRNA-mediated knockdown of MCT2 or MCT4 did not significantly reduce succinate secretion (figure 2.4c and S2.2b – S2.2c). Based on these findings, we treated cells with established MCT1 inhibitors all of which attenuated succinate secretion driven by cytosolic acidification (figure 2.4d – 2.4f and S2.2e)[24]. Similarly, chemical inhibition of MCT1 reduced hypoxia-induced succinate secretion (figure 2.4g). Pharmacological inhibition of MCT1 in EDL muscle, *ex vivo*, decreased succinate secretion driven by increased glycolytic flux (figure S2.2f) and inhibition of mitochondrial respiration (figure S2.2g).

We next directly examined the ability of MCT1 to transport succinate by expressing recombinant, human MCT1 in *Xenopus oocytes*. This system allows for the expression of functional MCT1 protein on the plasma membrane and has been used to determine the transport capabilities of the protein[25,26]. Using this reductionist system, we observe MCT1 facilitated succinate transport at pH 6.4 (figure 2.4h and S2.2h – S2.2i). Transport in MCT1 expressing oocytes was blocked with MCT1 inhibitors (figure 2.4i). Notably, the rate of succinate transport is slower than that of lactate, in this system (figure S2.2j). This is in line with previous reports that show MCT1 has a preference for lactate over other transport substrates and illustrates that the

capacity for MCT1-facilitated transport of succinate is lower in comparison to its traditional substrate[27]. Together these data demonstrate that MCT1 facilitates transport of succinate in a pH dependent manner (figure 2.4b).

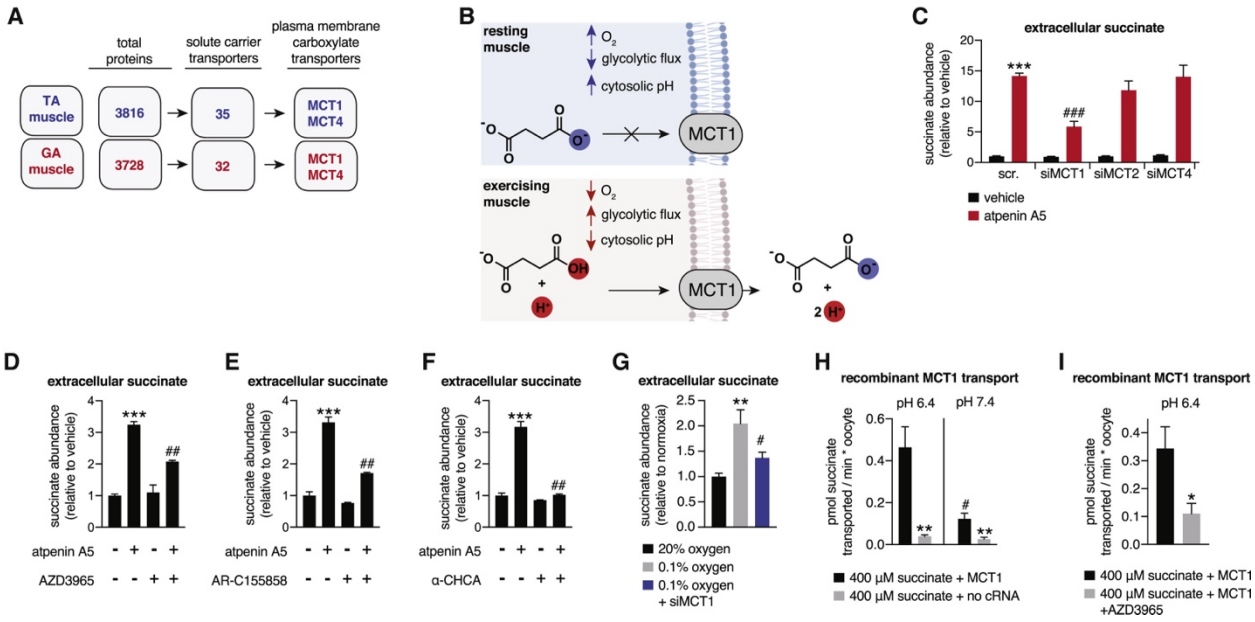


Figure 2.4 l pH-dependent secretion of succinate. (a) Schematic depicting total number of proteins identified in TA and GA muscle and candidate transporters of succinate. (b) Proposed mechanism of MCT1-mediated succinate release during exercise. (c) Genetic depletion of MCT1 in C2C12 myoblasts abrogates succinate secretion induced by cytosolic acidification with atpenin A5 (n = 6). (d) Pharmacological inhibition of MCT1 with AZD3965 in C2C12 myoblasts attenuates succinate release induced by cytosolic acidification with atpenin A5 (n = 6). (e) Chemical inhibition of MCT1 with AR-C155858 in C2C12 myoblasts abrogates succinate release induced by cytosolic acidification with atpenin A5 (n = 6). (f) Pharmacological inhibition of MCT1 with alpha-Cyano-4-hydroxycinnamic acid (α-CHCA) in C2C12 myoblasts reduces succinate secretion induced by cytosolic acidification with atpenin A5 (n = 6). (g) Genetic depletion of MCT1 in C2C12 myoblasts attenuates succinate secretion driven by hypoxia (n = 6). (h) Expression of recombinant human MCT1 facilitates succinate transport in *Xenopus oocytes*. All rates were obtained during the first 10 min following succinate addition, which corresponds to the linear phase of uptake (n = 5 – 8). (i) Pharmacological inhibition of recombinant human MCT1 with AZD3965 attenuates succinate

Figure 2.4 l pH-dependent secretion of succinate (cont). (i) secretion in *Xenopus oocytes*. Data are represented as mean ± SEM. *p or #p < 0.05, **p or ##p < 0.01, ***p or ###p < 0.005 (two-tailed Student's t test for pairwise comparisons, one-way ANOVA for multiple comparisons involving one independent variable). # label significance assessed by ANOVA when comparing to a condition other than control.

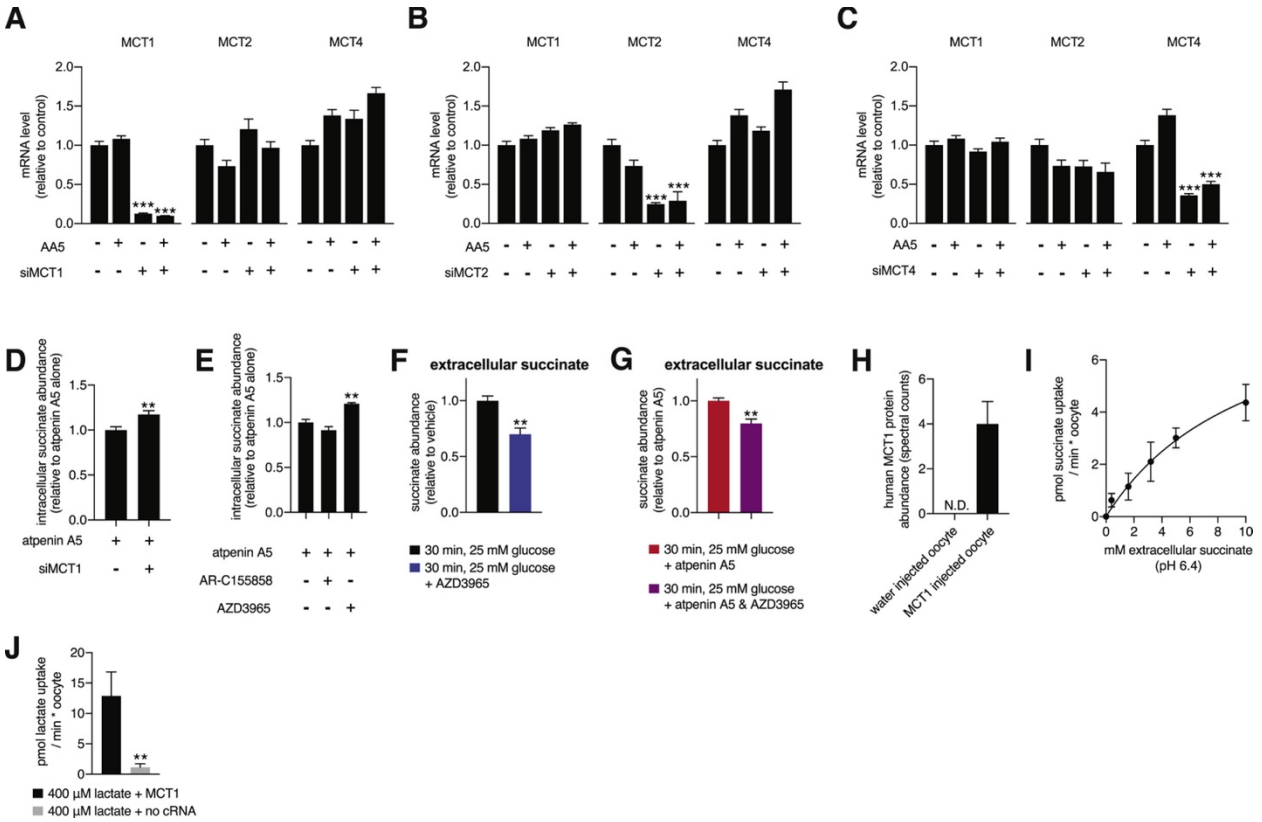


Figure S2.2 | Depletion of MCT isoforms in C2C12 myoblasts and characterization of MCT1-dependent succinate transport. (a) siRNA mediated knockdown of MCT1 is specific and does not deplete other MCT isoforms (n = 6). (b) siRNA mediated knockdown of MCT2 is specific and does not deplete other MCT isoforms (n = 6). (c) siRNA mediated knockdown of MCT4 is specific and does not deplete other MCT isoforms (n = 6). (d) Genetic depletion of MCT1 modestly increases intracellular succinate abundance following atpenin A5 treatment in C2C12 myoblasts (n = 6). (e) MCT inhibitors do not dramatically affect intracellular succinate abundance following atpenin A5 treatment in C2C12 myoblasts (n = 5). (f) Pharmacological inhibition of MCT1 with AZD3965 attenuates succinate release driven by increased glycolytic flux, *ex vivo* in intact EDL muscle (n = 6). (g) Pharmacological inhibition of MCT1 with AZD3965 attenuates succinate release driven by atpenin A5, *ex vivo* in intact EDL muscle (n = 6). (h) Protein expression of recombinant human MCT1 in *Xenopus oocytes* (n = 3). (i) Concentration

Figure S2.2 | Depletion of MCT isoforms in C2C12 myoblasts and characterization of MCT1-dependent succinate transport (cont). (i) dependent rate of succinate transport by recombinant human MCT1 in *Xenopus ooyctes*. (j) Recombinant human MCT1 transport of lactate in *Xenopus oocytes*. All rates were obtained during the first 10 min following succinate addition, which corresponds to the linear phase of uptake (n =3).

Data are represented as mean ± s.e.m. $**p < 0.01$; $***p < 0.005$ (two-tailed Student's t test for pairwise comparisons, one-way ANOVA for multiple comparisons involving one independent variable).

Non-myofibrillar cells in muscle respond to succinate signaling to drive muscle-remodeling transcriptional responses

Having demonstrated that skeletal muscle cells are capable of selective succinate secretion during exercise, we next wanted to determine if succinate could be initiating muscle-remodeling processes initiated by exercise. Succinate is a ligand for a g-protein coupled receptor (GPCR), succinate receptor 1 (SUCNR1)[28]. We hypothesized that succinate-SUCNR1 signaling may contribute to exercise-induced muscle remodeling. Basally, extracellular succinate concentrations are 20 μM and can rise to 60 – 200 μM with exercise (figure 2.2i). The half maximal effective concentration (EC_{50}) of succinate for SUCNR1 is 28 – 56 μM, with ~99% of responses achieved at a concentration of 200 μM[28]. Therefore, the concentration of extracellular succinate achieved with exercise is more than sufficient to initiate succinate-SUCNR1 signaling.

Succinate signaling is upstream several potential phosphorylation pathways that modulate various cell processes. However, many of the pathways downstream of SUCNR1 agonism are poorly defined[29]. We performed phosphoproteomics on TA muscle from wild-type (WT) and SUCNR1 KO mice immediately following exercise, when extracellular succinate concentration is

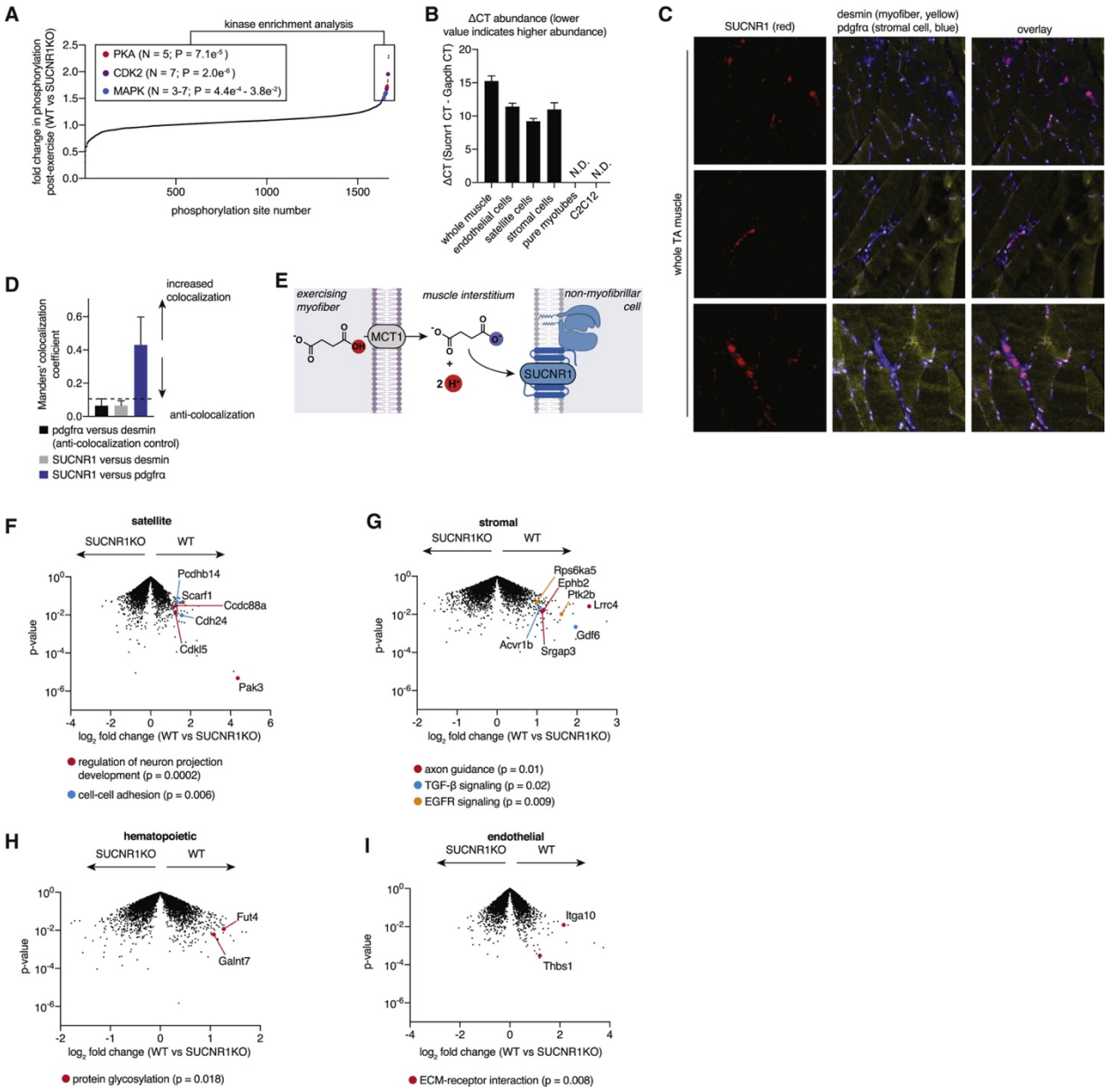


Figure 2.5 | Succinate-SUCNR1 signaling controls cell non-autonomous transcriptional responses to acute exercise. (a) Phosphoproteomics analysis of WT and SUCNR1 KO TA muscle following exercise. Sites exhibiting > 50% enrichment in WT TA compared to SUCNR1 KO TA were subjected to kinase analysis. Top enriched pathways and those established to be downstream of SUCNR1 agonism are highlighted (n = 4). (b) qPCR analysis of SUCNR1 transcript levels in whole muscle, purified myotubes, and resident non-myofibrillar cell populations. SUCNR1 transcripts detected on non-myofibrillar cell populations (endothelial,

Figure 2.5 | Succinate-SUCNR1 signaling controls cell non-autonomous transcriptional responses to acute exercise (cont). (b) immune, stromal, and satellite) and whole muscle, but were undetectable on purified myotubes or differentiated C2C12 myotubes (n = 3 – 4). (c) *in situ* hybridization in TA muscle to assess localization of SUCNR1. SUCNR1 transcripts are highlighted in red, desmin (muscle-specific) are highlighted in yellow, and PDGFRα is highlighted in blue. Three representative images are shown. (d) Manders' colocalization coefficient of TA muscle from *in situ* hybridization data shown in (c). Coefficient < 0.1 indicates anti-localization, which is validated by the anti-localization of controls, desmin and PDGFRα. SUCNR1 co-localized to non-myofibrillar stromal cells (PDGFRα) and anti-localizes with myofibers (desmin) (n = 3). (e) Model depicting succinate regulation of cell non-autonomous muscle remodeling, following exercise. (f) SUCNR1-dependent transcriptional responses in muscle satellite cells ($CD45^-$, $CD31^-$, $Sca1^-$, $Vcam^+$) following exercise in TA muscle. Differentially upregulated pathways are annotated. (g) SUCNR1-dependent transcriptional responses in stromal cells ($CD45^-$, $CD31^-$, $Sca1^+$, $PDGFRa^+$) following exercise in TA muscle. Differentially upregulated pathways are annotated. (h) SUCNR1-dependent transcriptional responses in muscle immune cells ($CD45^+$) following exercise in TA muscle. Differentially upregulated pathways are annotated. (i) SUCNR1-dependent transcriptional responses in endothelial cells ($CD45^-$, $CD31^+$) following exercise in TA muscle. Differentially upregulated pathways are annotated.

the highest. We observe SUCNR1-dependent phosphorylation of many kinase pathways during exercise (figure 2.5a). Two pathways of these pathways, mitogen-activated protein kinase (MAPK) and protein kinase A (PKA), are known to be downstream of SUCNR1 agonism[29,30]. We also observed an enrichment in CDK2-dependent phosphorylation cascades, which has not been

previously reported (figure 2.5a). Taken together, these data indicate succinate-SUCNR1 mediated phosphorylation occurs rapidly following acute exercise.

The SUCNR1-dependent signaling cascades we identified above are upstream of a broad range of transcriptional responses that are largely dependent on the nature of the target cell. Accordingly, we determined the cell populations where SUCNR1 agonism elicits transcriptional responses following acute exercise. A recent study suggested that SUCNR1 localized to myotubes and regulates muscle fiber remodeling[31]. However, while we were able to detect SUCNR1 in whole muscle, the receptor was absent in purified myotubes or C2C12 myoblasts (figure 2.5b). Instead, we determine muscle-resident non-myofibrillar cells, including satellite, endothelial, and stromal cell populations, to express the receptor (figure 2.5b). To confirm this, we performed *in situ* hybridization (ISH) to assess localization of SUCNR1 in skeletal muscle tissue. ISH is highly sensitive and can accurately detect transcripts within a tissue[32,33]. SUCNR1 was not detected on muscle fibers, as seen by the anti-colocalization of this receptor with desmin, a myofibrillar specific protein, corroborating our previous findings (figures 2.5c and 2.5d). Instead, we observe a strong colocalization between SUCNR1 and stromal cell populations, as defined by the expression of platelet-derived growth factor receptor-alpha (pdgfrα) (figures 2.5c. and 2.5d). Additionally, we do not observe any direct effect of succinate on myoblast differentiation, myoblast proliferation, or transcriptional expression of myosin heavy chains in differentiated myotubes (figures S2.3a – S2.3e). Taken together with the lack of expression of SUCNR1 on muscle fibers, our data indicates succinate-SUCNR1 signaling regulates muscle remodeling in a cell non-autonomous manner.

We hypothesized that succinate released during exercise could control transcriptional responses in non-myofibrillar cell in muscle tissue through SUCNR1 agonism (figure 2.5e). To explore this hypothesis, we isolated muscle-resident non-parenchymal cells from TA tissue: endothelial,

Figure S2.3 | Direct effect of succinate on muscle cells and comparison of WT and SUCNR1 TA proteomes. (a) qPCR analysis of myogenic differentiation markers and myosin isoforms following 72 h treatment with sodium succinate, in C2C12 muscle cells (n = 5). (b) Effect of succinate on myoblast proliferation (n = 6). (c) Representative images of myotubes stained for myosin heavy chain (MyHC) and DAPI following succinate treatment. (d) Quantification of $MyHC^+$ nuclei following succinate treatment (n = 8). (e) qPCR analysis of myogenic differentiation markers and myosin isoforms following 2 h treatment with sodium succinate in primary myotubes (n = 5). (f) Distance run of WT and SUCNR1 KO mice prior to isolation of non-myofibrillar cell populations (n = 3). (g) Myosin protein abundance in TA muscle from WT and SUCNR1 KO mice following training and under sedentary conditions (n = 4). Trained data is replotted from figure 2.6 for ease of comparison. (h) ECM protein abundance in TA muscle from WT and SUCNR1 KO mice following training and under sedentary conditions (n = 4). Trained data is replotted from figure 2.6 for ease of comparison. (i) Abundance of inflammatory complement pathway proteins in TA muscle from WT and SUCNR1 KO mice following training and under sedentary conditions (n = 4). Trained data is replotted from figure 2.6 for ease of comparison.

Data are represented as mean ± s.e.m. $*p < 0.05$; $**p < 0.01$ (two-tailed Student's t test for pairwise comparisons, one-way ANOVA for multiple comparisons involving one independent

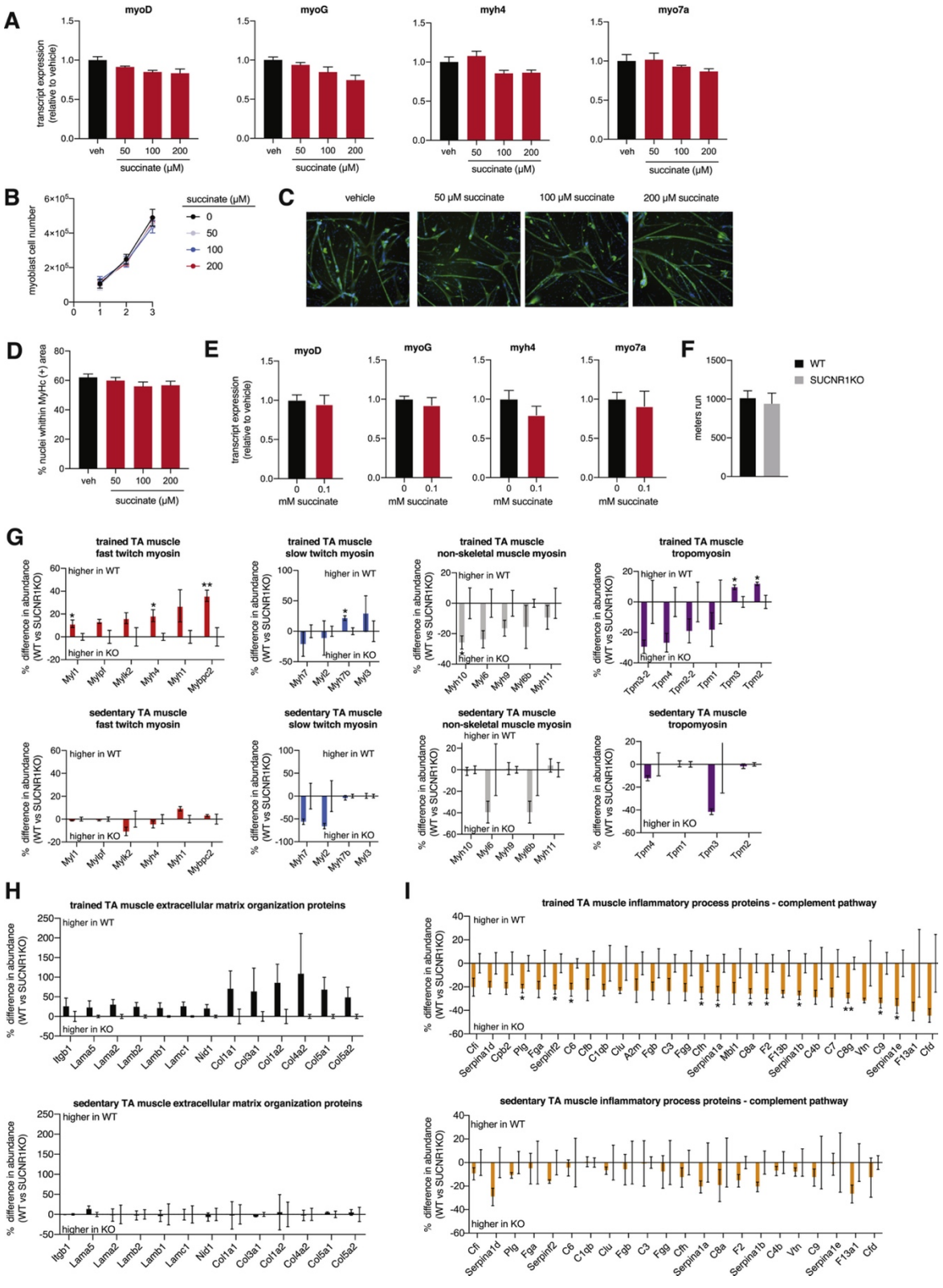


Figure S2.3 I (caption on preceding page)

satellite, stromal, and hematopoietic cells (immune cells)[34]. We subjected WT and SUCNR1 KO mice to a bout of acute treadmill running, to drive succinate release, and isolated these cell populations immediately following exercise (figure S2.3f). We performed RNA sequencing (RNA-seq) on purified cell populations to assess differential expression of transcripts in WT and SUCNR1 KO mice. We then performed pathway analysis to identify SUCNR1-dependent biological processes based on an enrichment of transcripts in WT compared to SUCNR1 KO cells. In satellite and stromal cells, we observe a SUCNR1-dependent increase in transcripts relating to axonal guidance and neuronal projection (figures 2.5f and 2.5g). SUCNR1 KO satellite cells had a decrease in transcripts relating to cell-cell adhesion, while SUCNR1 KO stromal cells had decreased expression of transcripts involved in transforming growth factor β (TGF-β) signaling and epidermal growth factor receptor (EGFR) signaling (figures 2.5f and 2.5g). Notably, we observe a SUCNR1 dependent enrichment in growth differentiation factor 6 (GDF6), an important growth factor that mediates muscle repair[35]. Hematopoietic and endothelial cell populations experienced fewer consequences of SUCNR1 ablation, with only few transcripts in protein glycosylation and extracellular matrix (ECM) remodeling demonstrating differential expression (figures 2.5h and 2.5i). Overall, our data demonstrates that lack of succinate-SUCNR1 signaling results in a decrease in transcripts relating to muscle innervation, regeneration, and ECM repair in numerous non-myofibrillar cell populations.

Succinate-SUCNR1 Signaling Mediates Muscle Adaptation to Exercise

Our data supports a model whereby succinate released from skeletal muscle during exercise regulates non-myofibrillar responses, specifically innervation and ECM remodeling. These processes are necessary for the muscle response to exercise training. Therefore, we investigated the role of succinate-SUCNR1 signaling in exercise training-induced muscle remodeling. To do so, we subjected WT and SUCNR1 KO mice to a 3-week voluntary resistance wheel running protocol (figure 2.6a)[4,36]. Resistance wheel running promotes many systemic

health benefits within 3-weeks, including improved insulin sensitivity and increased strength. We subjected WT and SUCNR1 KO mice to this training protocol. Sedentary WT and SUCNR1 KO mice did not experience any differences in strength (figure 2.6b). Interestingly SUCNR1 KO mice ran more than WT mice (figure 2.6c). However, SUCNR1 KO mice did not experience an increase in strength, despite running more. We observed ~20% increase in grip strength in WT mice, following the training period (figure 2.6d and 2.6e).

Figure 2.6 | Succinate signaling mediates muscle adaptation to exercise. (a) Schematic depicting resistance-wheel training protocol. (b) Grip strength of sedentary WT and SUCNR1 KO mice (n = 15 WT, n = 12 KO). (c) Distance run by WT and SUCNR1 KO mice during training period (n = 15 WT, n = 12 KO). (d-e) Grip strength of WT and SUCNR1 KO mice during training period (n = 15 WT, n = 12 KO). (f) Proteomics analysis of WT and SUCNR1 KO TA muscle following training. Pathways that contain proteins that are differentially enriched > 20% are annotated (n = 4). (g) Abundance of actin and myosin proteins in WT and SUCNR1 KO TA muscle following training (n = 4). (h) Abundance of ECM proteins in WT and SUCNR1 KO TA muscle following training (n = 4). (i) Abundance of inflammatory complement pathway proteins in WT and SUCNR1 KO TA muscle following training (n = 4) (j) Quantification of TUBB3 staining in WT and SUCNR1 KO TA muscle following training and under sedentary conditions (n = 5). (k) Representative flattened z-stack images of TUBB3 staining. Top and bottom rows are top and side views, respectively. (l) Schematic depicting experimental design of hyperinsulinemic-euglycemic clamp. (m) Correlation between peak venous succinate concentration and post-exercise insulin sensitivity (n = 10). (n) Insulin tolerance test of WT and SUCNR1 KO mice 3h following acute treadmill running (n = 6 – 7).

Data are represented as mean ± SEM. $*p < 0.05$, $**p < 0.01$, $***p < 0.005$ (two-tailed Student's t test for pairwise comparisons, one-way ANOVA for multiple comparisons involving one independent variable).

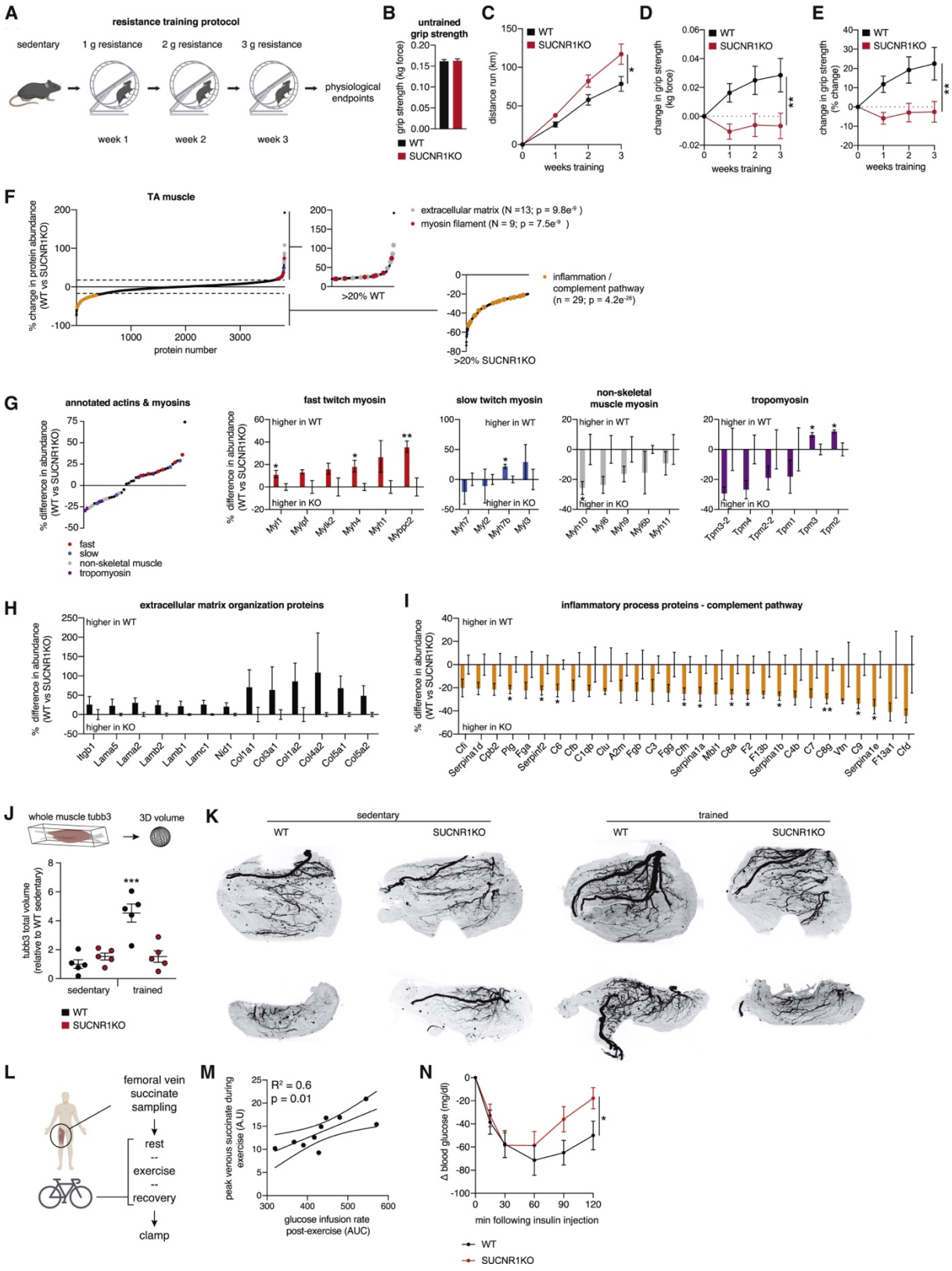


Figure 2.6 l (caption on preceding page)

To elucidate the molecular mechanism underlying this strength differential, we examined the proteomes of TA muscle from WT and SUCNR1 KO mice. SUCNR1 KO muscles demonstrated a decrease in numerous proteins involved in muscle adaptation to exercise (figure 2.6f). We observed a decrease in myosin complex protein abundance in SUCNR1 KO mice compared to WT mice following exercise training (figure 2.6f). Moreover, there was a difference in the nature of myosin heavy chains expressed between the two genotypes. WT mice had an enrichment of fast-twitch myosin heavy chains while SUCNR1 KO mice experienced remodeling of non-skeletal muscle myosin chains and tropomyosin proteins (figure 2.6g). SUCNR1 KO mice also experienced a decrease in ECM related proteins, including collagens and laminins (figures 2.6f and 2.6h). These proteins play a critical role in myogenesis, force transmission, and muscle innervation[37]. Conversely, SUCNR1 KO muscle experienced an increase in proteins involved in the complement pathway and the inflammatory response, many of which are associated with insulin resistance (figure 2.6f and 2.6i)[38]. Notably, we did not observe any differences in the muscle of untrained WT and SUCNR1 KO mice, indicating an exercise-dependent requirement for SUCNR1 to mediate these adaptations (figures S2.3G – S2.3I).

Our proteomics analysis revealed a SUCNR1-depedent expression of ECM related proteins that are involved in muscle innervation following exercise. Additionally, we observed a SUCNR1-dependent increase in transcripts related to neuronal development and axonal guidance in non-myofibrillar cells following acute exercise. Neuronal adaptations occur during the early months of exercise training and play a critical role in increased strength[39,40]. Therefore, we hypothesized the difference in strength we observed in the WT and SUCNR1 KO mice may be attributed to differences in muscle innervation. To examine this hypothesis, we performed whole-tissue staining of the neural-specific tubulin TUBB3 in TA muscle from WT and SUCNR1 KO mice. Strikingly, we observed a significant increase in neural volume in WT TA muscle following training that was absent in SUCNR1 KO muscle (figure 2.6j and 2.6k). We also assessed muscle

vascularization and fiber volume but did not observe any differences between the genotypes (figure S2.4a – S2.4d).

Taken together, these data illustrate the critical role succinate-SUCNR1 signaling plays in exercise training-induced muscle adaptations, specifically ECM remodeling, regulation of myosin

Figure S2.4 | Quantification of blood vessel and fiber volume in WT and SUCNR1 KO TA muscle and correlation analysis of human physiological parameters and peak venous succinate concentration following exercise. (a) Quantification of blood vessel volume, with CD31, in WT and SUCNR1 KO TA muscle following training and under sedentary conditions (n = 5). (b) Representative flattened z-stack images of CD31 staining. (c) Quantification of myofiber volume in WT and SUCNR1 KO TA muscle following training and under sedentary conditions (n = 10). (d) Representative 2D compressed images of muscle myofiber volume. (e) Multiple linear regression analysis actual vs predicted plot assessing co-variates and peak exercise venous succinate concentration. (f) Multiple linear regression analysis residual plot assessing co-variates from panel E on peak exercise succinate release. (g) Correlation between peak venous succinate concentration and peak VO_2 (n = 10). (h) Correlation between peak venous succinate concentration and peak load (n = 10, W; watts). (i) Glucose tolerance test on WT and SUCNR1 KO mice following i.p. injection of 1g/kg glucose (n = 6).

Data are represented as mean ± s.e.m. $**p < 0.01$; (two-tailed Student's t test for pairwise comparisons, one-way ANOVA for multiple comparisons involving one independent variable).

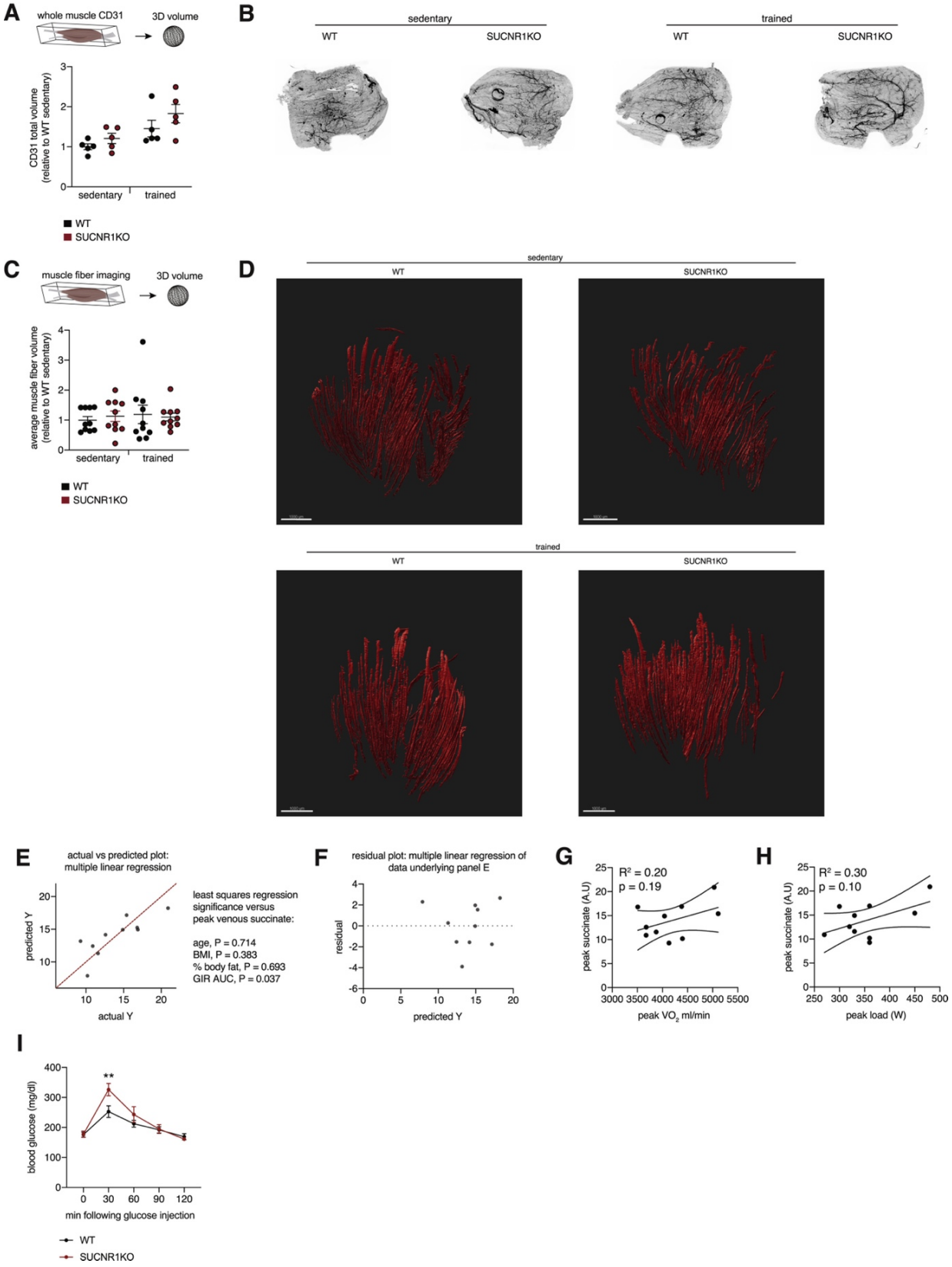


Figure S2.4 I (caption on preceding page)

complex proteins, and increased strength. Notably, neural adaptations in muscle are seen early following resistance training and contribute to increases in strength independent of hypertrophy[39]. Moreover, motor neurons directly influence myotube content and volume, while sympathetic innervation controls regeneration, strength, and blood flow to the muscle[41-43]. Therefore, it is likely that SUCNR1-dependent differences in strength and muscle remodeling can be at least partly attributable to a difference in muscle innervation.

Finally, we further explored our finding that succinate-SUCNR1 antagonizes muscle inflammation, which is associated with insulin resistance (figure 2.6i). In humans, a single bout of exercise improves insulin sensitivity for several hours post-exercise, and our data indicate an anti-inflammatory role for succinate signaling[44]. Therefore, we examined whether post-exercise succinate concentrations are predictive of insulin sensitivity following an acute bout of exercise, in humans (figure 2.6l). Individuals were sampled as described in figure 2.2h, and were subjected to a hyperinsulinemic-euglycemic clamp, following recovery. Strikingly, we observed a significant correlation between peak succinate concentration in the femoral vein and post-exercise insulin sensitivity (figure 2.6m). This correlation was distinct from other covariates tested (figures S2.4e and S2.4f) and occurred independently of VO_2 max (figure S2.4g) and peak muscle load (figure S2.4h). Based on these findings, we examined whether succinate-SUCNR1 signaling regulates post-exercise insulin sensitivity. We observed a decrease in post-exercise insulin sensitivity in SUCNR1 KO mice, which also exhibited a modest basal glucose insensitivity (figures 2.6n and S2.4i). Of note, previous studies on SUCNR1 KO mice found obesogenesis-dependent glucose insensitivity, induced by high-fat feeding[44]. Therefore, the effect of succinate signaling on insulin sensitivity observed here may be specific to exercise.

Discussion

Together our data highlights the role of succinate as a signaling molecule that relays the bioenergetic status of exercising muscle to the surrounding environment to initiate muscle remodeling processes. During exercise, the transient acidification of the cytosol, due to decreased oxygen tension and increased glycolytic flux, promotes the protonation of succinate converting the metabolite from a dicarboxylate to a monocarboxylate. This transformation of succinate is possible because of the metabolite's relatively high pka, compared to other TCA cycle intermediates. This allows for a significant portion of the intracellular succinate pool to be protonated at pH levels achieved by exercise. In the protonated form, succinate is now able to be secreted by MCT1. Once secreted, succinate engages its cognate receptor, SUCNR1, which is expressed by muscle resident non-myofibrillar cells. Succinate-SUCNR1 signaling controls transcriptional responses in muscle non-parenchymal cells, including neuronal projection and axonal guidance. During prolonged training, succinate-SUCNR1 signaling mediates several key exercise adaptions in muscle including ECM remodeling, innervation, and increased strength.

It is worth noting, that a previous study investigated the effects of orally administered sodium succinate on skeletal muscle function[31]. In that study, dietary succinate improved certain aspects of muscle performance such as strength and time to fatigue, in a SUCNR1-dependent manner. These adaptations were attributed to SUCNR1 signaling in myofibrils. It may be tempting to attribute the effects of dietary succinate to the paracrine signaling initiated by exercise-induced succinate secretion as determined in this work. However, orally administered succinate effects many systemic processes including whole-body energy expenditure, systemic glucose homeostasis, and intestinal fuel utilization[14,45,46]. These processes are linked to muscle metabolism. Therefore, any effects on skeletal muscle observed, following several weeks of dietary succinate supplementation, must consider these upstream processes when determining

the mechanism. However, it would be interesting to determine the extent to which dietary succinate can initiate ECM remodeling and muscle innervation similar to exercise-induced succinate release.

Our findings propose a general model where changes in bioenergetic status can be communicated to the surrounding environment through transient changes in pH. This pH-gated mechanism of secretion reconciles the view of succinate as an intracellular metabolite with the numerous processes that are regulated by extracellular succinate or SUCNR1 signaling, including increased energy expenditure, tissue inflammation, and renin-angiotensin system[14,47-49]. It also supports the hypothesis that extreme conditions such as tissue ischemia or pH gradients between neurons and astrocytes could drive succinate secretion via MCT1, which was recently shown in the context of myocardial infarction[50-52]. Overall, our model predicts that hypoxia or intracellular acidification will promote succinate release as a general mechanism to initiate paracrine modes of physiological regulation.

Experimental Model and Subject Details

Mouse Lines

Animal experiments were performed according to procedures approved by the Institutional Animal Care and Use Committee of the Beth Israel Deaconess Medical Center. Unless otherwise stated, mice used were male C57BL/6J (8 ± 12 weeks of age; Jackson Laboratories) and housed in a temperature-controlled (23°C) room on a 12-h light-dark cycle. Male WT and SUCNR1KO littermate matched controls were used.

Human exercise study recruitment

Ten men were recruited for the study, which was approved by the Copenhagen Ethics Committee (Reg. number H-16040740) and performed in accordance with the Declaration of Helsinki. Informed written consent was received from each participant prior to study inclusion. All subjects

were healthy, moderately physically active and with no family history of diabetes. The subjects were 27 ± 0.8 (means ± SEM) years old, with a body weight of 85 ± 2.5 kg, body mass index (BMI) of 24 ± 0.5 kg·m-2 and maximal oxygen uptake (VO2 peak) of 49 ± 1 ml·kg-1·min-1. Maximal oxygen uptake was measured by an incremental exercise test on a Monark Ergomedic 839E bicycle ergometer (Monark). Before the trial subjects consumed a eucaloric controlled diet for 3 days to eliminate dietary differences between subjects. The daily energy requirements were individually determined from weighed dietary registrations and predicted equations from WHO/FAO/UNU. All food items were weighed and prepared in the metabolic kitchen and menus were delivered to the subjects and ingested at home. The diet consisted of 60 energy-percent (E%) carbohydrate, 25E% fat and 15E% protein.

Cell lines

C2C12 murine myoblasts (obtained from ATCC) were in growth media consisting of DMEM and 10% fetal bovine serum and 1% penicillin/streptomycin. Upon reaching confluency, growth media was exchanged for differentiation media consisting of DMEM containing 2% horse serum. Seven days post differentiation cells appeared mostly as phase-bright fused myotubes[53].

Isolation of muscle satellite cells

Mouse satellite cells were isolated as previously described[54]. Briefly, gastrocnemius and tibialis anterior muscles were dissected and digested with Collagenase type 2 and Dispase (Worthington Biochemical Corporation) for a total of 90-120 min. Cell suspension was strained with a 40 µm filter and stained cells the following antibodies: anti-CD45 (BD Biosciences), anti-CD11b (BD Biosciences), anti-CD31 (eBiosciences) and anti-Sca1 (BD Biosciences). Next, cells were incubated with streptavidin microbeads (Miltenyi Biotech), SA Texas Red (Invitrogen), PE labeled anti-integrin α7 antibody labeled with phycoerythrin (AbLab) and anti-CD34 eFluor660 (eBioscience). Dead cells were identified using propidium iodide staining. Cells were sorted on a FACS Aria 2 and routinely yielded > 95% CD34+ α7 integrin+ cells from a single round of sorting.

Scatterplots were analyzed using FlowJo (TreeStar). Live cells were plated in collagen coated plates (Corning) and maintained in growth media (50:50 DMEM /F10, 15% FBS, 1% penicillin/streptomycin, and 2.5 ng/ml bFGF). For *in vitro* differentiation satellite cells were washed with PBS and subjected to differentiation media (DMEM supplemented with 5% horse serum) for three days. Depending on experimental condition, vehicle (PBS) or succinate (50, 100 and 200 μM) were added to growth and differentiation media.

Method Details

Acute exercise training protocol

Eight-week old mice were acclimated to a motorized treadmill (Columbus Instruments) for three days prior to forced running protocol. Training sessions consisted of mice walking on the treadmill for 5 min at 12 m/min followed by a 1 min rest and then 5 min at 12 m/min and 5 min at 14 m/min. On the day of running, all mice were subjected to the training protocol. Mice in the sedentary group were taken off the treadmill after the training protocol was complete while mice in the exercise group remained on the treadmill. After the training period, exercised mice remained on the treadmill and the speed was ramped up 2 m/min every 4 min, until a final speed of 26 m/min was reached. Exercised mice were removed from the treadmill once exhausted, which was deemed to be the point where they refused to step on the treadmill.

Sample preparation for metabolite profiling

Following intervention, animals were sacrificed immediately by cervical dislocation and tissues were rapidly extracted and immediately snap frozen in liquid nitrogen for metabolite profiling. For metabolite extraction, tissues were weighed and then homogenized with extraction buffer which consisted of 80% methanol containing inosine15N4, thymine-d4 and glycocholate-d4 internal standards (Cambridge Isotope Laboratories) at a 4:1 volume to wet weight ratio. Samples were then centrifuged twice (5 min, 10,000 g, 4°C). Supernatant was then further diluted with 80%

HPLC grade methanol at a ratio of 1:10 extracted metabolite to methanol. Interstitial fluid was extracted from muscles immediately upon extraction using a rapid isolation procedure described previously[1,2]. Muscles were subjected to centrifugation (10 min, 800 g, 4°C) following placement in a 20 µm nylon mesh filter (EMD Millipore). Metabolites were extracted by adding extraction buffer at a ratio of 1:100 interstitial fluid to methanol. Samples were then centrifuged twice (5 min, 10,000 g, 4°C) and supernatant was collected. For plasma collection, blood was taken via cheek bleed from mice, collected into a heparin column (Becton Dickson), centrifuged (10 min, 1,000 g, 4°C), and subsequently snap-frozen. Metabolites were extracted from plasma by adding extraction buffer in a 1:4 ratio plasma to methanol. Samples were then centrifuged twice (5 min, 10,000 g, 4°C) and supernatant was collected. For media metabolite extraction, media samples were collected and centrifuged (1 min, 21,100 g, 4°C) to remove any debris or cell contaminants. Metabolites from media were extracted by adding extraction buffer in a ratio of 1:4 media to methanol. Samples were then centrifuged twice (5 min, 10,000 g, 4°C) and supernatant was collected.

Metabolite analyses by mass spectrometry

All extracted samples were then subjected to LC/MS analysis as previously described[14]. Metabolite extracts were loaded onto a Luna- HILIC column (Phenomenex) using an UltiMate-3000 TPLRS LC with 10% mobile phase A (20 mM ammonium acetate and 20 mM ammonium hydroxide in water) and 90% mobile phase B (10 mM ammonium hydroxide in 75:25 v/v acetonitrile/methanol). A 10 min linear gradient to 99% mobile phase A was used to separate metabolites. Subsequent analysis was carried out using a QExactive HF-X mass spectrometer (Thermo Fisher Scientific). Negative and positive ion modes were used with full scan analysis over m/z 70-750 m/z at 60,000 resolution, 1e6 AGC, and 100 ms maximum ion accumulation time. Additional MS settings were: ion spray voltage, 3.8 kV; capillary temperature, 350°C; probe heater temperature, 320°C; sheath gas, 50; auxiliary gas, 15; and S-lens RF level 40. Targeted

processing of a subset of known metabolites and isotopologues was conducted using TraceFinder software version 4.1 (Thermo Fisher Scientific). Compound identities were confirmed using reference standards. In all case metabolite abundance was normalized using internal standards and relative changes were assessed by comparison with metabolite extracted from the same sample type (i.e., tissue, IF, plasma).

Human exercise study protocol

After three days on the control diet, subjects ingested a light standardized breakfast (1.6 MJ) at 6 A.M at home. Subjects arrived at the laboratory at 8 A.M, and after 10-15 min of supine rest, teflon catheters were inserted into the femoral artery in one leg and the femoral vein of the other leg under local anesthesia. After continued supine rest, basal blood samples were obtained from the femoral artery and vein at 10 A.M (0 min). Subjects then initiated a 60 min exercise bout on the Monark Ergomedic 839E bicycle ergometer at 67 ± 1% of maximal oxygen uptake (VO2max). VO2 peak was determined by an incremental test performed on a bike ergometer (Monark) at least 1 week prior to the experiment. Femoral arterial and femoral venous samples were collected simultaneously during exercise at 20, 40 and 60 min and again after 10 and 120 min of resting supine recovery without food intake. Femoral arterial blood flow at rest was measured by high frequency 12-3 MHz linear array transducer in Power Doppler mode interfaced to an Affiniti70 ultrasound machine (Phillips Ultrasound). During exercise, leg blood flow was estimated based on pulmonary oxygen uptake and the A-V difference for oxygen as described[55]. The pulmonary oxygen consumption was measured using a MasterScreen CPX system (Becton).

Euglycemic hyperinsulinemic clamp

Two hours after completion of the exercise trial, a 2 h euglycemic, hyperinsulinemic clamp was initiated. Subjects were clamped at their individual ambient plasma glucose level obtained prior to initiation of the insulin infusion. Insulin was infused at 1.4 $mU.kg^{-1}.min^{-1}$ resulting in a plasma insulin concentration ∼ 100 μU/ml. Plasma glucose concentration was measured every ~7 min

and a variable glucose infusion (20% Fresenius Kabi, SE) into a forearm vein was adjusted to clamp euglycaemia as previously described[56]. Insulin sensitivity was calculated as the glucose infusion rate over the last 30 min of the 120 min clamp.

Human blood sample preparation

Blood was sampled in heparinized syringes and transferred to EDTA-containing tubes and centrifuged at 4°C at 3000 g for 5 min. Plasma was aspirated, frozen, and stored at –80°C until analysis.

Acute muscle cell hypoxia experiments

C2C12 myoblasts were seeded at a density of 80,000 cells per well, 24 h prior to use. A minimal media was made consisting of 8.3 g/L DMEM, 4 mM L-glutamine, 1 mM pyruvate, 10 mM glucose, and 10 mM HEPES. Media was place in a sealed hypoxic chamber set to 0.1% oxygen tension, 24 h prior to use. On the day of the experiment, cells were placed in the hypoxic chamber for 2 h and previously degassed media was added to each well. After the 2 h, media from each well was collected inside the chamber, and snap frozen for metabolomic analysis.

Intracellular pH modulation

Pharmacological acidification of intracellular pH in C2C12 cells was achieved by acute inhibition of mitochondrial oxidative phosphorylation with 100 nM atpenin A5 (Cayman Chemical) and 0.5 mM antimycin A (Sigma Aldrich) for 1 h and 2 h, respectively. 100 µM monensin (Sigma Aldrich) were added 1h before administration of atpenin A5 or hypoxia to prevent cellular acidification. Intracellular pH acidification by extracellular equilibration was achieved as previously described[57]. Briefly, cells were incubated with pH 6.4 medium supplemented with 30 mM NH_4Cl and 10 µM 5-(N-ethyl-N-isopropyl) amiloride (EIPA) for 15 min, followed by reincubation in pH 6.4 medium with 10 µM EIPA alone for 4 hours.

Intracellular pH measurement

Intracellular pH was determined using the ratiometric fluorescent intracellular pH probe BCECF-AM (Invitrogen)[58]. Briefly, cells were loaded with BCECF (1 mM) for 30 min at 37°C. We used dual-excitation ratio of 480 nm and 440 nm and fixed emission at 535 nm to measure changes in BCECF-AM fluorescence. A calibration curve of the intracellular pH response in terms of the ratio of fluorescence intensities was performed using the high K^+ nigericin technique.

MCT1 inhibition

Pharmacological inhibition of MCT1 in C2C12 cells was achieved by preincubation with 5 mM α-cyano-4-hydroxycinnamic acid, 100 nM AZD 3965, and 100 nM ARC155858 for 30 min, followed by hypoxia or acidification of intracellular pH experiments

Muscle cell siRNA

Opti-MEM media (Thermo Fisher Scientific) was incubated with lipofectamine (Life Technologies) for 10 min at room temperature. In a separate 1.5 mL tube, Opti-MEM media was incubated with 2 uL of siRNA (10 µM stock; Sigma Aldrich) for 5 min. The lipofectamine mixture was added dropwise to the siRNA mixture and left to incubate (20 min, room temperature). This final solution was added dropwise to a 12-well plate. C2C12 myoblasts were then added at a density of 40,000 cells/well. The media was changed 24 h later and the cells were used 48 h after plating. Knock-down efficiency was confirmed via qPCR.

Succinate transport assay in *Xenopus laevis* oocytes

Xenopus laevis oocytes were purchased from EcoCyte Bioscience and the transport assay was conducted as previously described[59,60]. Oocytes were injected with MCT1 cRNA (24 ng) prepared by *in vitro* transcription using the mMessage mMachine kit (Thermo Fisher Scientific) from the human MCT1 cloned in the plasmid pcDNA3.1 (GeneScript). Controls were injected with equivalent volume of water. Oocytes were cultured in modified Barth's solution (88 mM NaCl, 1 mM KCl, 0.82 mM $MgSO_4$, 0.4 mM $CaCl_2$, 0.33 mM $Ca(NO_3)_2$, 2.4 mM $NaHCO_3$, 10 mM HEPES, 10 U/ml penicillin, 10 µg/ml streptomycin, pH 7.4) for 3 days. For succinate uptake

measurements, groups of 5 oocytes were incubated in OR2 buffer (82.5 mM NaCl, 2.5 mM KCl, 1 mM $CaCl_2$, 1 mM $MgCl_2$, 1 mM Na_2HPO_4, 5 mM HEPES, pH 6.4 or pH 7.4) containing [U13C] succinate or lactate at different concentrations for 10 min, which we established as the time point for linear kinetics of transport. Inhibition of MCT1 was achieved by incubating oocyte with 100 nM AZD3965 5 min prior to the addition of [U13C] succinate. Oocytes were washed three times in ice cold OR2 buffer, lysed with metabolite extraction buffer, and subjected to LC/MS analysis, as described above.

***Ex vivo* skeletal muscle experiments**

Extensor digitorum longus and soleus muscles were rapidly isolated, transferred to 12 well plates containing DMEM supplemented with 25 mM glucose and maintained at 37°C - adapted from (Campos et al., 2018)[61]. When applicable, muscles were incubated with 10 µM AZD, 100 µM monensin for 30 min with or without 1 µM atpenin A5 for additional 60 min. Following interventions, media from each well was collected and snap frozen for metabolomic analysis.

Muscle tissue proteomics

Muscle tissues were homogenized in 100 mM HEPES pH 8.5, 8 M urea, 2% SDS, 1 p/15 mL protease and phosphatase inhibitors (Thermo Fisher Scientific). The mixture was clarified by centrifugation and the supernatant was subjected to BCA protein concentration measurement and reduced with 5 mM tris(2-carboxyethyl) phosphine (TCEP) and alkylated with 15 mM iodoacetamide. Proteins were then purified using the methanol-chloroform precipitation method and reconstituted in 200 mM EPPS at pH 8.5 and digested by Lys-C and trypsin overnight 1:100 enzyme-to-substrate ratio and an additional 6 h by trypsin the next day. Resulting peptides were labeled by TMT-pro 16plex (Thermo Fisher Scientific) following the SL-TMT protocol[62], and quench by adding 5% hydroxylamine. A ratio-check is then performed by mixing 1% sample from each TMT channel, and the TMT-labeled peptides were evenly mixed based on the ratio-check. The mixture was desalted using Sep-pak cartridges (Waters), dried, and fractionated using an

Agilent 1100 quaternary HPLC system. Peptides were separated using a 50 min linear gradient from 18% to 40% acetonitrile in 10 mM ammonium bicarbonate, pH 8, into a total of 96 fractions that were consolidated into 8. Samples were dried and desalted via StageTip and reconstituted in 5% formic acid and 5% ACN for liquid chromatography tandem mass spectrometry (LC-MS/MS) analysis. The proteomics samples were either analyzed using an Orbitrap Fusion Lumos or an Orbitrap Eclipse mass spectrometer (Thermo Fisher Scientific) coupled with an Easy-nLC 1200 (Thermo Fisher Scientific) ultra-high pressure liquid chromatography (LC) pump were used to analyze the samples. The columns are packed in house with 100 mm inner diameter microcapillary column packed with 40 cm of GP-18 resin (2.6 mm, 200 A, Sepax). A FAIMSPro (Thermo Fisher Scientific) device for FAIMS separation of precursors[63]. The FAIMS device was operated with default settings and multiple compensation voltages (40V/-60V/-80V).

For protein abundance measurements on the Orbitrap Fusion Lumos instrument, samples were analyzed using a single 135 min run with 9%–24% ACN at 500 nL min^{-1} flow rate. Fractionated peptides were injected. Under each FAIMS voltage, the full MS was operated with a scan range 375-1500 m/z at 120,000 resolution in the Orbitrap. Tandem mass spectra (MS2) were matched in real time to targeted proteins[64]. When a peptide match was observed to a targeted protein, a quantitative SPS-MS3 scan was acquired[65]. For protein abundance measurements on the Orbitrap Eclipse instrument with TMT, all samples were analyzed with a 180 min gradient consisting of 2% - 23% ACN, 0.125% FA at 500 nl/min flow rate. Under each FAIMS voltage, peptide ions were collected in data-dependent mode using a mass range of m/z 400 - 1600 using 2 s cycles. Resolution for MS1 was set at 120,000, with standard automatic gain control (AGC) target. Multiply-charged ions were selected and subjected to fragmentation at 35% normalized collisional energy (NCE) for MS2 with a dynamic exclusion of 120 s. Quantification was performed using multinotch SPS-MS3 as described previously (McAlister et al., 2014). For phosphoproteomics, unfractionated samples were analyzed with a 150 min gradient consisting of

2% - 27% ACN, 0.125% FA at 525 nl/min flow rate. The samples were first analyzed with multistage activation (MSA) based on 97.9763 Da neutral loss and quantified using SPSMS3, then analyzed again using high-resolution MS2 as described previously[66]. For label-free quantification, unfractionated samples were analyzed with a 180 min gradient consisting of 2% - 23% ACN, 0.125% FA at 500 nl/min flow rate. Peptide ions were collected in data-dependent mode using a mass range of m/z 400-1600 using 2 s cycles. Each ion is selected for further fragmentation in MS2. Maximum injection time was set to 50 ms and dynamic exclusion was 120 s.

The Comet algorithm[67] was used to search all MS/MS spectra against a database containing sequences of human (*Mus musculus*) proteins downloaded from UniProt (https://www.uniprot.org/). Reversed sequences were appended as decoys for FDR filtering, and common contaminant proteins (e.g., human keratins, trypsin) were included. Peptides were searched using following parameters: 25 ppm precursor mass tolerance; 1.0 Da product ion mass tolerance; fully tryptic digestion; up to three missed cleavages; variable modification: oxidation of methionine (+15.9949); static modifications: TMT (+304.2071) on lysine and peptide N terminus, carboxyamidomethylation (+57.0214637236) on cysteines. The target-decoy method was employed to control the false discovery rate (FDR)[68-70]. To distinguish correct and incorrect peptide identifications, linear discriminant analysis (LDA) was used to control peptide-level FDR to less than 1%. Peptides shorter than six amino acids were discarded. Protein-level FDR was also controlled to 1% and as a result the number of peptide reverse hits were further decreased. Peptides were matched to the least number of proteins. TMT reporter ion signal-to-noise ratios for all quantified peptides matched to the same protein were summed up to report protein abundance. Spectral counts were used to quantify proteins in label-free samples. KEGG pathway GO enrichment analyses were performed using Enrichr (https://amp.pharm.mssm.edu/Enrichr/)[71,72].

Phosphoproteomics

Samples were homogenized using TissueLyser II (QIAGEN) in a lysis buffer containing 50 mM HEPES pH 8.5, 8 M urea, 2% SDS, 150 mM NaCl plus 1X Roche cOmplete protease and PhosStop phosphatase inhibitors. Following a BCA assay to estimate protein concentration, all lysates were reduced with 5 mM TCEP for 30 min at room temperature, then alkylated with 15 mM iodoacetamide for 30 min at room temperature in the dark. Proteins were precipitated by chloroform-methanol precipitation, digested, and 100 µg peptides from each sample were labeled by TMT-pro (Thermo Fisher Scientific) following the SL-TMT. Samples were then combined according to a ratio-check, then desalted using a sep-pak cartridge (Waters). Ten percent of the resulting peptides were used for protein abundance analysis and fractionated using a High-pH fractionation kit (Thermo Fisher Scientiic) into 8 fractions and purified by stagetipping. The rest were subjected to phosphopeptide enrichment using the High-Select Fe-NTA kit[73]. The resulting phosphopeptides were desalted using a stage-tip and analyzed by mass spectrometry. Kinase enrichment analysis was performed using Enrichr (https://amp.pharm.mssm.edu/Enrichr/)[71,72].

Oocyte mass spectrometry

Proteins from control and MCT1 expressing oocytes were extracted and digested as described above. After digestion, peptides from each sample were then purified using stage-tips and 2 µg peptides were analyzed by mass spectrometry.

Isolation of pure cell populations from muscle

The tibialis anterior, gastrocnemius, and quadricep muscles were isolated from each mouse and placed in a 1.5 mL tube containing 500 µL of phenol-free, serum-free DMEM (GIBCO). Tissues were then minced until disintegrated. Minced tissues were further digested (30 min, 37°C) in DMEM containing collagenase VIII (Sigma Aldrich) and dispase (Thermo Fisher Scientific). Tissue homogenate was filtered into a new 50 mL conical using a 70 µM filter and washed with phenol-free DMEM (GIBCO) containing 2% FBS and EDTA (staining buffer). Cells were then centrifuged

(10 min, 1500 rpm, 4°C) and resuspended in staining buffer, twice. Buffer was aspirated and pellet was resuspended in 250 µL of staining buffer containing the following antibodies (Biolegend): CD45 BV605 (1:100), CD31 PE-Cy7 (1:100), CD140a APC (1:50), Sca1 PerCP-Cy5.5 (1:50), and Vcam1 PE (1:100). Cells were incubated for 20 min then washed twice (5 min, 1500 rpm, 4°C) and resuspended in 200 µL of staining buffer. Stained cells were then sorted using a FACS Aria II (Becton Dickinson). Cells were sorted twice to ensure purity.

Immunostaining

Cells were fixed with 100% methanol (chilled at –20°C) for 5 min and then permeabilized with 0.1% Triton in PBS for 15 min. Nonspecific binding was blocked with 2% BSA in PBS at room temperature for 60 min. Incubation with anti-MyHC (1:400; Sigma Aldrich) diluted in PBS with 0.1% BSA was performed overnight at 4°C. Cells were then incubated with Alexa Fluor 488 (Thermo Fisher Scientific) and DAPI (Invitrogen) diluted in PBS for 1 h.

Cell proliferation assay

C2C12 myoblasts were seeded at a density of 40,000 cells per well in a 12 wells plate, 24h prior to use. Cells were then brought into suspension using trypsin, followed by resuspension in fresh medium. Cell suspension was mixed with trypan blue (1:1) and transferred to a hemocytometer. Number of cells was counted 24, 48 and 72 h after the beginning of the experiment.

RNA-Seq analysis

Cell suspensions were stained with antibodies against CD45, CD31, Sca-1, CD140a (PDGFRα), and Vcam1 and sorted using FACS Aria II (Becton Dickson). DAPI was used for cellular viability. The following populations were isolated: hematopoietic ($CD45^+$), endothelial ($CD31^+$), stromal ($CD45^-CD31^-PDGFR\alpha^+Sca\text{-}1^+$), and satellite ($CD45^-CD31^-Sca\text{-}1^-Vcam1^+$). One thousand cells from each population were double-sorted and collected into 5 µL Buffer TCL (QIAGEN) containing 1% beta-mercaptoethanol (Sigma Aldrich). Samples were placed on ice for 5 minutes, transferred to dry ice, and eventually stored at –80°C until submitted for sequencing. Smart-Seq2 libraries

were prepared by the Broad Technology Labs and were sequenced using the Broad Genomics Platform[74]. Transcripts were quantified by the Broad Technology Labs computational pipeline using Cufflinks version 2.2.1[75]. For pathway analysis, differentially expressed genes were defined using the following cutoffs: expression (> 10), fold-change (> 2, WT versus KO), p value (< 0.05), and coefficient of variation (< 0.3). KEGG pathway and GO enrichment analyses were performed using Enrichr (https://amp.pharm.mssm.edu/Enrichr/)[71,72,76,77].

GTT and ITT

For insulin tolerance testing (ITT), 13-week old mice were fasted for 3.5h. At 2 h following initial fasting time, mice were subjected to a single bout of acute treadmill running for 45 min and then were allowed to rest of 45 min. Insulin (0.9 U/kg) was administered i.p. Blood glucose measurements were taken at 0, 15, 30, 60, 90, and 120 min using a glucometer. For glucose tolerance testing (GTT), mice were fasted for 6h and were administered glucose (1 g/kg) i.p. Blood glucose measurements were taken at 0, 15, 30, 60, 90, and 120 min using a glucometer.

RNA *in situ* hybridization

Tissues were fixed overnight in 4% paraformaldehyde at 4°C. Tissues were then washed three times in PBS and stored in 70% ethanol until paraffin embedded. Following embedding, tissues were sectioned into 5 µM thick slices and placed onto superfrost slides. *In situ* hybridization was performed using the RNAscope multiplex v2 assay and 4-plex ancillary kits from ACD. Slides were first deparaffinized by washing in xylene twice (room temperature, 5 min) followed by 2 methanol washes (room temperature, 2 min). Slides were then allowed to dry completely before H_2O_2 treatment (room temperature, 10 min). Slides were subsequently washed twice in dH_2O (room temperature, 1 min). Samples were then incubated in RNAscope 1X Target Retrieval Reagent (100°C, 30 min). Following target retrieval, slides were rinsed in dH_2O and then washed in methanol (room temperature, 3min). Slides were then allowed to dry before RNAscope Protease Plus reagent was applied to each section (40°C, 30 min). All 40°C incubations were

performed in the HybEZ Oven. Slides were washed twice with dH_2O. Following washes, RNAscope probes for desmin, pax7, pdgfrα, and SUCNR1 were administered to each section (40°C, 2 h). Slides were then washed twice with 1X Wash Buffer (room temperature, 2 min). Amp 1 was then applied to each section (40°C, 30 min). The slides were then washed twice with wash buffer (room temperature, 2min). These steps were repeated with Amp 2 (40°C, 30 min) and Amp 3 (40°C, 15 min). HRP-C1 reagent was then applied to each section (40°C, 15 min) followed by two washes (RT, 2 min). Opal 520 fluorophore was applied (1:750, 40°C, 30 min). Slides were washed twice and then HRP blocker was applied to each section (40°C, 15 min). These steps were repeated for HRP-C2 using opal 570, HRP-C3 using opal 620, and HRP-C4 using opal 690. All opal dyes were diluted 1:750 using TSA buffer. Samples were then mounted using ProLong Gold Antifade Mountant and allowed to dry overnight. Samples were then imaged using a fluorescent microscope. Colocalization analysis was performed in Fiji using the Coloc2 plugin for determination of the Manders' colocalization coefficient.

Resistance training protocol

A resistance training wheel was created by attaching brass spacers to a standard running wheel as previously described[78]. Twelve-week old mice were singly housed and half of them were placed in cages containing a running wheel for 3 weeks. Wheels were weighted to 1 g of resistance at the start of the experiment and was increased by 1 g/week till a final weight of 3 g was reached. Distance run was continually recorded (Starr Life) and grip strength was assessed weekly in both trained and untrained mice using a force meter. Lean and fat mass were measured by MRI at the beginning and at the end of the 3 weeks. Mice were sacrificed after 3 weeks and the tibialis anterior and gastrocnemius were harvested for further processing.

iDISCO three-dimensional muscle imaging

Tibialis anterior and gastrocnemius muscles were fixed in 4% paraformaldehyde (Thermo Fisher Scientific). Muscles were then processed for whole-tissue clearing and imaging, using the iDISCO

method[79]. All washes were performed in a 2 mL tube with end-over-end shaking. Tissues were first dehydrated by washing in a series of methanol/H_2O buffers: 20%, 40%, 60%, 80%, 100%, 100% (1 h each, room temperature). Samples were chilled (4°C) and then incubated in 66% dichloromethane (Sigma Aldrich)/ 33% methanol (o/n, room temperature). Tissues were then washed twice in 100% methanol (room temperature) and then chilled (4°C). Samples were bleached in fresh 5% H_2O_2 (Sigma Aldrich) diluted in methanol (o/n, 4°C). Tissues were then rehydrated by washing in a series of methanol/H2O buffers: 80%, 60%, 40%, 20%, PBS (1 h each, room temperature). Samples were then washed twice (1 h, room temperature) with PBS containing 2% Triton X-100 (Sigma Aldrich). To stain the whole tissue, samples were permeabilized (2 days, 37°C) using PBS containing 2% Triton X-100, glycine (Sigma Aldrich), and DMSO (Sigma Aldrich). Exogenous binding of antibodies was prevented by incubating samples in a blocking solution containing PBS, Triton X-100, DMSO, and FBS (2 days, 37°C). Following blocking, half of the samples were incubated with a TUBB3 antibody (1:2000, Biolegend) and the other half were incubated with a CD31 antibody (1:250, Biolegend) for 4 days at 37°C. Tissues were then washed 5 times with PBS containing 2% Tween-20 (Sigma Aldrich) and heparin (Sigma Aldrich). Samples were then incubated with secondary antibody (1:500, Invitrogen) for 4 days at 37°C. Tissues were then again washed 5 times with PBS containing 2% Tween-20. Samples were dehydrated by washing in a series of methanol/H_2O buffers: 20%, 40%, 60%, 80%, 100%, 100% (1 h each, room temperature). Following dehydration, tissues were incubated in 66% dichloromethane/ 33% methanol (3 h, room temperature). Samples were then washed twice with 100% dichloromethane (15 min each, room temperature). Finally, tissues were cleared using dibenzyl ether (Sigma Aldrich). Whole tissues were then imaged at 0.66x magnification using a light sheet microscope. 3D reconstructions and renderings were made using the software Imaris (Bitplane). Further imaging analysis was performed using ImageJ.

Gene expression analysis

Stromal, endothelial, immune, and satellite cells were isolated from hindlimb muscles as previously described and collected into RLT buffer (QIAGEN) for RNA extraction. RNA was further purified using the RNAeasy Micro Kit (QIAGEN). RNA was then quantified using a Nanodrop 2000 UV-visible spectrophotometer. 100 ng of RNA was used to synthesize cDNA via reverse-transcription polymerase chain reaction (RT-PCR) using a high-capacity cDNA reverse transcription kit (Thermo Fisher Scientific). cDNA was then diluted in a 1:4 ratio cDNA to water and used for real-time quantitative PCR (qPCR) analysis. qPCR reactions were performed in 384-well plates using GoTaq qPCR Master Mix (Promega). Samples were run on a Quant Studio 6 Flex Real-Time PCR machine (Applied Biosystems). Relative abundance of Sucnr1 was calculated by the ΔCt method using GAPDH as an endogenous control.

Quantification and Statistical Analysis

Data analysis was performed in Excel, R, and Prism as described above. All data (unless otherwise noted) was presented as mean ± SEM. Unless otherwise noted, P values were calculated using a two-tailed Student's t test for pairwise comparisons and one-way ANOVA for multiple comparisons involving a single variable. * $p < 0.05$; ** $p < 0.01$; *** $p < 0.005$. Details of statistical analyses and n values are found in the Figure Legends. For *in vivo* experiments, n indicates number of mice or humans. For all other experiments, n indicates biological replicates.

References

1. Spinelli, J.B.*, et al.* Metabolic recycling of ammonia via glutamate dehydrogenase supports breast cancer biomass. *Science* **358**, 941-946 (2017).
2. Sullivan, M.R.*, et al.* Quantification of microenvironmental metabolites in murine cancers reveals determinants of tumor nutrient availability. *Elife* **8**(2019).
3. Martinez-Reyes, I. & Chandel, N.S. Mitochondrial TCA cycle metabolites control physiology and disease. *Nat Commun* **11**, 102 (2020).
4. Ghosh, S., Golbidi, S., Werner, I., Verchere, B.C. & Laher, I. Selecting exercise regimens and strains to modify obesity and diabetes in rodents: an overview. *Clin Sci (Lond)* **119**, 57-74 (2010).
5. Hawley, J.A., Hargreaves, M., Joyner, M.J. & Zierath, J.R. Integrative biology of exercise. *Cell* **159**, 738-749 (2014).

6. Kemi, O.J., Loennechen, J.P., Wisloff, U. & Ellingsen, O. Intensity-controlled treadmill running in mice: cardiac and skeletal muscle hypertrophy. *J Appl Physiol (1985)* **93**, 1301-1309 (2002).
7. Sylow, L., Kleinert, M., Richter, E.A. & Jensen, T.E. Exercise-stimulated glucose uptake - regulation and implications for glycaemic control. *Nat Rev Endocrinol* **13**, 133-148 (2017).
8. Henriquez-Olguin, C*., et al.* Cytosolic ROS production by NADPH oxidase 2 regulates muscle glucose uptake during exercise. *Nat Commun* **10**, 4623 (2019).
9. Kleinert, M*., et al.* Exercise increases circulating GDF15 in humans. *Mol Metab* **9**, 187-191 (2018).
10. Kiens, B., Essen-Gustavsson, B., Christensen, N.J. & Saltin, B. Skeletal muscle substrate utilization during submaximal exercise in man: effect of endurance training. *J Physiol* **469**, 459-478 (1993).
11. Ehinger, J.K*., et al.* Cell-permeable succinate prodrugs bypass mitochondrial complex I deficiency. *Nat Commun* **7**, 12317 (2016).
12. Hems, R., Stubbs, M. & Krebs, H.A. Restricted permeability of rat liver for glutamate and succinate. *Biochem J* **107**, 807-815 (1968).
13. MacDonald, M.J., Fahien, L.A., Mertz, R.J. & Rana, R.S. Effect of esters of succinic acid and other citric acid cycle intermediates on insulin release and inositol phosphate formation by pancreatic islets. *Arch Biochem Biophys* **269**, 400-406 (1989).
14. Mills, E.L*., et al.* Accumulation of succinate controls activation of adipose tissue thermogenesis. *Nature* **560**, 102-106 (2018).
15. Hochachka, P.W., Owen, T.G., Allen, J.F. & Whittow, G.C. Multiple end products of anaerobiosis in diving vertebrates. *Comp Biochem Physiol B* **50**, 17-22 (1975).
16. Hochachka, P.W. & Dressendorfer, R.H. Succinate accumulation in man during exercise. *Eur J Appl Physiol Occup Physiol* **35**, 235-242 (1976).
17. Murphy, M.P. & O'Neill, L.A.J. Krebs Cycle Reimagined: The Emerging Roles of Succinate and Itaconate as Signal Transducers. *Cell* **174**, 780-784 (2018).
18. Hagberg, H. Intracellular pH during ischemia in skeletal muscle: relationship to membrane potential, extracellular pH, tissue lactic acid and ATP. *Pflugers Arch* **404**, 342-347 (1985).
19. Robergs, R.A., Ghiasvand, F. & Parker, D. Biochemistry of exercise-induced metabolic acidosis. *Am J Physiol Regul Integr Comp Physiol* **287**, R502-516 (2004).
20. Sahlin, K., Edstrom, L., Sjoholm, H. & Hultman, E. Effects of lactic acid accumulation and ATP decrease on muscle tension and relaxation. *Am J Physiol* **240**, C121-126 (1981).
21. Bright, C.M. & Ellis, D. Intracellular pH changes induced by hypoxia and anoxia in isolated sheep heart Purkinje fibres. *Exp Physiol* **77**, 165-175 (1992).
22. Lin, H.J., Herman, P. & Lakowicz, J.R. Fluorescence lifetime-resolved pH imaging of living cells. *Cytometry A* **52**, 77-89 (2003).
23. Markovich, D. & Murer, H. The SLC13 gene family of sodium sulphate/carboxylate cotransporters. *Pflugers Arch* **447**, 594-602 (2004).
24. Halestrap, A.P. The monocarboxylate transporter family--Structure and functional characterization. *IUBMB Life* **64**, 1-9 (2012).
25. Broer, S*., et al.* Characterization of the high-affinity monocarboxylate transporter MCT2 in Xenopus laevis oocytes. *Biochem J* **341 (Pt 3)**, 529-535 (1999).
26. Nancolas, B., Sessions, R.B. & Halestrap, A.P. Identification of key binding site residues of MCT1 for AR-C155858 reveals the molecular basis of its isoform selectivity. *Biochem J* **466**, 177-188 (2015).
27. Broer, S*., et al.* Characterization of the monocarboxylate transporter 1 expressed in Xenopus laevis oocytes by changes in cytosolic pH. *Biochem J* **333 (Pt 1)**, 167-174 (1998).

28. He, W.*, et al.* Citric acid cycle intermediates as ligands for orphan G-protein-coupled receptors. *Nature* **429**, 188-193 (2004).
29. Mills, E. & O'Neill, L.A. Succinate: a metabolic signal in inflammation. *Trends Cell Biol* **24**, 313-320 (2014).
30. Ariza, A.C., Deen, P.M. & Robben, J.H. The succinate receptor as a novel therapeutic target for oxidative and metabolic stress-related conditions. *Front Endocrinol (Lausanne)* **3**, 22 (2012).
31. Wang, T.*, et al.* Succinate induces skeletal muscle fiber remodeling via SUNCR1 signaling. *EMBO Rep* **20**, e47892 (2019).
32. Wang, F.*, et al.* RNAscope: a novel in situ RNA analysis platform for formalin-fixed, paraffin-embedded tissues. *J Mol Diagn* **14**, 22-29 (2012).
33. Wang, Z.*, et al.* Automated quantitative RNA in situ hybridization for resolution of equivocal and heterogeneous ERBB2 (HER2) status in invasive breast carcinoma. *J Mol Diagn* **15**, 210-219 (2013).
34. Wang, K.*, et al.* Neuronal, stromal, and T-regulatory cell crosstalk in murine skeletal muscle. *Proc Natl Acad Sci U S A* **117**, 5402-5408 (2020).
35. Hisamatsu, D., Ohno-Oishi, M., Nakamura, S., Mabuchi, Y. & Naka-Kaneda, H. Growth differentiation factor 6 derived from mesenchymal stem/stromal cells reduces age-related functional deterioration in multiple tissues. *Aging (Albany NY)* **8**, 1259-1275 (2016).
36. Roemers, P.*, et al.* Burrowing as a novel voluntary strength training method for mice: A comparison of various voluntary strength or resistance exercise methods. *J Neurosci Methods* **300**, 112-126 (2018).
37. Sanes, J.R. The basement membrane/basal lamina of skeletal muscle. *J Biol Chem* **278**, 12601-12604 (2003).
38. Phieler, J., Garcia-Martin, R., Lambris, J.D. & Chavakis, T. The role of the complement system in metabolic organs and metabolic diseases. *Semin Immunol* **25**, 47-53 (2013).
39. Folland, J.P. & Williams, A.G. The adaptations to strength training : morphological and neurological contributions to increased strength. *Sports Med* **37**, 145-168 (2007).
40. Gabriel, D.A., Kamen, G. & Frost, G. Neural adaptations to resistive exercise: mechanisms and recommendations for training practices. *Sports Med* **36**, 133-149 (2006).
41. Buller, A.J., Eccles, J.C. & Eccles, R.M. Interactions between motoneurones and muscles in respect of the characteristic speeds of their responses. *J Physiol* **150**, 417-439 (1960).
42. Barker, D. & Saito, M. Autonomic innervation of receptors and muscle fibres in cat skeletal muscle. *Proc R Soc Lond B Biol Sci* **212**, 317-332 (1981).
43. Beitzel, F.*, et al.* Beta2-adrenoceptor agonist fenoterol enhances functional repair of regenerating rat skeletal muscle after injury. *J Appl Physiol (1985)* **96**, 1385-1392 (2004).
44. Richter, E.A., Mikines, K.J., Galbo, H. & Kiens, B. Effect of exercise on insulin action in human skeletal muscle. *J Appl Physiol (1985)* **66**, 876-885 (1989).
45. De Vadder, F.*, et al.* Microbiota-Produced Succinate Improves Glucose Homeostasis via Intestinal Gluconeogenesis. *Cell Metab* **24**, 151-157 (2016).
46. de Vadder, F. & Mithieux, G. Gut-brain signaling in energy homeostasis: the unexpected role of microbiota-derived succinate. *J Endocrinol* **236**, R105-R108 (2018).
47. Littlewood-Evans, A.*, et al.* GPR91 senses extracellular succinate released from inflammatory macrophages and exacerbates rheumatoid arthritis. *J Exp Med* **213**, 1655-1662 (2016).
48. Peruzzotti-Jametti, L.*, et al.* Macrophage-Derived Extracellular Succinate Licenses Neural Stem Cells to Suppress Chronic Neuroinflammation. *Cell Stem Cell* **22**, 355-368 e313 (2018).

49. Deen, P.M. & Robben, J.H. Succinate receptors in the kidney. *J Am Soc Nephrol* **22**, 1416-1422 (2011).
50. Andrienko, T.N., Pasdois, P., Pereira, G.C., Ovens, M.J. & Halestrap, A.P. The role of succinate and ROS in reperfusion injury - A critical appraisal. *J Mol Cell Cardiol* **110**, 1-14 (2017).
51. Molnar, T.*, et al.* gamma-Hydroxybutyrate binds to the synaptic site recognizing succinate monocarboxylate: a new hypothesis on astrocyte-neuron interaction via the protonation of succinate. *J Neurosci Res* **86**, 1566-1576 (2008).
52. Prag, H.A.*, et al.* Mechanism of succinate efflux upon reperfusion of the ischaemic heart. *Cardiovasc Res* **117**, 1188-1201 (2021).
53. Ramesh, M.*, et al.* Mitophagy protects against statin-mediated skeletal muscle toxicity. *FASEB J* **33**, 11857-11869 (2019).
54. Sampath, S.C.*, et al.* Induction of muscle stem cell quiescence by the secreted niche factor Oncostatin M. *Nat Commun* **9**, 1531 (2018).
55. Jorfeldt, L. & Wahren, J. Leg blood flow during exercise in man. *Clin Sci* **41**, 459-473 (1971).
56. DeFronzo, R.A., Tobin, J.D. & Andres, R. Glucose clamp technique: a method for quantifying insulin secretion and resistance. *Am J Physiol* **237**, E214-223 (1979).
57. Nadtochiy, S.M.*, et al.* Acidic pH Is a Metabolic Switch for 2-Hydroxyglutarate Generation and Signaling. *J Biol Chem* **291**, 20188-20197 (2016).
58. Khacho, M.*, et al.* Acidosis overrides oxygen deprivation to maintain mitochondrial function and cell survival. *Nat Commun* **5**, 3550 (2014).
59. Broer, S.*, et al.* Comparison of lactate transport in astroglial cells and monocarboxylate transporter 1 (MCT 1) expressing Xenopus laevis oocytes. Expression of two different monocarboxylate transporters in astroglial cells and neurons. *J Biol Chem* **272**, 30096-30102 (1997).
60. Markovich, D. Expression cloning and radiotracer uptakes in Xenopus laevis oocytes. *Nat Protoc* **3**, 1975-1980 (2008).
61. Campos, J.C.*, et al.* Exercise prevents impaired autophagy and proteostasis in a model of neurogenic myopathy. *Sci Rep* **8**, 11818 (2018).
62. Navarrete-Perea, J., Yu, Q., Gygi, S.P. & Paulo, J.A. Streamlined Tandem Mass Tag (SL-TMT) Protocol: An Efficient Strategy for Quantitative (Phospho)proteome Profiling Using Tandem Mass Tag-Synchronous Precursor Selection-MS3. *J Proteome Res* **17**, 2226-2236 (2018).
63. Schweppe, D.K.*, et al.* Characterization and Optimization of Multiplexed Quantitative Analyses Using High-Field Asymmetric-Waveform Ion Mobility Mass Spectrometry. *Anal Chem* **91**, 4010-4016 (2019).
64. Schweppe, D.K.*, et al.* Full-Featured, Real-Time Database Searching Platform Enables Fast and Accurate Multiplexed Quantitative Proteomics. *J Proteome Res* **19**, 2026-2034 (2020).
65. McAlister, G.C.*, et al.* MultiNotch MS3 enables accurate, sensitive, and multiplexed detection of differential expression across cancer cell line proteomes. *Anal Chem* **86**, 7150-7158 (2014).
66. Schweppe, D.K., Rusin, S.F., Gygi, S.P. & Paulo, J.A. Optimized Workflow for Multiplexed Phosphorylation Analysis of TMT-Labeled Peptides Using High-Field Asymmetric Waveform Ion Mobility Spectrometry. *J Proteome Res* **19**, 554-560 (2020).
67. Eng, J.K., Jahan, T.A. & Hoopmann, M.R. Comet: an open-source MS/MS sequence database search tool. *Proteomics* **13**, 22-24 (2013).

68. Elias, J.E. & Gygi, S.P. Target-decoy search strategy for increased confidence in large-scale protein identifications by mass spectrometry. *Nat Methods* **4**, 207-214 (2007).
69. Huttlin, E.L.*, et al.* A tissue-specific atlas of mouse protein phosphorylation and expression. *Cell* **143**, 1174-1189 (2010).
70. Peng, J., Elias, J.E., Thoreen, C.C., Licklider, L.J. & Gygi, S.P. Evaluation of multidimensional chromatography coupled with tandem mass spectrometry (LC/LC-MS/MS) for large-scale protein analysis: the yeast proteome. *J Proteome Res* **2**, 43-50 (2003).
71. Chen, E.Y.*, et al.* Enrichr: interactive and collaborative HTML5 gene list enrichment analysis tool. *BMC Bioinformatics* **14**, 128 (2013).
72. Kuleshov, M.V.*, et al.* Enrichr: a comprehensive gene set enrichment analysis web server 2016 update. *Nucleic Acids Res* **44**, W90-97 (2016).
73. Paulo, J.A., Navarrete-Perea, J., Erickson, A.R., Knott, J. & Gygi, S.P. An Internal Standard for Assessing Phosphopeptide Recovery from Metal Ion/Oxide Enrichment Strategies. *J Am Soc Mass Spectrom* **29**, 1505-1511 (2018).
74. Picelli, S.*, et al.* Full-length RNA-seq from single cells using Smart-seq2. *Nat Protoc* **9**, 171-181 (2014).
75. Trapnell, C.*, et al.* Differential gene and transcript expression analysis of RNA-seq experiments with TopHat and Cufflinks. *Nat Protoc* **7**, 562-578 (2012).
76. Eden, E., Lipson, D., Yogev, S. & Yakhini, Z. Discovering motifs in ranked lists of DNA sequences. *PLoS Comput Biol* **3**, e39 (2007).
77. Eden, E., Navon, R., Steinfeld, I., Lipson, D. & Yakhini, Z. GOrilla: a tool for discovery and visualization of enriched GO terms in ranked gene lists. *BMC Bioinformatics* **10**, 48 (2009).
78. Call, J.A., McKeehen, J.N., Novotny, S.A. & Lowe, D.A. Progressive resistance voluntary wheel running in the mdx mouse. *Muscle Nerve* **42**, 871-880 (2010).
79. Renier, N.*, et al.* iDISCO: a simple, rapid method to immunolabel large tissue samples for volume imaging. *Cell* **159**, 896-910 (2014).

Chapter 3

Monocarboxylate transporters facilitate succinate uptake into brown adipocytes

Citation. This chapter has been assembled with minor modification from the following manuscript:

Monocarboxylate transporters facilitate succinate uptake into brown adipocytes

bioRxiv, (2023).

Anita Reddy[1,2]*, Sally Winther[3]*, Nhien Tran[4,5], Haopeng Xiao[1,2], Josefine Jakob[1,2], Ryan Garrity[1], Arianne Smith[1], Martha Ordonez[1,2], Dina Laznik-Bogoslavski[1], Evanna L. Mills[4,5], and Edward T. Chouchani[1,2,6]

[1] Department of Cancer Biology, Dana-Farber Cancer Institute, Boston, MA, USA

[2] Department of Cell Biology, Harvard Medical School, Boston, MA, USA

[3] Novo Nordisk Foundation Center for Basic Metabolic Research, Faculty of Health and Medical Sciences University of Copenhagen, Copenhagen, Denmark

[4] Department of Cancer Immunology and Virology, Dana-Farber Cancer Institute, Boston, MA, USA

[5] Department of Immunology, Department of Immunology, Harvard Medical School, Boston, MA, USA

[6] Corresponding author

* Equal contribution

Author contributions: A.R and E.T.C. wrote the manuscript. S.W. conducted and designed all 14C4-succinate experiments. E.L.M, R.G, and S.W performed the in vivo tracing experiment following acute MCT inhibition using AZD3965. A.R. and N.T. conducted in vivo tracing experiment in MCT1 KO mice. H.X. performed proteomics to confirm MCT1 KO using BAT harvested from MCT1 KO mice. J.J. and R.G. conducted in vitro 13C4-succinate tracing experiment following treatment with AZD3965. A.R. performed imaging experiments to determine cytosolic pH. A.R. performed in vitro 13C4-succinate tracing experiment with NE. E.T.C, S.W., E.L.M, and A.R. oversaw the experiments and data analysis. All authors edited the manuscript.

Acknowledgements: This work was supported by The Novo Nordisk Foundation Center for Basic Metabolic Research is an independent Research Center, based at the University of Copenhagen, and partially funded by an unconditional donation from the Novo Nordisk Foundation (Grant number NNF18CC0034900), a fellowship from the Novo Nordisk Foundation (NNF18OC0032380) (S.W), the Claudia Adams Barr Program (E.T.C), the Lavine Family Fund (E.T.C), the Pew Charitable Trust (E.T.C), NIH DK123095 (E.T.C), NIH AG071966 (E.T.C), The Smith Family Foundation (E.T.C), and the American Federation for Aging Research (E.T.C).

Abstract

Uptake of circulating succinate by brown adipose tissue (BAT) and beige fat elevates whole-body energy expenditure, counteracts obesity, and antagonizes systemic tissue inflammation in mice. The plasma membrane transporters that facilitate succinate uptake in these adipocytes remain undefined. Here we elucidate a mechanism underlying succinate import into BAT via monocarboxylate transporters (MCTs). We show that succinate transport is strongly dependent on the proportion of it present in the monocarboxylate form. MCTs facilitate monocarboxylate succinate uptake, which is promoted by alkalinization of the cytosol driven by adrenoreceptor stimulation. In brown adipocytes, we show that MCT1 primarily facilitates succinate import. In male mice, we show that both acute pharmacological inhibition of MCT1 and congenital depletion of MCT1 decrease succinate uptake into BAT and consequent catabolism. In sum, we define a mechanism of succinate uptake in BAT that underlies its protective activity in mouse models of metabolic disease.

Introduction

Beyond its role as a tricarboxylic acid (TCA) cycle intermediate, succinate is now known to regulate several physiological and pathophysiological processes[1-3]. Succinate elicits biological adaptation via its accumulation and subsequent modulation of intracellular processes[1]. One consequence of accumulated succinate arises from its capacity to contribute reducing power to the mitochondrial respiratory chain, and in doing so to regulate the production of superoxide and hydrogen peroxide[4]. Accumulated succinate is also readily released from mitochondria and can regulate cellular adaptation through inhibition of alpha-ketoglutarate (αKG) dependent

dioxygenases, a large family of enzymes with broad roles ranging from oxygen sensing, fatty acid catabolism, and regulation of the epigenome[5].

Additionally, accumulated succinate is now well appreciated to regulate physiology through its secretion and ligation of the G-protein coupled receptor, succinate receptor 1 (SUCNR1)[6-12]. Recent studies have shown that succinate is selectively released from cells via the plasma membrane monocarboxylate transporter (MCT)[1,8,13-15]. This process is initiated by intracellular acidification, for example in response to acute metabolic perturbations such as muscle exercise or tissue hypoxia[8,14]. Acute acidification causes a portion of the intracellular succinate pool to become protonated, converting the metabolite from a dicarboxylate to a monocarboxylate, which renders it a transport substrate for MCT1. Following secretion, succinate signaling via SUCNR1 has been shown to regulate numerous physiological processes, including increased innervation following exercise training and cytokine production by macrophages[7,8,10,12,16-20].

A major factor that antagonizes SUCNR1 signaling by succinate is the rate of succinate sequestration by tissues following its release. SUCNR1 activation occurs at a half-maximum effective concentration (EC50) between 28–56 μM, with ~99% responses achieved at 200 μM[21]. Extracellular succinate readily achieves these concentrations following release[7,8,11,22,23]. Also, depending on the physiological context, extracellular succinate levels can rapidly renormalize, or remain chronically elevated[7,8,11,23]. The varied kinetics and fates of circulating succinate coincide with distinct physiological outcomes. For example, pulsatile elevation of extracellular succinate is associated with physiological remodeling of muscle tissue following exercise, while chronic elevation of extracellular succinate is linked to pro-fibrotic and pro-inflammatory signaling[7,8,11,23,24].

Brown adipose tissue (BAT) can sequester extracellular succinate[7,25]. Uptake of succinate by BAT is linked to protection against various aspects of metabolic disease. Succinate uptake by BAT promotes uncoupling protein 1 (UCP1)-dependent thermogenesis, energy expenditure, and

protection against obesity and glucose intolerance in mice[25]. Additionally, sequestration of extracellular succinate by BAT antagonizes chronic SUCNR1 mediated liver inflammation and fibrosis in the context of non-alcoholic fatty liver disease (NAFLD)[7]. While succinate uptake into BAT results in beneficial systemic effects, little is known about the mechanism of succinate transport in BAT or how it is regulated. Here we identify a key role for MCTs and pH-gradient facilitated succinate uptake.

Results

Brown adipocytes import extracellular succinate in a pH dependent manner.

We first used 14C4-succinate to characterize the properties of the succinate transport system in differentiated mouse primary brown adipocytes. As expected, externally applied succinate resulted in concentration-dependent transport across the range of 0.01–20 mM extracellular succinate (**figure 3.1a**). Succinate transport occurred at a maximal rate of 800 pmol/mg protein/min (**figure 3.1a**). We next monitored the fate of internalized succinate by tracking uptake and metabolism of $^{13}C_4$-succinate using mass spectrometry (**figure 3.1b**). At external concentrations as low as 10 μM, uptake and mitochondrial metabolism of extracellularly applied succinate occurred rapidly, with $^{13}C_4$-fumarate and $^{13}C_4$-malate accumulating within cells as early as two minutes following application of $^{13}C_4$-succinate (**figure 3.1c**). We observed a comparable capacity for succinate uptake and catabolism in human brown adipocytes, where sequestration and metabolism of 13C4-succinate occurred readily when external concentrations as low as 10 μM were applied (**figure 3.1d**).

Previous work performed in muscle, myotubes, and the ischemic heart showed that decreasing intracellular pH promotes succinate export[8,14]. On this basis, we examined whether succinate uptake into brown adipocytes could be stimulated by decreasing extracellular pH (**figure 3.1e**). We observed an inverse relationship between extracellular pH and the amount of

succinate transported: as extracellular pH lowered, brown adipocytes imported more succinate (**figure 3.1e**). Increased uptake was attributable to elevation in initial linear rate of transport of succinate as extracellular pH lowered (**figure 3.1f**). Next, we monitored whether capacity for brown adipocyte succinate uptake depended on differentiation state. Using primary brown adipocytes, we assessed the ability of pre-adipocytes to transport succinate. Pre-adipocytes exhibited significantly reduced capacity for succinate uptake compared to differentiated brown adipocytes (**figure 3.1g**). Previous work showed BAT preferentially accumulates succinate upon cold exposure[25]. Adrenergic signaling stimulated by norepinephrine (NE) release from sympathetic nerves in BAT is a key signaling event that occurs in response to cold[26-28]. Moreover, previous work has demonstrated cytosolic alkalinization following activation of β-adrenergic signaling[29-31]. In line with this we observed that stimulation of brown adipocytes with NE resulted in a rapid alkalinization of cytosolic pH by ~0.6 pH units. (**figure 3.1h**), which was paralleled by an elevation of local extracellular pH of ~0.8 pH units (**figure 31h**). Based on the ΔpH dependence of succinate export[8,14], we hypothesized that a ΔpH imposed by cytoplasmic alkalinization induced by adrenergic signaling could promote succinate uptake by brown adipocytes. In support of this hypothesis, we observed that upon NE treatment uptake of succinate into brown adipocytes was significantly potentiated (**figure 3.1i**). Taken together these findings indicate that succinate transport occurs at physiological pH but can be enhanced by a ΔpH gradient across the plasma membrane.

Monocarboxylate transporters (MCTs) facilitate succinate uptake in brown adipocytes.

We next sought to determine the protein(s) responsible for mediating succinate uptake in brown adipocytes. We first assessed a role for the canonical transporter of succinate, solute carrier family 13 member 3 (SLC13A3). We tested the relevance of SLC13A3 contribution to succinate uptake at an externally applied pH of 6.5 to ensure high uptake of succinate under the

experimental conditions and maximal dynamic range for measuring putative inhibitory effects.

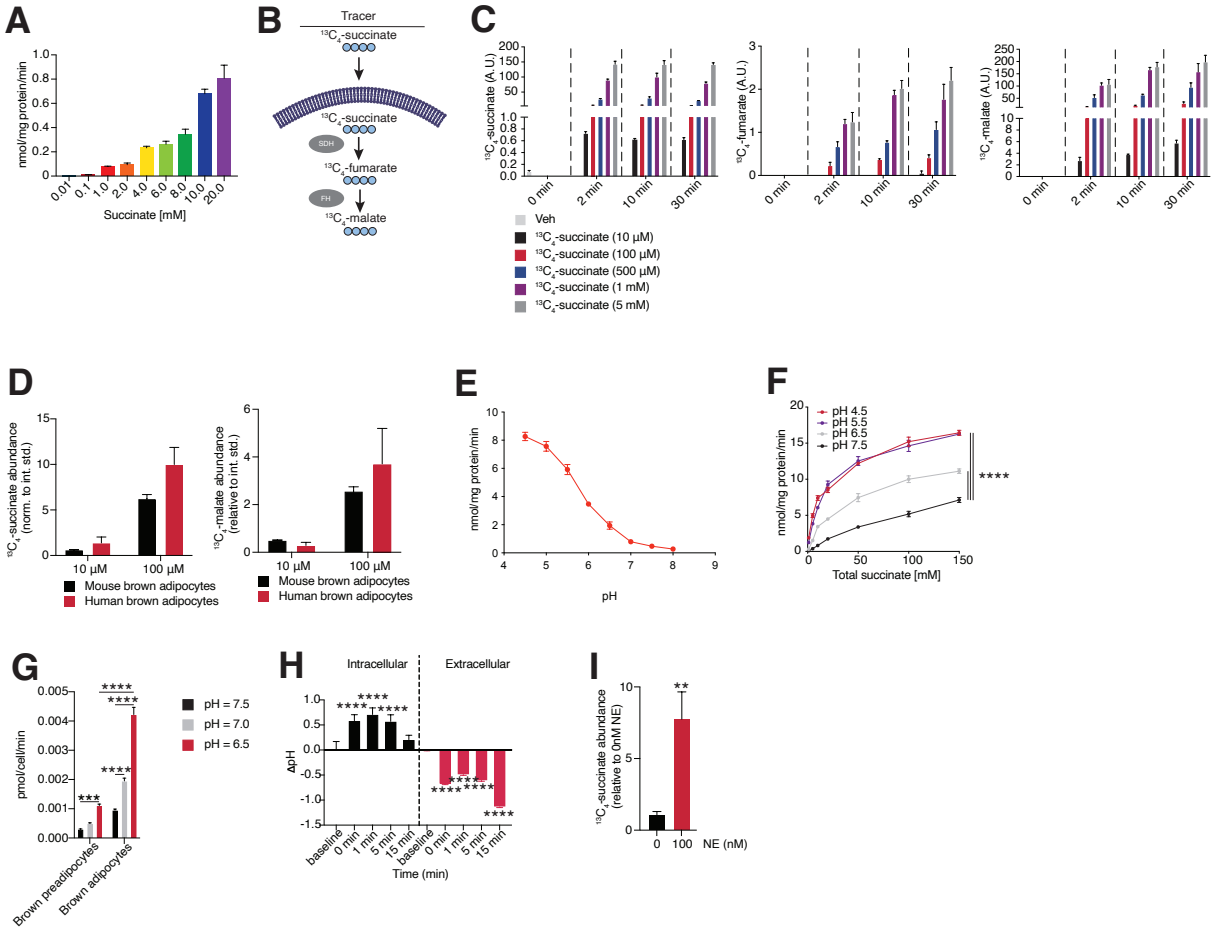


Figure 3.1 | Brown adipocytes import extracellular succinate in a pH dependent manner.

(a) Brown adipocytes were treated with $^{14}C_4$-succinate (pH = 7.45) and uptake was monitored (n = 3). (b) Schematic depicting transport and metabolism of $^{13}C_4$-succinate tracer. (c) Brown adipocytes were treated with $^{13}C_4$-succinate (pH 7.45) and intracellular, relative metabolite abundance was assessed (n = 4). (d) Human (n = 6, pH = 7.0, 15 min) and mouse (n = 4, pH = 7.45, 10 min) brown adipocytes were treated with $^{13}C_4$-succinate. Intracellular, relative metabolite abundance was assessed and normalized to cell number. Mouse data replotted from figure 1c. (e) Cells were treated with $^{14}C_4$-succinate under different media pH conditions and uptake was monitored (n = 3). Brown adipocyte protein concentration was determined by bicinchoninic acid (BCA) assay.

Figure 3.1 | Brown adipocytes import extracellular succinate in a pH dependent manner (cont) (f) Cells were treated with $^{14}C_4$-succinate at indicated concentrations under different media pH conditions, as shown. $^{14}C_4$-succinate uptake was monitored (n = 3). Brown adipocyte protein concentration was determined by BCA assay. (g) Primary brown adipocytes and preadipocytes were treated with $^{14}C_4$-succinate under various media pH conditions, as indicated. $^{14}C_4$-succinate uptake was monitored (n = 3). (h) Cells were stained with intra- (n = 143) or extracellular (n = 151) pH-sensitive dye and were then treated with 1 μM norepinephrine (NE). Images were collected at 0 min, 1 min, 5 min, and 15 min following NE. A baseline image, before NE administration, was also collected. (i) Brown adipocytes were treated with 100 μM $^{13}C_4$-succinate in the presence or absence of 100 nM NE for 2 min. Relative abundance of intracellular $^{13}C_4$-succinate was determined by LC/MS analysis (n = 6).

Selective depletion of SLC13A3 in brown adipocytes had no effect on succinate uptake (**Figure 3.2a**). We next considered the fact that succinate uptake in brown adipocytes is pH-dependent. Succinate is a dicarboxylate with a monocarboxylic pKa of 5.69 and a fully protonated pKa of 4.21 [32]. The monocarboxylic pKa of succinate is much higher than that of other TCA cycle intermediates, rendering this metabolite amenable to protonation at physiological pH [33]. As such, across the pH range 4.5 - 7.5 the proportion of succinate existing in the monocarboxylate form will vary substantially. We examined the relationship between brown adipocyte succinate uptake rate, extracellular pH, and the proportion of succinate existing as a monocarboxylate. This analysis demonstrated a strong relationship between the amount of succinate present in the monocarboxylate form and the rate of succinate sequestration by brown adipocytes (**Figure 3.2b,c**). Taken together, this data strongly suggests that the monocarboxylate form of succinate is the major transported form.

We next examined which small molecule carboxylate transporters are present in brown and beige adipocytes that could explain the basis for transport of monocarboxylic succinate

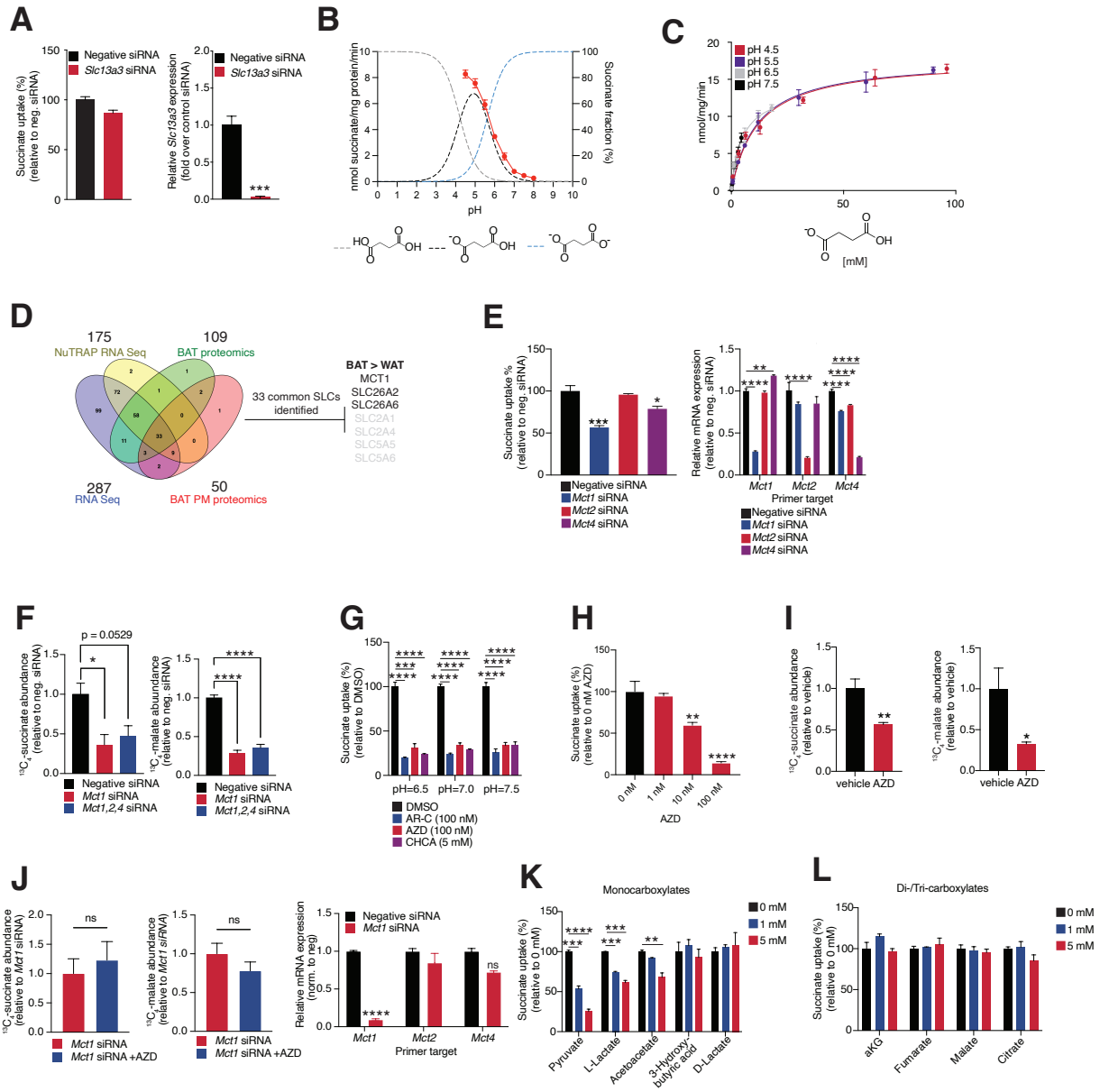


Figure 3.2 | Monocarboxylate transporters (MCTs) facilitate succinate uptake in brown adipocytes. (a) WT and Slc13a3 knockdown cells were treated with $^{14}C_4$-succinate (n = 3) and uptake was monitored. Knockdown was confirmed by qPCR. **(b)** Schematic of figure 1e and succinate pKa curve.

Figure 3.2 | Monocarboxylate transporters (MCTs) facilitate succinate uptake in brown adipocytes (cont.) (c) Rate of $^{14}C_4$-succinate transport determined in figure 1f was recalculated to reflect the concentration of protonated $^{14}C_4$-succinate present. **(d)** Comparative screen to identify potential plasma membrane (PM) transporters of succinate present in brown adipose tissue (BAT). **(e)** MCT knockdown cells were treated with $^{14}C_4$-succinate (pH = 7.0) and uptake was monitored (n = 3). Knockdown was confirmed by qPCR. **(f)** MCT1 and MCT1,2,4 knockdown cells were treated with 10 µM $^{13}C_4$-succinate (pH = 7.0) for 15 min. Relative, intracellular metabolite abundance was assessed (n = 6). Knockdown was confirmed by qPCR. **(f)** Brown adipocytes were treated with MCT inhibitors. $^{14}C_4$-succinate was administered to cells and uptake was monitored (n = 3). **(g)** Brown adipocytes were treated with AZD3965 and $^{14}C_4$-succinate and transport was monitored (n = 3). **(h)** Cells were pre-treated with 100 nM of AZD3965 for 30 min and then were administered 10 µM $^{13}C_4$-succinate for 2 min (pH = 7.45). Relative intracellular metabolite abundance was assessed. (n = 6). **(i)** Cells were pre-treated with 100 nM of AZD3965 for 30 min and then were administered 10 µM $^{13}C_4$-succinate for 2 min (pH = 7.45). Relative intracellular metabolite abundance was assessed. (n = 6). **(j)** 10 µM $^{13}C_4$-succinate was applied to MCT1 knockdown cells for 15 min. Knockdown was confirmed by qPCR. Relative, intracellular metabolite abundance was assessed (n = 6). **(k-l)** Cells were treated with $^{14}C_4$-succinate for 5 min in the presence of structurally similar metabolites, monocarboxylates (k) and di/tricarboxylates (l). $^{14}C_4$-succinate uptake was assessed (n = 3).

across the plasma membrane. We compared four RNA and proteomic data sets comprising mouse brown, beige, and white adipocytes to identify potential transporters of succinate [34]. From this comparative analysis, MCT1 emerged among the common small molecule carboxylate transporters (**Figure 3.2d**). MCT1 belongs to the MCT family of proteins that include MCT1, 2, and 4. These transporters facilitate the diffusion of small monocarboxylates such as L-lactate and pyruvate across the plasma membrane. This transport is proton-linked and is driven by changes in proton concentration [35]. Previous studies show MCT1 expression to be induced upon differentiation and cold exposure and to be specifically localized to brown and beige adipocytes[36,37]. The cold-inducibility of MCT1 appears to be specific, with other MCT isoforms remaining unchanged upon cold exposure [36]. Moreover, previous studies of muscle, heart, and recombinant protein have shown that MCT1 can transport succinate in its monocarboxylate form [8,13-15].

Genetic depletion of MCT1 in brown adipocytes resulted in an attenuation in succinate uptake, whereas depletion of MCT4 had minimal effect and MCT2 no effect on uptake (**Figure 3.2e**). Knockdown of all three MCT isoforms did not further inhibit succinate uptake compared to knockdown of MCT1 alone **(Figure 3.2f)**. Chemical inhibition of the MCTs resulted in a similar attenuation of succinate transport (**Figure 3.2g**). AZD-3965, a potent inhibitor of MCT1 (IC_{50} = 1.6 nM) [38,39] and at higher concentrations an inhibitor of MCT2 (IC_{50} = 20 nM) [39], induced a concentration-dependent decrease in $^{14}C_4$-succinate uptake (**Figure 3.2h**). Administering AZD-3965 at concentrations that inhibit MCT1 and MCT2 similarly resulted in a decrease in $^{13}C_4$-succinate uptake and its downstream product of mitochondrial catabolism, $^{13}C_4$-malate (**Figure 3.2i**). AZD-3965 elicited no significant additional inhibition of succinate transport in MCT1-KD cells, suggesting that the major uptake pathway is via MCT1 **(Figure 3.2j)**. Extracellular co-application of known transport substrates of the MCT family of proteins also decreased succinate uptake by brown adipocytes, suggesting that these metabolites are competing for the same

transporter as succinate (**Figure 3.2k**). Conversely, there was no effect on succinate uptake in the presence of excess di- or tricarboxylates (**Figure 3.2l**). In competition experiments, we tested the relevance of metabolite competition with succinate uptake at pH 6.5 to drive elevated uptake of succinate under the experimental conditions.

Inhibition of MCT1 attenuates succinate uptake into mouse BAT *in vivo.*

We next examined whether MCT1 regulates succinate uptake into mouse BAT *in vivo.* We generated an adipocyte-specific MCT1 knockout (KO) mouse by crossing a MCT1 flox mouse with a mouse expressing cre under the adiponectin promoter (**Figure 3.3a**). We confirmed ablation of MCT1 by performing quantitative proteomics on interscapular BAT from MCT1 KO and wild-type (WT) mice. We observed a significant decrease in MCT1 protein abundance along with its accessory protein basigin (BSG) (**Figure 3.3b**). This analysis provided no evidence for compensatory upregulation of other transporters in the fat-specific KO animals (**Figure 3.3c**). We next injected WT and MCT1 KO animals housed at room temperature with $^{13}C_4$-succinate and harvested interscapular BAT and subcutaneous adipose tissue (SAT), which contains both white and beige adipocytes [40,41], and performed liquid chromatography/mass spectrometry (LC/MS) analysis to assess succinate uptake and metabolism in these tissues (**Figure 3.3d**). We observed a significant decrease in BAT succinate uptake and catabolism in MCT1KO mice when compared to WT **(Figure 3.3e)**. We noted that brown adipocyte uptake of succinate is strongly potentiated by adrenoreceptor agonism, **(Figure 3.1i)**. At room temperature, mouse BAT is subject to adrenergic activation, which is significantly diminished at thermoneutral housing temperatures. We repeated the above tracing experiment in mice housed at thermoneutrality and found MCT1 mediated succinate uptake and metabolism was significantly diminished. **(Figure 3.3f)**.

The discordance of our *in vivo* observations between thermoneutral housed mice and room temperature housed mice led us to consider explanations for residual transport capacity in BAT in MCT1KO. One potential difference arose in the nature of acute versus chronic MCT

depletion or inhibition. Our *in vitro* studies employed siRNA mediated knockdown (several days), or pharmacological inhibition (minutes). Conversely, our *in vivo* analysis was performed in mice with a congenital lack of MCT1, which could lead to altered development of thermogenic adipocytes and reliance on alternative modes of monocarboxylate transport. However, triple knockdown of MCT1/MCT2/MCT4 did not further inhibit succinate uptake in brown adipocytes **(Figure 3.2f)**, suggesting that additional succinate transport activity in BAT is not attributable to MCTs. To examine this possibility further, we acutely inhibited MCT1 and 2 in WT mice using AZD-3965 and injected $^{13}C_4$-succinate (**Figure 3.3g**). AZD-3965 treatment significantly decreased $^{13}C_4$-succinate uptake by BAT but not SAT (**Figure 3.3h**), with an effect size approximating that which we observed in MCT1KO mice **(Figure 3.3e)**. An additional factor to consider when interpreting *in vivo* tracing into BAT is contaminating signal from non-adipocyte sources, including non-adipocyte cell types and local blood. ^{13}C-succinate signal in BAT *in vivo* will include these factors, which likely leads to an underrepresentation of the effect of MCT1KO in this context. It is noteworthy that ^{13}C-malate signal reported on succinate uptake and metabolism by mitochondria, presumably explaining why effects of MCT1KO were clearer when assessing conversion to malate. Taken together, these data indicate that MCT1 facilitates succinate uptake into BAT *in vivo*, with strongest effects at room temperature, and suggests a role for other non-MCT transporters in addition to MCT1 that may be most relevant under conditions of ow adrenoreceptor agonism.

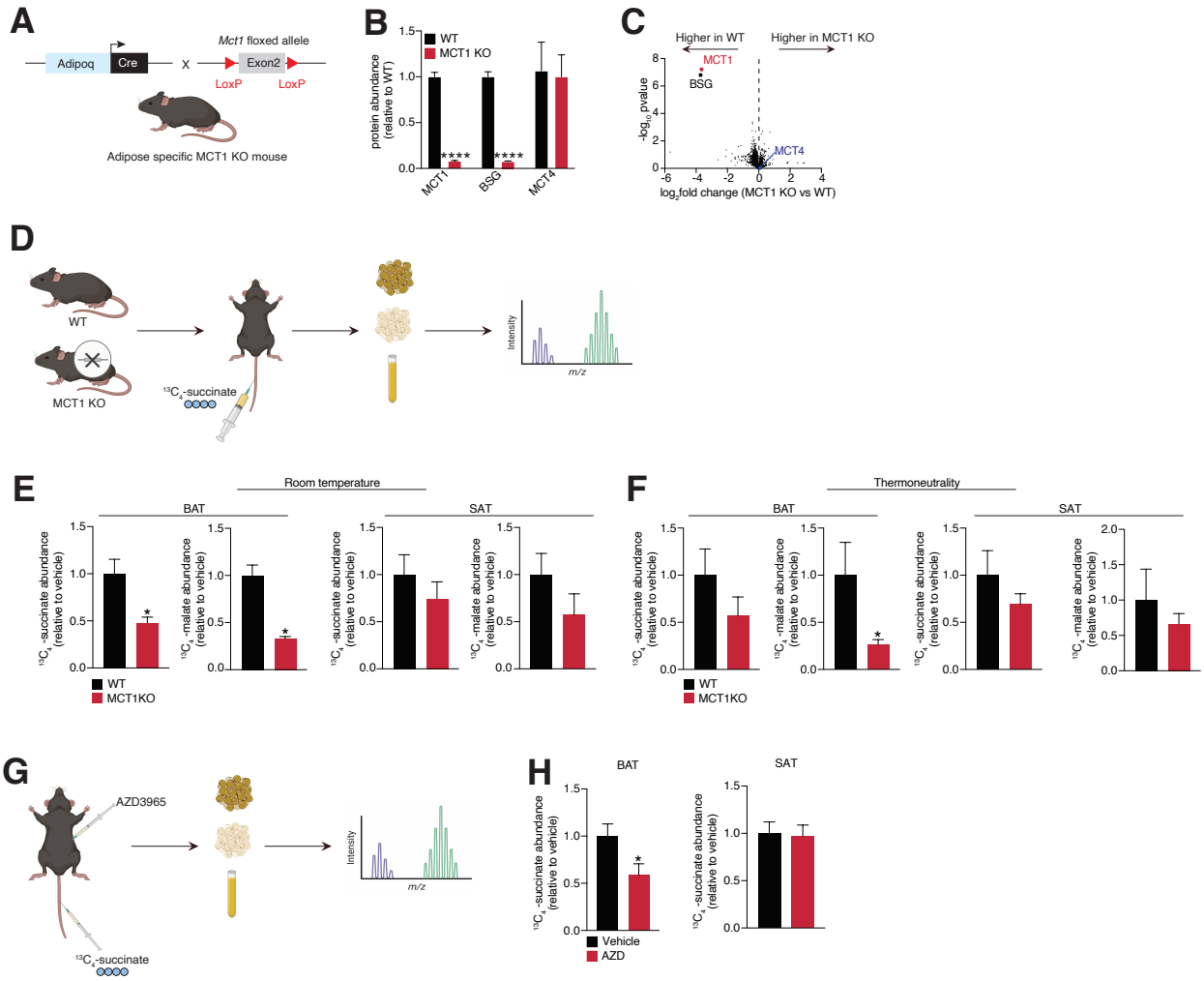


Figure 3.3 l Inhibition of MCT1 attenuates succinate uptake into mouse BAT *in vivo.* (a) Schematic detailing the generation of the fat-specific MCT1 KO mouse. (b) Proteomic analysis was performed on BAT harvested from wild-type (WT) and MCT1 KO mice to assess the relative abundance of MCT1, MCT4, and accessory protein basigin (BSG) (n = 4). (c) Global proteomic analysis was performed on BAT harvested from WT and MCT1 KO mice to determine possible off-target changes in protein abundance in the absence of MCT1 (n = 4). (d) Schematic outlining experimental procedure of *in vivo* $^{13}C_4$-succinate tracing in WT and MCT1 KO mice.

Figure 3.3 | Inhibition of MCT1 attenuates succinate uptake into mouse BAT *in vivo* (cont.) (e) WT or fat-specific MCT1 KO mice were administered tail-vein injection of $^{13}C_4$-succinate (10 mg/kg) at room temperature. 2 min following $^{13}C_4$-succinate injection, BAT and SAT were harvested. Metabolite extraction was performed on tissues and relative $^{13}C_4$-succinate and malate abundance were assessed via LC/MS analysis. (n = 3-6). (f) WT or fat-specific MCT1 KO mice were administered tail-vein injection of $^{13}C_4$-succinate (10 mg/kg) at thermoneutrality. 2 min following $^{13}C_4$-succinate injection, BAT and SAT were harvested. Metabolite extraction was performed on tissues and relative $^{13}C_4$-succinate and malate abundance were assessed via LC/MS analysis. (n = 5-6). (g) Schematic detailing experimental procedure of *in vivo* $^{13}C_4$-succinate tracing following AZD3965 administration. (h) WT mice were administered either 5 mg/kg AZD3965 (n = 10) or saline (n =16) via i.p. injection 2h prior to tail-vein injection of $^{13}C_4$-succinate (10 mg/kg). 2 min following $^{13}C_4$-succinate injection, BAT and SAT were harvested. Metabolite extraction was performed on tissues and relative $^{13}C_4$-succinate abundance was assessed via LC/MS analysis.

Discussion

Regulation of SUCNR1 by circulating succinate has emerged as a key node of metabolite control over tissue remodeling. The dynamics of succinate-SUCNR1 signaling appear to be a major component dictating the nature of the biological consequence of succinate action. Acute, pulsatile elevation in extracellular succinate elicits distinct remodeling processes compared to chronic elevation. Additionally, SUCNR1 agonism appears to promote distinct adaptive responses depending on the SUCNR1-expressing cell type sensing extracellular succinate.

The dynamic nature of SUCNR1 agonism by succinate requires a better understanding of the mechanisms that control succinate secretion into, and sequestration from, extracellular fluids. Here we focused our attention on brown adipocytes, a cell type with a particular avidity for uptake of extracellular succinate. Brown adipocyte succinate uptake regulates thermogenic respiration in BAT and beige fat and whole-body energy expenditure. Moreover, succinate uptake by these cells has been shown to antagonize pathogenic SUCNR1 activation caused by chronically elevated circulating succinate. Here we show that brown adipocyte uptake of succinate depends on the proportion of it in the monocarboxylic form, and relies substantially on MCT family proteins, in particular MCT1. It is noteworthy that a mechanism through which brown adipocytes acquire succinate appears to be an inversion of the succinate export mechanism recently discovered in a variety of cell types [8,13,14].

Studies in exercising muscle, ischemic heart, and mouse retinas have shown succinate export via MCT1 to be dependent on intracellular acidification occurring in response to changes in cellular metabolism. For example, during exercise, the combination of decreased oxygen tension and increased glycolytic flux results in acute intracellular acidification, with cytosolic pH falling as low as 6.4 [42]. Other physiological conditions, such as ischemia, can also lead to acute acidification of the cytosol [14]. This pH regulation of succinate export positions succinate as an ideal signaling molecule since it can relay changes in bioenergetic status to the surrounding environment. Because the pKa of succinate is high compared to other mitochondrial dicarboxylates, a significant portion of the intracellular pool is readily protonated at physiological pH, converting the

metabolite from a dicarboxylate to a monocarboxylate. Once protonated, succinate is then secreted from the cell via MCT1. The decrease in pH serves a dual purpose, not only does it increase the pool of monocarboxylate succinate, but it also supplies protons required for MCT-facilitated transport.

MCTs facilitate the diffusion of carboxylates across the plasma membrane, with the rate and directionality dictated by the concentration gradient of the carboxylate and protons. Notably, transport of the monocarboxylate form of succinate by MCTs would carry two protons across the membrane, as opposed to one, in the case of lactate or pyruvate. Therefore, succinate transport by MCTs is presumably more sensitive to ΔpH across the plasma membrane than for other MCT substrates. Succinate export from cells by MCTs is highly pH dependent, due to the requirement for intracellular succinate to exist as a monocarboxylate, and ΔpH driving proton release with succinate. However, in the case of succinate import into brown adipocytes, the intracellular concentration of succinate would be equivalent to or higher than the extracellular concentration, which peaks in the hundreds of micromolar. How then is uptake and metabolism of micromolar concentrations of succinate achieved via MCTs, if transport is operating against the succinate concentration gradient? One contributing factor is likely to be ΔpH across the plasma membrane. Since succinate uptake would bring two molar equivalents of protons, relative alkalinization of the cytosol could preferentially drive proton import using succinate as a co-transported species. This supposition is supported by the observation that interventions driving cytosolic alkalinization, i.e. adrenoreceptor agonism, promote succinate uptake into brown adipocytes. Indeed, the highly innervated nature of BAT and

beige fat, coupled with the high capacity of these cells for succinate oxidation to support thermogenesis, may be a major reason why these cells avidly acquire extracellular succinate. The above parameters dictating succinate transport by MCTs also suggest that the metabolic state of BAT could be a major factor regulating succinate uptake in these cells. For example, it would be expected that intracellular acidification in brown adipocytes would promote succinate export, as opposed to import. This concept is supported by our findings that elevated glycolytic lactate production antagonizes succinate uptake by brown adipocytes. Such local metabolic changes could also affect the capacity of BAT to handle systemic succinate.

Understanding the metabolic and environmental conditions that foster succinate uptake into BAT will offer us greater insight into how BAT regulates systemic health. Succinate transport into BAT promotes a range of physiological responses that are beneficial for systemic health. These include increased thermogenic activity, protection from metabolic disease, and decreased inflammation. Here we show both *in vivo* and *in vitro* that MCT proteins, particularly MCT1, have a capacity to sequester extracellular succinate, which is potentiated by adrenoreceptor agonism. We demonstrate a pH dependency of succinate transport and show BAT preferentially transports protonated succinate. Our *in vivo* MCT1 KO data suggests a compensatory pathway for succinate uptake, presumably through an MCT-independent mechanism. Future studies will need to be conducted to further elucidate the full repertoire of transporters capable of transporting succinate into BAT.

Materials and Methods

Mouse Lines

Animal experiments were performed according to procedures approved by the Institutional Animal Care and Use Committee of the Beth Israel Deaconess Medical Center. Unless otherwise stated, male C57BL/6J were used (10 ± 2 weeks of age; Jackson Laboratories). MCT1 flox mice were a gift from the Rothstein lab [43]. All mice were housed in a temperature-controlled (23°C) room on a 12-h light-dark cycle at ambient humidity.

Primary brown adipocyte isolation

Primary brown adipocytes were obtained and handled as previously described [25,44]. Briefly, intrascapular brown adipose tissue was dissected from 2- to 10-day-old pups, washed in PBS and minced. The minced tissue was digested for 45 min at 37°C in PBS buffer containing 1.5 mg ml^{-1} collagenase B, 123 mM NaCl, 5 mM KCl, 1.3 mM $CaCl_2$, 5 mM glucose, 100 mM HEPES, and 4% essentially fatty-acid-free BSA. The tissue suspension was filtered first through a 100 μm and then a 40 μm cell strainer and spun at 600 g for 5 min in-between to pellet the stromal vascular fraction. The cell pellet was resuspended in adipocyte culture medium, plated, and maintained at 37°C in 10% CO_2. Primary brown pre-adipocytes were counted and diluted to a concentration of 150,000 cell/ml and plated in the evening 12h before differentiation start. Plating was scaled according to surface area, for 24-well plates 0.5 ml (75,000 cells) were used/well. Brown preadipocytes were induced to differentiate with an adipogenic cocktail diluted in adipocyte culture medium (1 μM rosiglitazone, 0.5 mM IBMX, 5 μM dexamethasone, 0.114 μg ml^{-1} insulin, 1 nM T3, and 125 μM indomethacin). Two days after induction, and subsequently every 48hrs, cells were re-fed adipocyte culture medium containing 1 μM rosiglitazone, 1 nM T3, and 0.5 μg ml^{-1} insulin. Cells were fully differentiated 7 days after induction.

Human brown adipocyte differentiation

A41 hWAT-SVF pre-adipocytes were a gift from the Tseng lab and were plated in a 10 cm dish with high-glucose DMEM (Gibco) supplemented with 10% FBS and 1% penicillin-streptomycin (Thermo Fisher) and maintained at 37°C in 5% CO_2. Upon differentiation, cells were re-plated in a 24-well dish (20,000 – 40,000 cells/ml) and given induction media (high-glucose DMEM, 2% FBS, 1% penicillin-streptomycin, 33 μM biotin, 0.5 μM human insulin, 17 μM pantothenate, 0.1 μM dexamethasone, 2 nM T3, 500 μM IBMX, 30 μM indomethacin). Fresh induction media was added every three days. Cells reached full differentiation 12 – 24 days following induction. Once differentiation was achieved, $^{13}C_4$-succinate uptake assays were performed.

$^{14}C_4$-Succinate uptake assay

For radioactive uptake assays cells were grown in 24-well plates. On day of experiment tissue culture media was aspirated and the cells were washed once in pre-warmed (37°C) PBS. The cells were then preincubated for 30 min in assay buffer (DPBS with $MgCl_2$ & $CaCl_2$ supplemented with 2% BSA and 1 mM glucose; pH 7.5) at 37°C. For MCT inhibitor experiments the inhibitors were added at the specified concentrations in the preincubation buffer. After preincubation buffer was removed and replaced with 200 μl assay buffer containing [1,4-^{14}C] succinic acid (American Radiolabeled chemicals) for 15 min (unless otherwise stated) at 37°C. pH of the assay buffer was adjusted with NaOH to pH 6.5, unless otherwise stated. The radioactive assay buffer contained 0.5 μCi/ml ^{14}C-succinate and was supplemented with sodium succinate to a final concentration of 5 mM (unless otherwise stated). For metabolite competitor studies the indicated metabolite was added to the uptake buffer together with succinate. At the end of the 15 min cells were placed on ice and washed 3x with ice-cold PBS. Cells were lysed by pipetting in 200 μl 1% SDS, and 150 μl was transferred to a scintillation vial (Wheaton) containing 6 ml Ultima Gold scintillation cocktail (Perkin Elmer). Radiation in each sample was measured as counts/minute (CPM) using a TRI-CARB 2900TR scintillation counter. For each experiment at blank sample was run to determine

background counts, and this value was subtracted from all experimental readings. For normalization total protein concentration was measured on an aliquot of the cell lysate with the Pierce BCA protein kit (Thermo Fisher) following the manufacturer's instructions. Radioactive CPM was converted to succinate concentrations using the specific activity (55 mCi/ml) of ^{14}C-succinic acid. The uptake was then normalized to total protein amount for each sample. (For experiments with preadipocytes and cell lines uptake data was normalized to cell counts instead of protein concentration).

In vitro $^{13}C_4$-Succinate uptake assay

For $^{13}C_4$-succinate uptake assays, cells were grown in 24-well plates. On the day of the experiment, serum-free media (Gibco) containing $^{13}C_4$-succinate (Cambridge Isotopes) was prepared and pH was adjusted to pH 7.4 using NaOH. For norepinephrine (NE) stimulation experiments, a specified amount of NE (Sigma Aldrich) was added to the $^{13}C_4$-succinate containing media just prior to incubation. For MCT1 inhibitor experiments, cells were pre-incubated with AZD-3965 for 30 min. After pre-incubation, $^{13}C_4$-succinate containing media was added and cells were incubated for specified amount of time. Media was aspirated and cells were washed three times on dry ice with ice-cold PBS. 100 µL of metabolite extraction buffer consisting of 80% HPLC MeOH containing D4-thymine, D4-glycocholate, and 15N4-inosine was added to each well. Cells were scraped and lysates were collected for further LC/MS analysis.

Cytosolic pH measurements

Intracellular pH was measured using the ratiometric pH dye BCECF-AM (Invitrogen) [45]. Preadipocytes were plated in a 12-well plate and differentiated. On day 7, mature adipocytes were loaded with dye (5 µM) and incubated for 30 min at 37°C. Cells were imaged using a dual-excitation ratio of 480 nm and 440 nm and a fixed emission at 535 nm. A baseline image was

obtained before norepinephrine (Sigma Aldrich) was administered. A calibration curve was created using nigericin and high K^+.

Local extracellular pH measurements

Extracellular pH was measured using the ratiometric pH dye fluorescein DHPE (Life Technologies) [46]. Pre-adipocytes were plated in a 24-well plate and differentiated. On day 7, mature adipocytes were loaded with dye (8 μM) and incubated for 30 min at 37°C. Cells were imaged using a dual-excitation ratio of 470 nm and 440 nm and a fixed emission at 500 nm. A baseline image was collected before norepinephrine (Sigma Aldrich) was administered. A calibration curve was created using different pH media conditions (6.4, 7.4, and 8.4).

siRNA mediated knockdown in brown adipocytes

Forward and reverse siRNA transfections were performed as previously described [47]. Transfections were carried out on day 4 of differentiation and experiments were conducted on day 7. For forward transfections, pre-adipocytes were plated in a 24-well plate at a concentration of 50,000 cells/well. For reverse transfections, day 4 differentiated brown adipocytes were plated at a concentration of 475,000 cells/well in a 24-well plate. Final concentrations of siRNA and lipofectamine RNAiMAX was 90 nM and 9 μl/ml, respectively. siRNAs (Sigma-Aldrich) used were: Mct1 (SASI_Mm01_00112354), Mct2 (SASI_Mm01_00096521), Mct4 (SASI_Mm01_00119743), Slc13a3 (SASI_Mm01_00057701). MISSION® siRNA Universal Negative Control #1 (Sigma-Aldrich, SIC001) was used as control siRNA.

Sample preparation for metabolite analysis

Following intervention, 100 uL of ice-cold extraction buffer consisting of 80% methanol containing D4-thymine, D4-glycocholate, and 15N4-inosine was added to each well of a 24-well plate. Cells were immediately harvested by scraping on dry ice and transferred to a 1.5 mL microcentrifuge tube. Lysates were centrifuged twice at max speed (10 min, 21,100 g, 4°C) and supernatant was collected. For *in vivo* experiments, mice were sacrificed by cervical dislocation following

intervention and tissues were quickly harvested and immediately snap-frozen in liquid nitrogen. Samples were then weighed and homogenized with extraction buffer in a 4:1 (µL extraction buffer: mg of tissue) ratio. Tissues were centrifuged twice (10 min, 21,100 g, 4°C) and supernatant was collected. Supernatant was further diluted 1:10 (sample:80% methanol) with 80% HPLC grade methanol. For plasma collection, blood was collected via cheek bleed into a heparin column (Becton Dickson), centrifuged (10 min, 1,000 g, 4°C), and immediately snap-frozen. Metabolites were then extracted by adding extraction buffer in a 4:1 (µL of extraction buffer: µL of plasma) ratio. Extracted metabolites were further diluted 1:10 (sample:80% methanol) with 80% HPLC grade methanol.

LC/MS metabolite analysis

Metabolite separation was performed using a Luna-HILIC column (Phenomenex) on an UltiMate-3000 TPLRS LC. A linear 10-min gradient of 10% mobile phase A (20 mM ammonium acetate and 20 mM ammonium hydroxide in 95% water and 5% ACN) and 90% mobile phase B (10 mM ammonium hydroxide in 75:25 v/v ACN/MeOH) to 99% mobile phase A was used, and metabolites were analyzed by a Q-Exactive™ HF-X mass spectrometer (ThermoFisher). Negative ion mode was used with full scan analysis over m/z 70-750 m/z at 60,000 resolution, 1e6 AGC, and 100 ms maximum ion accumulation time. Ion spray voltage was set at 3.8 kV, capillary temperature was at 350°C, probe heater temperature was at 320 °C, sheath gas flow was set at 50, auxiliary gas was set at 15, and S-lens RF level was set at 40. TraceFinder (ThermoFisher) was used to annotate and quantify the metabolite peaks.

***In vivo* $^{13}C_4$-Succinate tracing**

Mice were housed at thermoneutrality (29°C) for one week prior to experiment. Mice were then injected with [U^{13}C] succinate (10 mg/kg, 2 min) (Cambridge Isotope Laboratories) via intravenous tail vein. Intravenous injections were performed as a bolus over 20 s. Mice were sacrificed by

cervical dislocation. Tissues were harvested and immediately snap frozen in liquid nitrogen and stored at -80°C for further analysis.

***In vivo* chemical inhibition of MCTs**

Mice were injected intraperitoneally with AZD 5 mg/kg, 2 h prior to intravenous tail vein injection with [U^{13}C] succinate (10 mg/kg, 2 min) (Cambridge Isotope Laboratories). Intravenous injections were performed as a bolus over 20 s. Tissues were extracted and snap frozen in liquid nitrogen and stored at –80°C until MS analysis was performed.

Gene expression analysis (qPCR)

Total RNA from cellular siRNA experiments were extracted using TRIzol (Invitrogen) and purified using phenol:chloroform extraction with isopropanol precipitation. Purified RNA was quantified using a Nanodrop 2000 UV-visible spectrophotometer. cDNA was prepared according to manufacturer's instructions from 2 ug total RNA using a high-capacity cDNA reverse transcription kit (Applied Biosystems). qPCR reactions were performed in a 384-well format using GoTaq qPCR Master Mix (Promega) and run on an ABI PRISM 7900HT real time PCR system (Applied Biosystems). Relative gene expression was calculated by the delta delta Ct method using mouse cyclophilin A expression as endogenous control. All fold changes are expressed normalized to the universal negative siRNA control. Primer pairs are as follows: *Cyclophilin A*, FW 5'-GGAGATGGCACAGGAGGAA-3', RV 5'- GCCCGTAGTGCTTCAGCTT-3'; *Mct1*, FW 5'-GTGCAACGACCAGTGAAGTA-3', RV 5'- ACAACCACCAGCGATCATT-3'; *Mct2,* FW 5'-GTTGGCTTCAATGGAGGTTT-3', RV 5'-AAAACAGGACTTCCAGCCAT-3'; *Mct4*, FW 5'-TCCTGCTGGCTATGCTCTA-3', RV 5'- CAAAGAGGCCACCCACAA-3'; *Slc13a3*, FW 5'-AGCTCAAGAGTTTCTTCCCA-3', RV 5'-CGTCAGCTCGTATCTTGGAT-3'.

Brown adipose tissue proteomics

BAT samples were lysed in the lysis buffer (100 mM 4-(2-hydroxyethyl)-1-piperazineethanesulfonic acid (HEPES) pH 8.5, 8 M urea, 2% SDS, 1p/15 mL Roche cOmplete™

protease inhibitors) to 1 mg/mL protein based on BCA assay results. Disulfides were reduction with 5 mM tris(2-carboxyethyl)phosphine (TCEP) at 37 °C for 1 h, followed by alkylation with 25 mM iodoacetamide for 25 min at room temperature in the dark. Protein precipitation was performed by the methanol-chloroform method [48], and proteins were digested resuspended in 200 mM N-(2-Hydroxyethyl)piperazine-N′-(3-propanesulfonic acid) (EPPS) buffer pH=8, using a combination of Lys-C and trypsin at an enzyme-to-protein ratio of 1:100 overnight at 37 °C, followed by an additional 4 h digestion with trypsin 1:100. Samples were then subjected to a microBCA measurement for peptide quantification, and 25 µg peptides from each sample were labeled by TMTpro-16 reagents [49] for 1 h at room temperature following the streamlined-TMT protocol [50]. The reaction was quenched using 2 µl of 5% hydroxylamine for 15 min. A ratio-check was performed by mixing 2 µL of peptides from each channel, desalted via StageTip, and analyzed by LC-MS. Samples were combined according to the ratio check to ensure equal loading of proteins from each sample, then desalted with Waters SepPak cartridges and dried. Peptide were fractionated using high-pH HPLC. Each fraction was then desalted via StageTip, dried in a speedvac, and reconstituted in a solution containing 5% ACN and 5% FA for liquid chromatography tandem mass spectrometry (LC-MS/MS).

LC-MS/MS

2 µg of peptides were loaded onto an in-house 100-µm capillary column packed with 35 cm of Accucore 150 resin (2.6 µm,150 Å). An Orbitrap Eclipse Tribrid Mass Spectrometer (Thermo) coupled with an Easy-nLC 1200 (Thermo) and FAIMSPro (Thermo) were used for protein measurements. Peptides were separated using a 180-min gradient consisting of 2% - 23% ACN, 0.125% FA at 500 nl/min flow rate. Field asymmetric waveform ion mobility spectrometry (FAIMS) separation of precursors [51] were carried out with default settings and multiple compensation voltages (-40V/-60V/-80V). Peptide ions were collected in data-dependent mode using a mass range of m/z 400-1600 using 2 s cycles and 120,000 resolution. Singly-charged ions were

discarded, and multiply-charged ions were selected and subjected to fragmentation with standard automatic gain control (AGC) and 35% normalized collisional energy (NCE) for MS2, with a dynamic exclusion window of 120 s and maximum ion injection time of 50 ms. Quantification of TMT reporter ion were performed using the multinotch SPS-MS3 method [52] with 45% NCE for MS3.

Database searching and protein quantification

Raw files were searched using the Comet algorithm [53] on Masspike reported previously [54]. Database searching included all mouse (Mus musculus) entries from UniProt (http://www.uniprot.org, downloaded July 29th, 2020) and the reversed sequences as well as common contaminants (keratins, trypsin, etc). Peptides were searched using the following parameters: 25 ppm precursor mass tolerance; 1.0 Da product ion mass tolerance; fully tryptic digestion; up to three missed cleavages; variable modification: oxidation of methionine (+15.9949); static modifications: TMTpro (+304.2071) on lysine and peptide N terminus, carboxyamidomethylation (+57.0214637236) on cysteines. The target-decoy method was used for false discovery rate (FDR) control [54-56]. FDR was < 1% on peptide level for each MS run and peptides that are shorter than seven amino acids were not used. Proteins were assembled to <1% protein-level FDR. TMT reporter ions were used for quantification of peptide abundance. Peptides with summed signal-to-noise (S/N) lower than 160 across 16 channels or isolation specificity lower than 70% were discarded. Normalization was performed to ensure equal protein loadings in every sample. Proteins were quantified by summing peptide TMT S/N.

Statistics and Reproducibility

All data are presented as ± SEM and p-values were calculated using two-tailed Student's t test for pairwise comparisons, one-way analysis of variance (ANOVA) test for multiple comparisons involving one independent variable, and two-way ANOVA test for comparisons involving two independent variables. Data distribution was assumed to be normal, but this was not formally

tested. Sample sizes were determined on the basis of previous experiments using similar methodologies and are sufficient to account for any biological or technical variabilities. No data was excluded. For LC/MS data, the sequence of samples run was randomized across treatment groups and time points. For all animal studies, mice were assigned to random groups. For MS analysis, samples were run in random order and experimenters were blinded to the experimental condition of each sample. For all other experiments, blinding was unnecessary since the results were quantitative and did not require any subjective judgment.

Acknowledgements: This work was supported by The Novo Nordisk Foundation Center for Basic Metabolic Research, an independent Research Center, based at the University of Copenhagen, and partially funded by an unconditional donation from the Novo Nordisk Foundation (Grant number NNF18CC0034900), a fellowship from the Novo Nordisk Foundation (NNF18OC0032380) (S.W), the Claudia Adams Barr Program (E.T.C), the Lavine Family Fund (E.T.C), the Pew Charitable Trust (E.T.C), NIH DK123095 (E.T.C), NIH AG071966 (E.T.C), The Smith Family Foundation (E.T.C), and the American Federation for Aging Research (E.T.C).We would also like to acknowledge The Nikon Imaging Center at Harvard Medical School for their help with the pH imaging experiments and the Tseng lab for the human brown adipocyte cell line.

References

1. Murphy, M.P. & Chouchani, E.T. Why succinate? Physiological regulation by a mitochondrial coenzyme Q sentinel. *Nat Chem Biol* **18**, 461-469 (2022).
2. Mills, E. & O'Neill, L.A. Succinate: a metabolic signal in inflammation. *Trends Cell Biol* **24**, 313-320 (2014).
3. Murphy, M.P. & O'Neill, L.A.J. Krebs Cycle Reimagined: The Emerging Roles of Succinate and Itaconate as Signal Transducers. *Cell* **174**, 780-784 (2018).
4. Murphy, M.P. How mitochondria produce reactive oxygen species. *Biochem J* **417**, 1-13 (2009).
5. Losman, J.A., Koivunen, P. & Kaelin, W.G., Jr. 2-Oxoglutarate-dependent dioxygenases in cancer. *Nat Rev Cancer* **20**, 710-726 (2020).
6. McCreath, K.J.*, et al.* Targeted disruption of the SUCNR1 metabolic receptor leads to dichotomous effects on obesity. *Diabetes* **64**, 1154-1167 (2015).
7. Mills, E.L.*, et al.* UCP1 governs liver extracellular succinate and inflammatory pathogenesis. *Nat Metab* **3**, 604-617 (2021).

8. Reddy, A.*, et al.* pH-Gated Succinate Secretion Regulates Muscle Remodeling in Response to Exercise. *Cell* **183**, 62-75 e17 (2020).
9. Gilissen, J., Jouret, F., Pirotte, B. & Hanson, J. Insight into SUCNR1 (GPR91) structure and function. *Pharmacol Ther* **159**, 56-65 (2016).
10. Aguiar, C.J.*, et al.* Succinate causes pathological cardiomyocyte hypertrophy through GPR91 activation. *Cell Commun Signal* **12**, 78 (2014).
11. Sadagopan, N.*, et al.* Circulating succinate is elevated in rodent models of hypertension and metabolic disease. *Am J Hypertens* **20**, 1209-1215 (2007).
12. van Diepen, J.A.*, et al.* SUCNR1-mediated chemotaxis of macrophages aggravates obesity-induced inflammation and diabetes. *Diabetologia* **60**, 1304-1313 (2017).
13. Bisbach, C.M., Hass, D.T., Thomas, E.D., Cherry, T.J. & Hurley, J.B. Monocarboxylate Transporter 1 (MCT1) Mediates Succinate Export in the Retina. *Invest Ophthalmol Vis Sci* **63**, 1 (2022).
14. Prag, H.A.*, et al.* Mechanism of succinate efflux upon reperfusion of the ischaemic heart. *Cardiovasc Res* **117**, 1188-1201 (2021).
15. Andrienko, T.N., Pasdois, P., Pereira, G.C., Ovens, M.J. & Halestrap, A.P. The role of succinate and ROS in reperfusion injury - A critical appraisal. *J Mol Cell Cardiol* **110**, 1-14 (2017).
16. Littlewood-Evans, A.*, et al.* GPR91 senses extracellular succinate released from inflammatory macrophages and exacerbates rheumatoid arthritis. *J Exp Med* **213**, 1655-1662 (2016).
17. Sapieha, P.*, et al.* The succinate receptor GPR91 in neurons has a major role in retinal angiogenesis. *Nat Med* **14**, 1067-1076 (2008).
18. Vargas, S.L., Toma, I., Kang, J.J., Meer, E.J. & Peti-Peterdi, J. Activation of the succinate receptor GPR91 in macula densa cells causes renin release. *J Am Soc Nephrol* **20**, 1002-1011 (2009).
19. Rubic, T.*, et al.* Triggering the succinate receptor GPR91 on dendritic cells enhances immunity. *Nat Immunol* **9**, 1261-1269 (2008).
20. Wu, J.Y.*, et al.* Cancer-Derived Succinate Promotes Macrophage Polarization and Cancer Metastasis via Succinate Receptor. *Mol Cell* **77**, 213-227 e215 (2020).
21. He, W.*, et al.* Citric acid cycle intermediates as ligands for orphan G-protein-coupled receptors. *Nature* **429**, 188-193 (2004).
22. Correa, P.R.*, et al.* Succinate is a paracrine signal for liver damage. *J Hepatol* **47**, 262-269 (2007).
23. Hochachka, P.W. & Dressendorfer, R.H. Succinate accumulation in man during exercise. *Eur J Appl Physiol Occup Physiol* **35**, 235-242 (1976).
24. Osuna-Prieto, F.J.*, et al.* Elevated plasma succinate levels are linked to higher cardiovascular disease risk factors in young adults. *Cardiovasc Diabetol* **20**, 151 (2021).
25. Mills, E.L.*, et al.* Accumulation of succinate controls activation of adipose tissue thermogenesis. *Nature* **560**, 102-106 (2018).
26. Young, J.B., Saville, E., Rothwell, N.J., Stock, M.J. & Landsberg, L. Effect of diet and cold exposure on norepinephrine turnover in brown adipose tissue of the rat. *J Clin Invest* **69**, 1061-1071 (1982).
27. Kawate, R., Talan, M.I. & Engel, B.T. Sympathetic nervous activity to brown adipose tissue increases in cold-tolerant mice. *Physiol Behav* **55**, 921-925 (1994).
28. Wang, Q.*, et al.* Brown adipose tissue in humans is activated by elevated plasma catecholamines levels and is inversely related to central obesity. *PLoS One* **6**, e21006 (2011).

29. Bast-Habersbrunner, A. & Fromme, T. Purine Nucleotides in the Regulation of Brown Adipose Tissue Activity. *Front Endocrinol (Lausanne)* **11**, 118 (2020).
30. Lee, S.C., Hamilton, J.S., Trammell, T., Horwitz, B.A. & Pappone, P.A. Adrenergic modulation of intracellular pH in isolated brown fat cells from hamster and rat. *Am J Physiol* **267**, C349-356 (1994).
31. Chinet, A., Friedli, C., Seydoux, J. & Girardier, L. Does cytoplasmic alkalinization trigger mitochondrial energy dissipation in the brown adipocyte? *Experientia Suppl* **32**, 25-32 (1978).
32. Gokel, G.W. & Dean, J.A. *Dean's handbook of organic chemistry*, (McGraw-Hill, New York, 2004).
33. Martell, A.E.S., R.M. Acid Dissociation Constants of Organics. in *Critical Stability Constants*, Vol. 1 - 4 (Plenum Press, New York, 1976).
34. Roh, H.C.*, et al.* Simultaneous Transcriptional and Epigenomic Profiling from Specific Cell Types within Heterogeneous Tissues In Vivo. *Cell Rep* **18**, 1048-1061 (2017).
35. Halestrap, A.P. & Price, N.T. The proton-linked monocarboxylate transporter (MCT) family: structure, function and regulation. *Biochem J* **343 Pt 2**, 281-299 (1999).
36. Petersen, C.*, et al.* MCT1 and MCT4 Expression and Lactate Flux Activity Increase During White and Brown Adipogenesis and Impact Adipocyte Metabolism. *Sci Rep* **7**, 13101 (2017).
37. Lagarde, D.*, et al.* Lactate fluxes mediated by the monocarboxylate transporter-1 are key determinants of the metabolic activity of beige adipocytes. *J Biol Chem* **296**, 100137 (2021).
38. Bola, B.M.*, et al.* Inhibition of monocarboxylate transporter-1 (MCT1) by AZD3965 enhances radiosensitivity by reducing lactate transport. *Mol Cancer Ther* **13**, 2805-2816 (2014).
39. Curtis, N.J.*, et al.* Pre-clinical pharmacology of AZD3965, a selective inhibitor of MCT1: DLBCL, NHL and Burkitt's lymphoma anti-tumor activity. *Oncotarget* **8**, 69219-69236 (2017).
40. Garcia, R.A., Roemmich, J.N. & Claycombe, K.J. Evaluation of markers of beige adipocytes in white adipose tissue of the mouse. *Nutr Metab (Lond)* **13**, 24 (2016).
41. Wu, J.*, et al.* Beige adipocytes are a distinct type of thermogenic fat cell in mouse and human. *Cell* **150**, 366-376 (2012).
42. Robergs, R.A., Ghiasvand, F. & Parker, D. Biochemistry of exercise-induced metabolic acidosis. *Am J Physiol Regul Integr Comp Physiol* **287**, R502-516 (2004).
43. Jha, M.K.*, et al.* Monocarboxylate transporter 1 in Schwann cells contributes to maintenance of sensory nerve myelination during aging. *Glia* **68**, 161-177 (2020).
44. Kir, S.*, et al.* Tumour-derived PTH-related protein triggers adipose tissue browning and cancer cachexia. *Nature* **513**, 100-104 (2014).
45. Khacho, M.*, et al.* Acidosis overrides oxygen deprivation to maintain mitochondrial function and cell survival. *Nat Commun* **5**, 3550 (2014).
46. Stuwe, L.*, et al.* pH dependence of melanoma cell migration: protons extruded by NHE1 dominate protons of the bulk solution. *J Physiol* **585**, 351-360 (2007).
47. Isidor, M.S.*, et al.* An siRNA-based method for efficient silencing of gene expression in mature brown adipocytes. *Adipocyte* **5**, 175-185 (2016).
48. Wessel, D. & Flugge, U.I. A Method for the Quantitative Recovery of Protein in Dilute-Solution in the Presence of Detergents and Lipids. *Anal Biochem* **138**, 141-143 (1984).
49. Li, J.*, et al.* TMTpro reagents: a set of isobaric labeling mass tags enables simultaneous proteome-wide measurements across 16 samples. *Nat Methods* **17**, 399-404 (2020).

50. Navarrete-Perea, J., Yu, Q., Gygi, S.P. & Paulo, J.A. Streamlined Tandem Mass Tag (SL-TMT) Protocol: An Efficient Strategy for Quantitative (Phospho)proteome Profiling Using Tandem Mass Tag-Synchronous Precursor Selection-MS3. *J Proteome Res* **17**, 2226-2236 (2018).
51. Schweppe, D.K.*, et al.* Characterization and Optimization of Multiplexed Quantitative Analyses Using High-Field Asymmetric-Waveform Ion Mobility Mass Spectrometry. *Anal Chem* **91**, 4010-4016 (2019).
52. McAlister, G.C.*, et al.* MultiNotch MS3 Enables Accurate, Sensitive, and Multiplexed Detection of Differential Expression across Cancer Cell Line Proteomes. *Analytical Chemistry* **86**, 7150-7158 (2014).
53. Eng, J.K., Jahan, T.A. & Hoopmann, M.R. Comet: An open-source MS/MS sequence database search tool. *Proteomics* **13**, 22-24 (2013).
54. Huttlin, E.L.*, et al.* A tissue-specific atlas of mouse protein phosphorylation and expression. *Cell* **143**, 1174-1189 (2010).
55. Elias, J.E. & Gygi, S.P. Target-decoy search strategy for increased confidence in large-scale protein identifications by mass spectrometry. *Nature Methods* **4**, 207-214 (2007).
56. Peng, J.M., Elias, J.E., Thoreen, C.C., Licklider, L.J. & Gygi, S.P. Evaluation of multidimensional chromatography coupled with tandem mass spectrometry (LC/LC-MS/MS) for large-scale protein analysis: The yeast proteome. *Journal of Proteome Research* **2**, 43-50 (2003).

Chapter 4

Discussion and Future Perspectives

Succinate-SUCNR1 signaling and muscle remodeling

We have defined a role for succinate as a bioenergetic signaling molecule that can relay the metabolic status of cells to their outside environment and initiate remodeling in response to physiological events. We (Reddy* and Bozi* *et al.*, *Cell* 2020) identified succinate as an exercise responsive metabolite that is selectively released by skeletal muscle in both mice and humans. We elucidated the transport mechanism of succinate from exercising skeletal muscle and implicate acute cytosolic acidification, associated with exercise, as a key driver of succinate secretion[1-4]. We propose a model whereby transient decreases in cytosolic pH, caused by increased glycolytic flux and decreased oxygen tension, results in the protonation of succinate transforming the metabolite from a dicarboxylate to a monocarboxylate. Once protonated, succinate is rendered amenable for transport via the plasma membrane protein, monocarboxylate transporter 1 (MCT1) (figure 4.1).

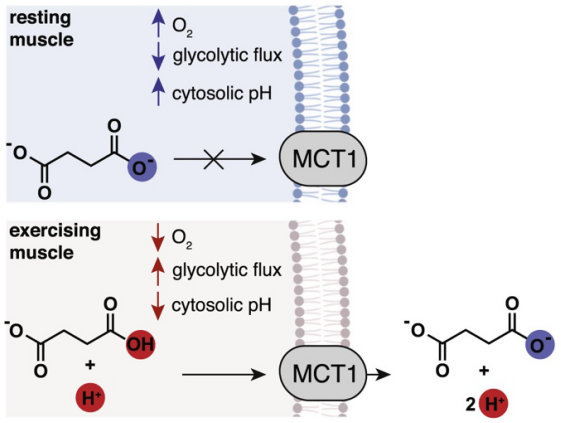


Figure 4.1 | Schematic depicting pH-gated succinate release from skeletal muscle. Transient decreases in cytosolic pH driven by decreased oxygen or increased glycolytic flux result in the protonation of succinate, rendering it amenable to secretion by MCT1. (Figure adapted from Reddy and Bozi *et al., Cell,* (2020).)

We demonstrate the requirement of cytosolic acidification, driven by acute hypoxia or mitochondrial inhibition, for succinate release from skeletal muscle cells. This release is MCT1 dependent, where genetic or pharmacological inhibition of the transporter results in reduced succinate release. This mode of pH-gated succinate release reconciles the previous observations of increased extracellular succinate during physiological interventions like hypoxia[5], cold-exposure,[6] and exercise[7] with the notion that succinate is largely confined intracellularly[6,8-10].

We show extracellular succinate engages its cognate receptor, succinate receptor 1 (SUCNR1), to drive transcriptional remodeling in muscle-resident non-myofibrillar cells (figure 4.2).

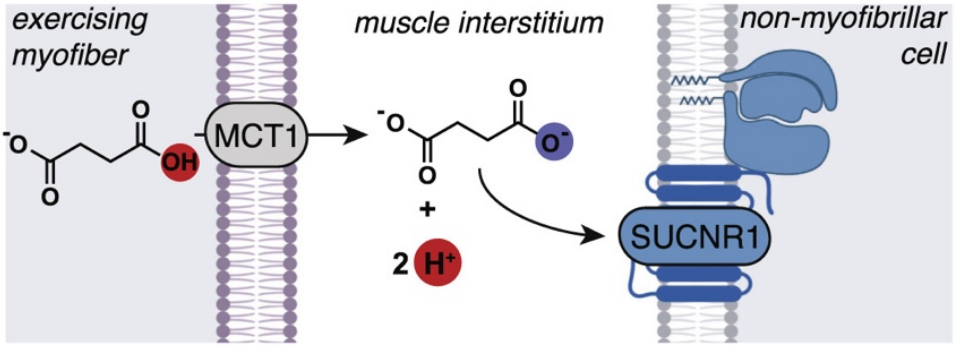


Figure 4.2 | Schematic depicting paracrine succinate-SUCNR1 signaling. (Figure adapted from Reddy and Bozi *et al.*, *Cell*, 2020.)

Using *in situ* hybridization (ISH) and qPCR analysis, we localize the receptor to non-myofibrillar cell populations, like stromal, satellite, and endothelial cells, that reside within the muscle. Contrary to previous findings, we were not able to detect SUCNR1 transcripts in muscle fibers[11]. We show that acute exercise is sufficient to drive SUCNR1-dependent phosphorylate of numerous signaling cascades, like protein kinase A (PKA) and mitogen-activated protein kinase (MAPK), both of which have been established to be downstream of SUCNR1 agonism[12,13]. When performing RNA-sequencing (RNA-seq) on non-myofibrillar cell populations isolated from exercised tibialis anterior (TA) muscle, we observe a distinct SUCNR1-dependent transcriptional

response in each isolated cell population. Notably, we see an enrichment in transcripts relating to neuronal projection and axonal guidance in satellite and stromal cells, respectively.

We further implicate succinate-SUCNR1 signaling in muscle adaptations following prolonged training. Using voluntary resistance-wheel running, we observe a significant difference in strength between wild-type (WT) and SUCNR1 KO mice, following three-weeks of exercise training. Moreover, we see distinct proteome remodeling responses to exercise training between the genotypes. In WT mice, we see an enrichment in fast twitch myosin and extracellular matrix (ECM) proteins. On the contrary, we observe an increase in complement pathway and inflammatory proteins in SUCNR1 KO mice, following training, indicating that these mice fail to appropriately respond to exercise. Additionally, we see an increase in total muscle innervation following the training period, in WT mice that was absent in SUCNR1 KO mice. Neuronal adaptations are commonly seen following resistance training and contributes to strength increases, independently of hypertrophy[14,15]. The difference in strength we observe may be partly attributed to a difference in neuronal content between the genotypes. However, more work is needed to determine if SUCNR1 is localized to neurons that innervate skeletal muscle or if an intermediary cell type facilitates this increase in innervation. Lastly, we implicate succinate-SUCNR1 signaling in post-exercise insulin sensitivity, a prominent adaptation seen with endurance exercise[16]. We observe a positive correlation between peak venous succinate concentration and post-exercise insulin sensitivity, in humans.

Succinate transport in brown adipocytes

We investigated whether the mechanism of succinate transport in skeletal muscle was applicable to other tissues. Previous findings from our lab have shown brown adipose tissue (BAT) to have a great affinity for succinate uptake[6,17]. However, the mechanism of succinate uptake by BAT remains poorly understood. We establish the MCT family of proteins, particularly MCT1, to facilitate succinate transport into brown adipocytes (Reddy and Winther *et al., bioRxiv*, 2023).

Succinate transport in BAT is pH-dependent and driven by proton differentials across the plasma membrane, which is characteristic of MCT mediated transport. Norepinephrine (NE)-stimulated

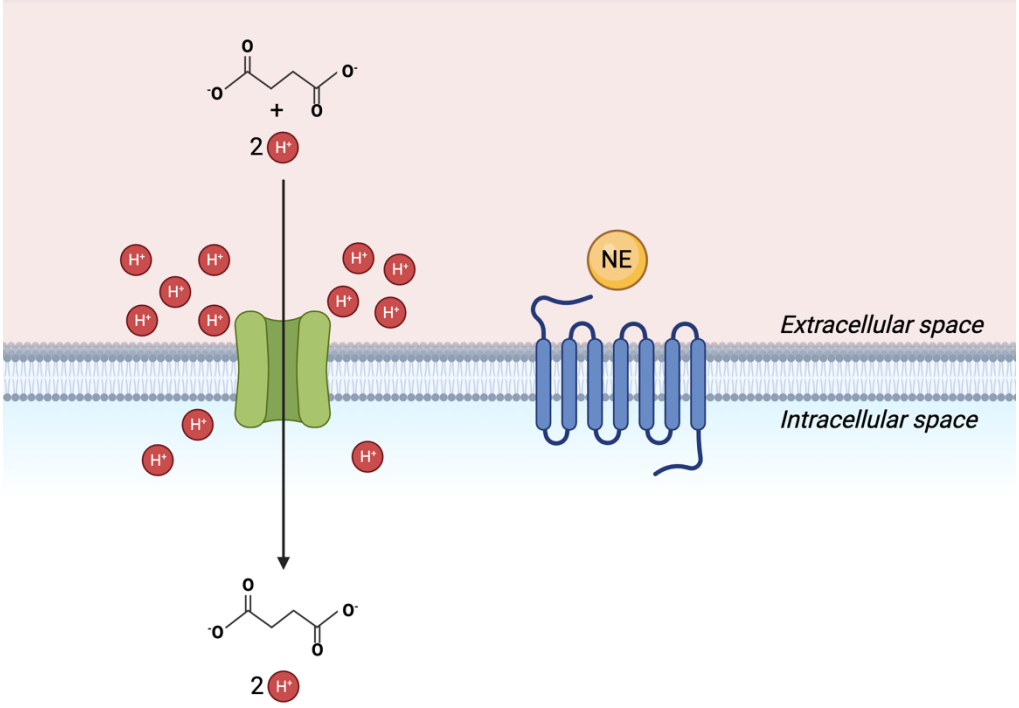


Figure 4.3 I Proposed model of NE-driven succinate transport. NE stimulation promotes a proton differential across the plasma membrane of brown adipocytes by inducing intracellular alkalinization and extracellular acidification. This proton differential may drive succinate transport and provide selectivity for succinate transport over other metabolites, since transport of succinate is accompanied by the transport of two protons.

β-adrenergic signaling, seen with cold exposure, promotes succinate uptake, which is in line with previous findings that report increased succinate transport upon cold exposure[6,17]. We attribute NE-driven succinate transport to changes in local intra- and extracellular pH. We observe a simultaneous increase in cytosolic pH and decrease in local extracellular pH upon NE treatment, in primary brown adipocytes. We posit this pH differential drives succinate transport. The proton gradient established by β-adrenergic signaling could foster a selectivity for succinate import,

which carries along 2 protons compared to lactate and pyruvate, that only have one associated proton (figure 4.3). Since succinate transport would result in transport of more protons, cytosolic alkalinization could potentially drive preferential import of succinate. However, more experiments would need to be conducted to fully examine this hypothesis.

Using CRE mice under an adiponectin (ADIPOQ) promoter, we generated a MCT1, fat-specific knockout mouse to examine the capacity of MCT1 to transport succinate, *in vivo*. We, surprisingly, did not see any difference in succinate transport between WT and MCT1 KO mice. However, when we acutely inhibit MCT1 by administering AZD3965, we reduce the amount of succinate transported into BAT. This difference may be attributed to the dose of AZD3965 used in this experiment, which was sufficient to inhibit both MCT1 and MCT2[18]. This coincides with our previous findings in primary brown adipocytes that acute inhibition of MCT1 and 2, with AZD3965, results in a greater reduction of succinate transport than inhibition of MCT1 alone. However, when we genetically inhibit all three MCT isoforms with siRNA, we do not observe a greater reduction in succinate uptake into primary brown adipocytes than with MCT1 knockdown alone. This incongruency may be due to a difference in acute inhibition versus genetic depletion of MCT isoforms. It is plausible that longer inhibition of MCT1 and other MCT isoforms may provide enough time for other proteins to adapt and fulfill the role of succinate transporter. However, more experiments would need to be conducted to fully identify the complete repertoire of succinate transporters in brown adipose tissue.

Acute vs. Chronic Succinate Signaling

Our work performed in exercising muscle (Reddy and Bozi *et al.*, *Cell*, 2020) highlighted the benefits of succinate signaling. However, many previous findings report succinate-SUCNR1 signaling to exacerbate inflammation associated with type II diabetes and obesity[17,19,20]. In fact, succinate sequestration by BAT reduces liver inflammation associated with non-alcoholic fatty liver disease (NAFLD) by limiting succinate-SUCNR1 signaling. The difference in beneficial and

deleterious effects of succinate signaling may lie in the duration of the signaling. In pathophysiological conditions, like type II diabetes, obesity, and hypertension, extracellular succinate concentrations rise and persist at high levels for an extended period[19-21]. On the contrary, during normal physiological events, like exercise, succinate rapidly accumulates and quickly renormalizes upon completion of the event[7]. This difference in the persistence of extracellular succinate translates to a difference in the frequency of succinate-SUCNR1 signaling. During exercise, the rapid accumulation and re-normalization of extracellular succinate results in short bursts of succinate-SUCNR1 signaling, which we show to be beneficial for muscle adaptation to exercise. Conversely, increased extracellular succinate leads to chronic, aberrant signaling which contributes to increased inflammation inflammation[17,21]. Thus, the favorable effects of succinate-SUCNR1 signaling seen with exercise can be largely attributed to quick decrease in extracellular succinate during recovery. Understanding the mechanism of succinate re-uptake during exercise could provide us with a better understanding as to how succinate signaling is regulated, in this context. One possibility may be that brown and beige adipocytes sequester extracellular succinate released by exercising muscle. It would be interesting to determine extracellular succinate concentrations following acute treadmill running in uncoupling protein 1 (UCP1) KO mice that lack functional brown and beige fat[22].

Localization of SUCNR1 in skeletal muscle

We previously report SUCNR1 to be exclusively localized to non-myofibrillar cell populations within skeletal muscle and implicate non-parenchymal succinate-SUCNR1 signaling in muscle adaptation to exercise. While we know generally that these cell populations play a critical role in SUCNR1-dependent muscle remodeling following exercise, it would be interesting to further elucidate the individual contributions of these populations in the adaptation process. Generation of SUCNR1 flox mice would allow us to fully interrogate this question. Our initial experiments were performed in whole body SUCNR1 KO mice. While this model provided an

initial insight into the role of succinate signaling in post-exercise muscle remodeling, knocking out SUCNR1 in specific cell populations will provide us with a more detailed understanding of this process. Moreover, determining if innervating neurons in skeletal muscle express SUCNR1 would provide more insight into the mechanism underlying SUCNR1-induced neuronal changes following exercise. This will allow us to determine if succinate directly signals to neurons post-exercise, or if an intermediary non-myofibrillar cell relays the signal. Additionally, it would be interesting to understand the universality of succinate-SUCNR1 signaling on neuronal remodeling. Is the role of succinate signaling in this process limited to exercise or are there additional physiological contexts where succinate promotes innervation? Further studies will need to be conducted to address these questions.

The Role of Succinate-SUCNR1 signaling in muscle inflammation

The inflammatory response to exercise is critical for proper muscle repair and remodeling to occur. In fact, administering non-steroidal anti-inflammatory drugs to individuals performing resistance exercise training blunted muscle hypertrophy and strength[23]. Additionally, pre-maturely expressing the anti-inflammatory cytokine interleukin-10 (IL-10) impairs muscle regeneration[24]. The role of inflammation in the muscle response to exercise can be largely attributed to its effects on satellite cells, a muscle-specific stem cell. Satellite cells can differentiate into new muscle fibers and play a key role in the hypertrophic response[25-28]. The initial burst of inflammation seen with the onset of exercise promotes proliferation of satellite cells while the resolution of this response fosters the fusion and differentiation of this stem cell niche. This is best highlighted by the proliferative effects of the pro-inflammatory cytokine interleukin-6 (IL-6) on satellite cells[29]. Conversely, the anti-inflammatory cytokine interleukin-4 (IL-4) promotes the fusion of these cells[30]. Thus, tight control of the inflammatory response is required for remodeling to occur. However, it is poorly understood how the inflammatory response is initiated following exercise.

Succinate has garnered much interest for its role in the inflammatory process and its immunomodulatory effects. Succinate stimulates the production of pro-inflammatory cytokine interleukin-1 beta (IL-1β), which can occur in both a SUCNR1-dependent and independent

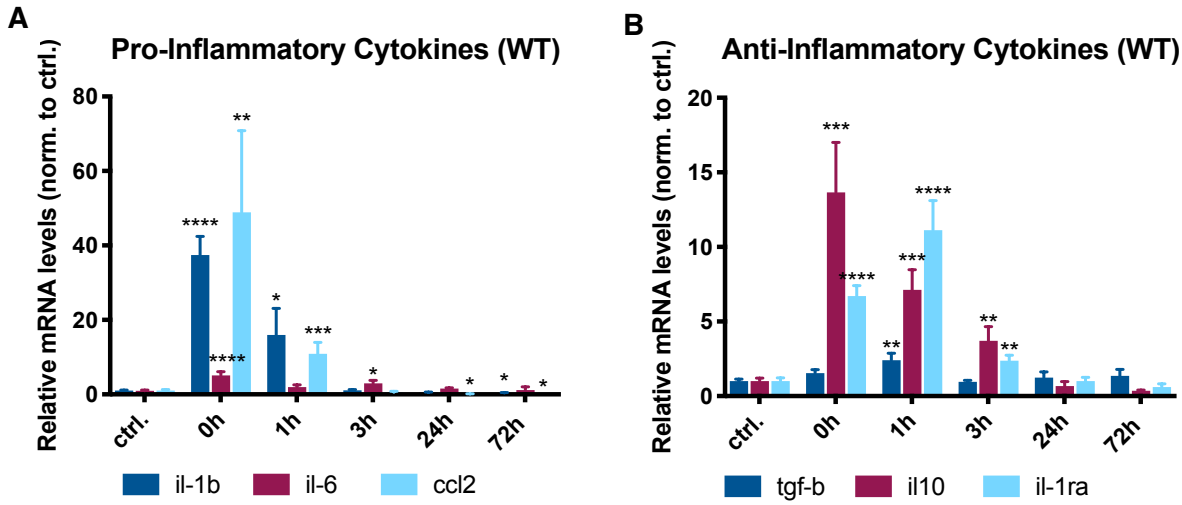


Figure 4.4 | Exercise promotes the transcription of pro- and anti-inflammatory cytokines. Mice were exercised to exhaustion and TA muscle was harvested at various times during the recovery period. qPCR analysis was performed to assess gene expression (n = 5). Pro-inflammatory cytokines il-1β, il-6, and ccl2 significantly increase immediately following and 1h after exercise (a). Anti-inflammatory cytokines tgf-β, il-10, and il-1rα significantly increase 0h, 1h, and 3h post-exercise (b).

Data are represented as mean ± SEM. *$p < 0.05$, **$p < 0.01$, ***$p < 0.005$, ****$p < 0.0001$ (one-way ANOVA for multiple comparisons involving one independent variable). Comparisons were made between individual genes at specific timepoints and their respective control.

manner[31-34]. Additionally, previous findings support the role of succinate as a chemokine for innate immune cells, which is dependent on SUCNR1[17,21,35]. Based on our previous findings (Reddy and Bozi *et al., Cell,* 2020) and others that report accumulation of extracellular succinate following exercise[19], we examined the role of succinate-SUCNR1 signaling in the inflammatory response

to exercise. We subjected WT mice to a single bout of graded treadmill running. Mice were exercised to exhaustion and sacrificed during various timepoints throughout recovery. We then assessed transcript levels of pro- and anti-inflammatory cytokines during the recovery period. In line with previous findings, we observe a significant increase in transcript levels of pro-inflammatory cytokines il-1β, il-6, and monocyte chemoattractant protein-1 (CCL2), a chemokine that recruits monocytes to sites of inflammation, during the early timepoints following exercise (figure 4.4). We then subjected WT and SUCNR1 KO mice to a single bout of treadmill running, and harvested TA muscle 1 hour following exercise. We performed qPCR analysis on exercised muscle to assess differential transcript expression of pro- and anti-inflammatory cytokines. We observe a significant decrease in pro-inflammatory cytokines il-6, ccl2, and tumor necrosis factor alpha (tnf-α) in SUCNR1 KO mice compared to WT (figure 4.5). While this data is preliminary, it suggests that SUCNR1 may be involved in establishing a pro-inflammatory environment in skeletal muscle following exercise. However, whether this difference in transcript levels translates to a difference in protein abundance, remains unknown. Additionally, the consequence of this difference in cytokine transcript levels is not known. Does a reduction in the transcript levels of these pro-inflammatory cytokines result in altered muscle adaptation to exercise? More work needs to be done to address these questions and fully understand the role of succinate-SUCNR1 signaling in the inflammatory response following exercise.

Conclusion

In this dissertation, we highlight the role of succinate as a signaling molecule that can relay changes in the bioenergetic status of the cell to the surrounding environment to promote remodeling. We implicate succinate-SUCNR1 signaling in muscle adaptation to exercise, specifically, extracellular matrix remodeling, innervation, and strength. Moreover, we define a new mode of regulation for transport whereby transient changes in cytosolic pH drive the release of succinate. In skeletal muscle, we observe a decrease in cytosolic pH, driven by hypoxia or acute

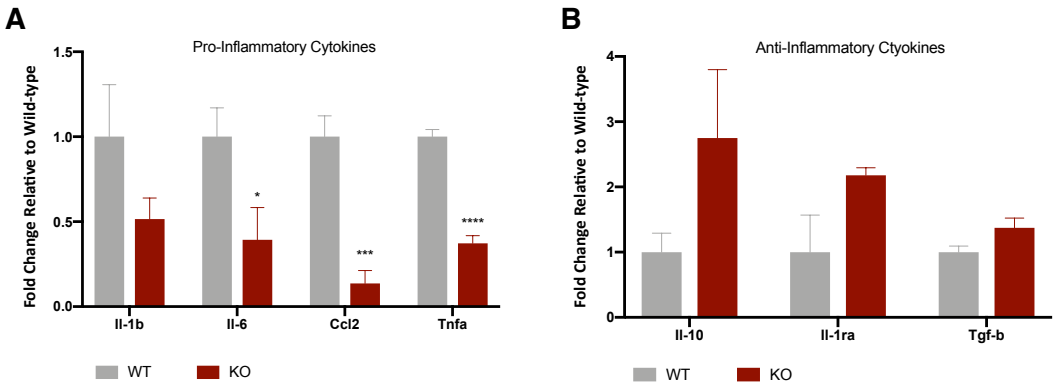


Figure 4.5 | Gene-expression data from WT and SUCNR1 KO mice following exhaustive treadmill running. WT and SUCNR1 KO mice were subjected to exhaustive treadmill running and sacrificed 1h following exercise. TA muscle was harvested, and qPCR analysis was performed. SUCNR1 KO mice had significant reduced transcript levels of pro-inflammatory cytokines il-6, ccl2, and tnf-α (a). No significant differences between genotypes were observed for transcript levels of anti-inflammatory cytokines il-10, il-1rα, and tgf-β (b).

Data are represented as mean ± SEM. *$p < 0.05$, **$p < 0.01$, ***$p < 0.005$, ****$p < 0.001$ (two-tailed Student's t test for pairwise comparisons).

mitochondrial inhibition, that fosters the protonation of succinate. In the protonated form, succinate can be secreted via MCT1. We show this transport mechanism to be applicable in brown adipocytes where changes in proton gradients driven by β-adrenergic signaling promote the uptake of succinate into brown adipocytes via MCT1. We demonstrate the capacity of MCT1 to facilitate succinate uptake in BAT, although there are most likely other transporters that are capable of transporting succinate. Overall, we describe a regulatory role for succinate during exercise and define a novel pH-gated mode of succinate transport that's mediated by MCT1. In sum, I hope this body of work provides the readers with an appreciation for the signaling capacities of metabolites and their role in tissue remodeling.

References

1. Hagberg, H. Intracellular pH during ischemia in skeletal muscle: relationship to membrane potential, extracellular pH, tissue lactic acid and ATP. *Pflugers Arch* **404**, 342-347 (1985).
2. Robergs, R.A., Ghiasvand, F. & Parker, D. Biochemistry of exercise-induced metabolic acidosis. *Am J Physiol Regul Integr Comp Physiol* **287**, R502-516 (2004).
3. Sahlin, K., Edstrom, L., Sjoholm, H. & Hultman, E. Effects of lactic acid accumulation and ATP decrease on muscle tension and relaxation. *Am J Physiol* **240**, C121-126 (1981).
4. Bright, C.M. & Ellis, D. Intracellular pH changes induced by hypoxia and anoxia in isolated sheep heart Purkinje fibres. *Exp Physiol* **77**, 165-175 (1992).
5. Hochachka, P.W., Owen, T.G., Allen, J.F. & Whittow, G.C. Multiple end products of anaerobiosis in diving vertebrates. *Comp Biochem Physiol B* **50**, 17-22 (1975).
6. Mills, E.L.*, et al.* Accumulation of succinate controls activation of adipose tissue thermogenesis. *Nature* **560**, 102-106 (2018).
7. Hochachka, P.W. & Dressendorfer, R.H. Succinate accumulation in man during exercise. *Eur J Appl Physiol Occup Physiol* **35**, 235-242 (1976).
8. Ehinger, J.K.*, et al.* Cell-permeable succinate prodrugs bypass mitochondrial complex I deficiency. *Nat Commun* **7**, 12317 (2016).
9. Hems, R., Stubbs, M. & Krebs, H.A. Restricted permeability of rat liver for glutamate and succinate. *Biochem J* **107**, 807-815 (1968).
10. MacDonald, M.J., Fahien, L.A., Mertz, R.J. & Rana, R.S. Effect of esters of succinic acid and other citric acid cycle intermediates on insulin release and inositol phosphate formation by pancreatic islets. *Arch Biochem Biophys* **269**, 400-406 (1989).
11. Wang, T.*, et al.* Succinate induces skeletal muscle fiber remodeling via SUNCR1 signaling. *EMBO Rep* **20**, e47892 (2019).
12. Ariza, A.C., Deen, P.M. & Robben, J.H. The succinate receptor as a novel therapeutic target for oxidative and metabolic stress-related conditions. *Front Endocrinol (Lausanne)* **3**, 22 (2012).
13. Mills, E. & O'Neill, L.A. Succinate: a metabolic signal in inflammation. *Trends Cell Biol* **24**, 313-320 (2014).
14. Folland, J.P. & Williams, A.G. The adaptations to strength training : morphological and neurological contributions to increased strength. *Sports Med* **37**, 145-168 (2007).
15. Gabriel, D.A., Kamen, G. & Frost, G. Neural adaptations to resistive exercise: mechanisms and recommendations for training practices. *Sports Med* **36**, 133-149 (2006).
16. Richter, E.A., Mikines, K.J., Galbo, H. & Kiens, B. Effect of exercise on insulin action in human skeletal muscle. *J Appl Physiol (1985)* **66**, 876-885 (1989).
17. Mills, E.L.*, et al.* UCP1 governs liver extracellular succinate and inflammatory pathogenesis. *Nat Metab* **3**, 604-617 (2021).
18. Curtis, N.J.*, et al.* Pre-clinical pharmacology of AZD3965, a selective inhibitor of MCT1: DLBCL, NHL and Burkitt's lymphoma anti-tumor activity. *Oncotarget* **8**, 69219-69236 (2017).
19. Sadagopan, N.*, et al.* Circulating succinate is elevated in rodent models of hypertension and metabolic disease. *Am J Hypertens* **20**, 1209-1215 (2007).
20. Osuna-Prieto, F.J.*, et al.* Elevated plasma succinate levels are linked to higher cardiovascular disease risk factors in young adults. *Cardiovasc Diabetol* **20**, 151 (2021).
21. van Diepen, J.A.*, et al.* SUCNR1-mediated chemotaxis of macrophages aggravates obesity-induced inflammation and diabetes. *Diabetologia* **60**, 1304-1313 (2017).

22. Kazak, L.*, et al.* UCP1 deficiency causes brown fat respiratory chain depletion and sensitizes mitochondria to calcium overload-induced dysfunction. *Proc Natl Acad Sci U S A* **114**, 7981-7986 (2017).
23. Lilja, M.*, et al.* High doses of anti-inflammatory drugs compromise muscle strength and hypertrophic adaptations to resistance training in young adults. *Acta Physiol (Oxf)* **222**(2018).
24. Perdiguero, E.*, et al.* p38/MKP-1-regulated AKT coordinates macrophage transitions and resolution of inflammation during tissue repair. *J Cell Biol* **195**, 307-322 (2011).
25. Pallafacchina, G., Blaauw, B. & Schiaffino, S. Role of satellite cells in muscle growth and maintenance of muscle mass. *Nutr Metab Cardiovasc Dis* **23 Suppl 1**, S12-18 (2013).
26. Abou Sawan, S.*, et al.* Satellite cell and myonuclear accretion is related to training-induced skeletal muscle fiber hypertrophy in young males and females. *J Appl Physiol (1985)* **131**, 871-880 (2021).
27. Goh, Q.*, et al.* Myonuclear accretion is a determinant of exercise-induced remodeling in skeletal muscle. *Elife* **8**(2019).
28. Masschelein, E.*, et al.* Exercise promotes satellite cell contribution to myofibers in a load-dependent manner. *Skelet Muscle* **10**, 21 (2020).
29. Serrano, A.L., Baeza-Raja, B., Perdiguero, E., Jardi, M. & Munoz-Canoves, P. Interleukin-6 is an essential regulator of satellite cell-mediated skeletal muscle hypertrophy. *Cell Metab* **7**, 33-44 (2008).
30. Horsley, V., Jansen, K.M., Mills, S.T. & Pavlath, G.K. IL-4 acts as a myoblast recruitment factor during mammalian muscle growth. *Cell* **113**, 483-494 (2003).
31. Tannahill, G.M.*, et al.* Succinate is an inflammatory signal that induces IL-1beta through HIF-1alpha. *Nature* **496**, 238-242 (2013).
32. Mills, E.L.*, et al.* Succinate Dehydrogenase Supports Metabolic Repurposing of Mitochondria to Drive Inflammatory Macrophages. *Cell* **167**, 457-470 e413 (2016).
33. Rubic, T.*, et al.* Triggering the succinate receptor GPR91 on dendritic cells enhances immunity. *Nat Immunol* **9**, 1261-1269 (2008).
34. Littlewood-Evans, A.*, et al.* GPR91 senses extracellular succinate released from inflammatory macrophages and exacerbates rheumatoid arthritis. *J Exp Med* **213**, 1655-1662 (2016).
35. He, W.*, et al.* Citric acid cycle intermediates as ligands for orphan G-protein-coupled receptors. *Nature* **429**, 188-193 (2004).